ISTANBUL TECHNICAL UNIVERSITY ★ GRADUATE SCHOOL OF SCIENCE ENGINEERING AND TECHNOLOGY

ELECTROSPUN P3ANA/PCL NANOFIBERS AS ELECTROACTIVE-BIOACTIVE BIOMATERIAL FOR BONE TISSUE REGENERATION: SYNTHESIS, CHARACTERIZATION AND CELL STUDIES

Ph.D. THESIS

Zeliha GÜLER

Department of Nanoscience and Nanoengineering

Nanoscience and Nanoengineering Programme

MAY 2016

ISTANBUL TECHNICAL UNIVERSITY ★ GRADUATE SCHOOL OF SCIENCE ENGINEERING AND TECHNOLOGY

ELECTROSPUN P3ANA/PCL NANOFIBERS AS ELECTROACTIVE-BIOACTIVE BIOMATERIAL FOR BONE TISSUE REGENERATION: SYNTHESIS, CHARACTERIZATION AND CELL STUDIES

Ph.D. THESIS

Zeliha GÜLER
(513112005)

Department of Nanoscience and Nanoengineering

Nanoscience and Nanoengineering Programme

Thesis Advisor: Prof. Dr. A. Sezai SARAÇ

MAY 2016

İSTANBUL TEKNİK ÜNİVERSİTESİ ★ FEN BİLİMLERİ ENSTİTÜSÜ

KEMİK DOKU REJENERASYONU İÇİN ELEKTROAKTİF-BİYOAKTİF BİYOMALZEME OLARAK P3ANA/PCL NANOFİBERLERİ: SENTEZ, KARAKTERİZASYON VE HÜCRE ÇALIŞMALARI

DOKTORA TEZİ

Zeliha GÜLER
(513112005)

Department of Nanoscience and Nanoengineering

Nanoscience and Nanoengineering Programme

Tez Danışmanı: Prof. Dr. A. Sezai SARAÇ

MAYIS 2016

Zeliha GÜLER, **a Ph.D.** student of ITU **Graduate School of Science Engineering and Technology** student ID **513112005**, successfully defended the **thesis** entitled "**ELECTROSPUN P3ANA/PCL NANOFIBERS AS ELECTROACTIVE-BIOACTIVE BIOMATERIAL FOR BONE TISSUE REGENERATION: SYNTHESIS, CHARACTERIZATION AND CELL STUDIES**", which she prepared after fulfilling the requirements specified in the associated legislations, before the jury whose signatures are below.

Thesis Advisor : **Prof. Dr. A. Sezai SARAÇ** .....
Istanbul Technical University

Jury Members : **Assoc. Prof. Dr. Fatma Neşe KÖK** .....
Istanbul Technical University

Prof. Dr. Mustafa ÖKSÜZ .....
Marmara University

Prof. Dr. Esra Özkan ZAYİM .....
Istanbul Technical University

Prof. Dr. Ayhan BOZKURT .....
Fatih University

Date of Submission : 13 April 2016
Date of Defense : 09 May 2016

To my father,

FOREWORD

I would like to first express my sincere gratitude to my supervisor Prof. Dr. A. Sezai SARAC for his guidance, support and inspiration throughout all period of my PhD. He always encouraged me to do better and to move forward.
I also thank my thesis committee members Assoc. Prof. Dr. Fatma Neşe KÖK and Prof. Dr. Mustafa ÖKSÜZ for their support, their valuable comments helped me in improving the quality of my work. I would like to thank to Prof. Dr. Jorge Carvalho SILVA from Tissue Engineering Group at Nova University of Lisbon for accepting me to his laboratory during my research period in Portugal, for his guidance and support in cell culture studies. I also appreciate his effort and time. I also want to thank to Prof. Dr. Gürsel TURGUT (MD), Kaya MOLO and Okan YAYLA from Genkord Stem Cell Technologies Corporation for providing facilities to carry out cell culture studies and for their hospitality.
I want to express my special thanks to Electropol-Nanotech Research group, especially my lab-mates Timuçin BALKAN and Rana GOLSHAEI for sharing their experience with me and for their support. I also want to give my sincere thanks to my friends and lab-mates; Başak DEMİRCİOĞLU, Aslı GENÇTÜRK, Mehmet Tolga SATICI, Mehmet Giray ERSÖZOĞLU and Dilek SUADİYE for their support. Their friendship is one of the most valuable thing that Electropol-Nanotech Research group brought me. Also I want to thank to Semra Zuhal BİROL for her friendship.
I would like to give my special thanks to Abdulmecit GÖKÇE for assisting statistical analyses on my thesis, for his patience, encouragement and love. I am grateful that even in challenging times you always find a way to create a beatiful moment for me.
Most of all, I would like to thank my mother Zeynep GÜLER, my father Hüseyin GÜLER and my sister Meliha GÜLER, for their endless patience and love. I will always feel your continuous support regardless of time and space. Also, I want to thank them for teaching me the importance of working hard and not to give up.
I want to express my thanks to Scientific and Technological Research Council of Turkey (TUBITAK) for the financial support on project 213M469 and on fellowship 2211C.

May 2016

Zeliha GÜLER
(Biologist)

TABLE OF CONTENTS

Page

ABBREVIATIONS

AC : Alternating Current
AFM : Atomic Force Microscope
ALP : Alkaline Phosphatase
ASC : Adult Stem Cell
ATR : Attenuated Total Reflectance
BCA : Bicinchoninic Acid
BMP : Bone Morphogenetic Protein
BMSC : Bone Marrow Mesenchymal Stem Cell
Ca : Calcium
CP : Conductive Polymer
DAPI : 40,6-diamidino-phenyindol
DC : Direct Current
DMA : Dynamic Mechanical Analyzer
DMEM : Dulbecco's Minimal Eagle Medium
DMF : Dimethyl Formamide
ECM : Extracellular Matrix
EDC : 1-ethyl-3-(dimethyl-aminopropyl) carbodiimide hydrochloride
EDX : Energy-Dispersive X-ray Spectroscopy
EF : Electric Field
EIS : Electrochemical Impedance Spectroscopy
ESC : Embryonic Stem Cell
FBS : Fetal Bovine Serum
FTIR : Fourier Transform Infrared Spectroscopy
HSC : Hematopoietic Stem Cell
Hz : Hertz
IGF : Insulin-like Growth Factor
ITO-PET : Indium Tin Oxide-Polyethylene Terephthalate
MES : 2-morpholinoethane Sulfonic Acid
MSC : Mesenchymal Stem Cell
MTT : 3-(4,5- dimethyl-2-thiazolyl)-2,5-diphenyltetrazolium bromide
NHS : N-hydroxysuccinimide
PANI : Polyaniline
P3ANA : Poly(m-anthranilic acid)
PBS : Phosphate Buffer Saline
PCL : Poly (ε-caprolactone)
RGD : Arginine, Glycine, Aspartic acid
SEM : Scanning Electron Microscopy
TE : Tissue Engineering
TGF : Transformation Growth Factor
THF : Tetrahydrofurane
UV-vis : Ultraviolet–visible

LIST OF TABLES

Page

LIST OF FIGURES

Page

ELECTROSPUN P3ANA/PCL NANOFIBERS AS ELECTROACTIVE-BIOACTIVE BIOMATERIAL FOR BONE TISSUE REGENERATION: SYNTHESIS, CHARACTERIZATION AND CELL STUDIES

SUMMARY

An electroactive and bioactive nanofiber scaffold which serves both chemical and physical bioactive signals for cells, was fabricated. Electrospun poly(ε-caprolactone)/poly(m-anthranilic acid) (PCL/P3ANA) nanofibers were fabricated by addition of increasing amounts of P3ANA to the PCL solutions. The addition of P3ANA in higher amount resulted a decrease in fiber diameter and high surface roughness and large surface area. The increased surface area of PCL/P3ANA nanofibers serves more available sites and carboxyl groups for biofunctionalization with growth factors. The mechanical properties of PCL/P3ANA nanofibers changed due to P3ANA amount which changed the structural properties of the nanofibers. Electrochemical impedance spectroscopy (EIS) measurements showed that the increase of P3ANA amount in the PCL/P3ANA nanofibers resulted lower charge transfer resistance values which indicates higher conductivity. Higher electroactivity is advantageous in terms of delivering electrical signals to cells. Therefore the PCL/P3ANA nanofiber scaffold containing the highest amount of P3ANA with highest surface area, best mechanical and electrochamical properties was chosen for biofunctionalization and electrical stimulation of cells.

PCL/P3ANA nanofiber scaffold was biofunctionalized with covalent protein attachment by using 1-ethyl-3-(dimethyl-aminopropyl) carbodiimide hydrochloride (EDC) and N-hydroxysuccinimide (NHS) activation process. The activation process was investigated and it was found that 50/50 mM of EDC/NHS was the most effective concentration for the activation of PCL/P3ANA nanofibers. After determination of the suitable nanofiber mat for cell culture studies and the optimum concentrations of EDC/NHS for covalent immobilization, PCL/P3ANA nanofiber scaffold was biofunctionalized with growth factors of bone morphogenetic protein-2 (BMP-2) and RGD peptide for *in vitro* cells studies. The amounts of covalently immobilized BMP-2 and RGD peptide were determined by bicinchoninic acid (BCA) protein assay and with elemental analyzes of N atoms by Energy-Dispersive X-ray Spectroscopy (EDX). Contact angle measurements showed the changes of the surface properties from hydrophobic to hydrophilic after protein immobilization. The increase in the double layer capacitance and charge transfer values of nanofibers after protein immobilization was showed with EIS. Nanofibers were nontoxic and enable for attachment and growth of Saos-2 cells. The cell proliferation was the highest for the RGD peptide immobilized nanofibers. Cell viability is in correlation with cellular adhesion and structure of the scaffold. Cell morphology was polygonal in shape on the PCL, PCL/P3ANA and PCL/P3ANA-RGD nanofibers is similar to each other. The cells on BMP-2 functionalized nanofibers exhibited osteocyte-like morphology. Alkaline phosphatase (ALP) activity and calcium deposition of Saos-2 cells cultured on cover glass, PCL, PCL/P3ANA, BMP-2/PCL/P3ANA and

PCL/P3ANA-RGD nanofibers were investigated. The cells on BMP-2 immobilized nanofibers had the highest ALP activity and the highest amount of calcium deposits among all nanofibers and cover glass, which indicates a higher degree of osteogenesis.

The effects of electrical stimulation on the differentiation of Bone Marrow Mesenchymal Stem Cells (BMSCs) into bone feature and the ability of PCL/P3ANA nanofibers to deliver the electrical signals to the cell were investigated. Electrical stimulation was applied to the cells with the electric field (voltage difference per unit distance) of 200 mV/mm, 400 mV/mm and 800 mV/mm at frequency of 0.5 kHz, 1 kHz, 5 kHz and 10 kHz. The viability of cells was the highest when frequency of 1 kHz was applied. At frequency of 0.5 kHz and 1 kHz, the highest viability was observed when cells stimulated with 400 mV/mm. When 800 mV/mm AC voltage at any frequency was applied, cell viability was below 50%. The higher frequencies (5 kHz and 10 kHz) caused a dramatic decrease in cell viability. The cells cultured on the PCL/P3ANA nanofibers under electrical stimulation, proliferated by spreading on the nanofiber mats. At 200 mV/mm and 400 mV/mm voltages BMSCs showed osteocyte-like morphology with adherent-cell type actin extensions. Osteogenic differentiation of BMSCs was investigated by staining for ALP activity and Ca deposits. ALP activity and Ca deposition data exhibited similar trend to the proliferation results. The cells stimulated with voltage of 800 mV/mm exhibited almost no ALP activity or mineralization. The highest mineralization and ALP activity was observed when BMSCs stimulated with 400 mV/mm at 1 kHz. The electrical stimulation data suggested that P3ANA in the nanofiber structure was capable of delivering, interacting and mediating the electrical signaling process within the seeded BMSCs.

KEMİK DOKU REJENERASYONU İÇİN ELEKTROAKTİF-BİYOAKTİF BİYOMALZEME OLARAK P3ANA/PCL NANOFİBERLERİ:SENTEZ, KARAKTERİZASYON VE HÜCRE ÇALIŞMALARI

ÖZET

Doku mühendisliği, organa özgün hücrelerin bir iskelet yapı üzerinde çoğaltılması ile yapay doku ve organların üretilmesini sağlamaktadır. Doku mühendisliğinde kullanılan iskelet, doğal hücredışı matrisi taklit ederek, hücrelere geçici olarak destek sağlayan üç boyutlu bir taslak olarak görev almaktadır. Hücreler, iskelet üzerinde çoğalır, göç eder ve özgün hücrelere farklılaşırlar. Kullanılan iskelet, hücrelere gerekli olan kimyasal, morfolojik ve yapısal sinyaller iletmektedir. Bu nedenle, istenilen şekil, boyut ve işleve sahip dokunun oluşturulması amacıyla iskelet seçimi oldukça önemlidir. İskelet tasarımında biyouyumluluk ve porozite gibi çeşitli özelliklerin gözönünde bulundurulması gereklidir. Porlu yapıları ve geniş yüzey alanına sahip olmalarından dolayı nanofiberler doku mühendisliği iskeleti olarak ideal yapılardır. Nanofiber, boyutları ve fibrilli yapıları dolayısıyla doğal hücredışı matrise benzerlik göstermektedir. Elektrospin yöntemi ile sentetik veya doğal polimerler kullanılarak, doku mühendisliği iskeleti olarak kullanılmak üzere nanofiberler üretilmektedir. Polimerik malzemeler arasında, poli(ε- kaprolakton) (PCL) ve PCL içeren kopilimer veya karışımlar doku mühendislik çalışmalarında yaygın olarak kullanılmıştır. PCL nanofiberleri biyobozunur, biyouyumludur ve özellikler kemik doku mühendisliği çalışmalarına uygun mekanik özelliklere sahiptir. Nanofiberlerin morfolojik özelliklerine rağmen, hücre ve nanofiber arasındaki etkileşimin arttırılması ve doku yenilenmesinin uyarılması amacıyla, hücrelerin fiziksel veya kimyasal faktörlerle uyarılması gerekmektedir. Nanofiberler, büyüme faktörlerinin nanofiber yüzeyinde bulunan fonksiyonel gruplara kovalent olarak immobilizasyonu ile kimyasal olarak modifiye edilebilirler. Fiziksel uyaran olarak ise, özellikle kemik dokusunu uyarmak üzere elektriksel uyarı kullanılabilir. Hem fiziksel hem de kimyasal uyarıların doku mühendisliğinde kullanılabilmesi için uygun bir iskelet malzemenin seçilmesi gerekmektedir. Bu doğrultuda iletken polimerin kullanımı uygun bir alternatif sağlamaktadır. Son yıllarda iletken polimerlerin doku mühendislik uygulamalarında kullanımı ilgi çekmektedir. Polianilin ve türevleri, biyouyumlu ve elektrokimyasal özellikleri tanımlanmış iletken polimerlerdir. Ancak, polianilin ve türevleri çeşitli çözücüler içerisindeki çözünürlüğünün sınırlı olması nedeniyle sınırlı işlenebilirliğe sahiptirler. Bu sorunun aşılması amacıyla anilin monomeri çeşitli fonksiyonel grupların monomere eklenmesi ile modifiye edilmektedir. Poli(m-antranilik asid) (P3ANA), anilin monomerine karboksil (-COOH) grubu eklemesi ile elde edilmiş bir polianilin türevidir. P3ANA yapısına eklenen karboksil grubu, polimerin sulu ve sulu olmayan çözücüler içerisinde çözünmesi sağlamaktadır. P3ANA, iyi tanımlanmış elektrokimyasal özellikleri, yapısında bulunan fonksiyonel grupların varlığı bakımından hem elektriksel uyarıların hücrelere iletilmesi hem de nanofiberlerin

biyomoleküller ile kovalent olarak modifiye edilemesi için uygun bir iletken polimerdir.

Hücrelere kimyasal ve fiziksel biyoaktif sinyaller ileten bir elektoaktif ve biyoaktif nanofiber hücre iskeleti üretilmiştir. Poli(ε-kaprolakton)/poli(m-antranilik asit) (PCL/P3ANA) nanofiberleri, PCL çözeltisine artan miktarda P3ANA ilave edilmesinin ardından elektrospin yöntemi ile elde edilmiştir. Fiber yapısına artan miktarda P3ANA eklenmesi, daha küçük fiber çapına, daha fazla yüzey pürüzlülüğüne ve yüzey alanına sahip nanofiberlerin üretilmesini sağlamıştır. PCL/P3ANA nanofiberlerinin geniş yüzey alanına sahip olması, nanofiberlerin büyüme faktörleri ile biyoişlevsel hale getirilmesi için daha fazla uygun bölge ve karboksil grubu sağlamaktadır. Nanofiber yapısına artan miktarda P3ANA ilave edilmesi, nanofiberlerin yapısal özelliklerinin değişmesine neden olarak nanofiberlerin mekanik özelliklerini iyileşmesine neden olmuştur. Elektrokimyasal empedans spektroskopik (EIS) ölçümler, PCL/P3ANA nanofiberlerinde bulunan P3ANA miktarının artmasıyla birlikte, oluşan nanofiberlerin yük transfer direncinin düştüğünü ve daha yüksek iletkenliğe sahip nanofiberlerin elde edildiğini göstermiştir. Bu yüksek elektroaktivite hücrelere elektriksel sinyallerin iletilmesi bakımından avantaj sağlamaktadır. Bu sepeble, yapısında en fazla miktarda P3ANA içeren PCL/P3ANA nanofiberlerinin en fazla yüzey alanına, en iyi mekanik ve elektokimyasal özelliğe sahip olmasından dolayı, bu nanofiberler büyüme faktörleri ile işlevsel hale getirilmiş ve hücrelerin elektriksel olarak uyarılması çalışmalarında kullanılmıştır.

Proteinlerin, PCL/P3ANA nanofiber hücre iskeletine kovalent olarak bağlanması sonucu biyoişlevsel hale getirilmesi 1-etil-3-(dimetil-aminopropil) karbodiimid hidroklorid (EDC) and N-hidroksisuksinimid (NHS) aktivayonu işlemi ile gerçekleştirilmiştir. Nanofiber yapısında bulunan karboksil gruplarının aktivasyon verimi, değişen EDC/NHS konsatrasyonuna bağlı olarak spektroskopik ve morfolojik olarak incelenmiştir. Elektrokimyasal empedans spektroskopik ölçümler, karboksil gruplarının aktivasyon derecesine bağlı olarak nanofiberlere kovalent bağlanan protein miktarının değiştiğini göstermiştir. Aktivasyon süreci detaylı olarak incelenmiş ve 50/50 mM EDC/NHS konsantrasyonunun nanofiberleri en etkili şekilde aktive eden konsatrasyon olduğu bulunmuştur. Elde edilen nanofiberler arasından hücre kültür çalışmalarında kullanılmak üzere uygun nanofiberlerin seçilmesinden ve kovalent protein immobilizasyonu için en etkili EDC/NHS konsatrasyonun belirlenmesinin ardından, PCL/P3ANA nanofiber hücre iskeleti, *in vitro* hücre kültür çalışmalarında kullanılmak üzere kemik morfogenetik protein-2 (BMP-2) ve RGD peptid büyüme faktörleri ile biyoişlevsel hale getilmiştir. BMP, kemik oluşumunu destekleyen güçlü bir osteoindüktif faktördür. BMP varlığı, mezenkimal kök hücrelerin alkalin fosfataz aktivitesinin artışına neden olarak osteoblastik fenotipe yönelimini uyarmaktadır. RGD peptid ise birincil kemik hücre cevabını arttırmak üzere bir adezyon peptidi olarak nanofiber yapısına dahil edilmiştir. RGD peptid, mezenkimal kök hücrelerin osteoblastik farklılaşmasını sağlar ve hücre çoğalmasını arttırır. Hücre ve nanofiber iskelet arasındaki etkileşimini arttırarak, hücrelerin nanofiber üzerinde yayılmasını sağlamaktadır. Nanofiberlere bağlanan BMP-2 ve RGD peptid miktarı bikinkoninik acit (BCA) protein deneyi ve Enerji-Dağılımlı X-ray Spektroskopisi (EDX) ile N atomlarının elemental analizleri sonucu belirlenmiştir. Temas açısı deneyleri sonucunda, yüzeye protein bağlanmasının ardından hidrofobik özellik gösteren nanofiber yüzeyinin hidrofilik özellik kazandığı görülmüştür. EIS ölçümleri, nanofiberlere bağlanan proteinlerin nanofiber çift tabaka kapasitansı ve yük transfer direncinin artmasına

neden olduğunu göstermiştir. Nanofiberler, Saos-2 hücreleri üzerinde toksik etki göstermemiş ve hücrelerinin tutunma ve büyüme özelliklerini desteklemiştir. En fazla hücre çoğalması RGD peptid immobilize edilen nanofiberler üzerinde gözlenmiştir. Hücre canlılığının, hücrelerin adhezyonu ve nanofiberin yapısal özellikleri ile ilişkili olduğu görülmüştür. PCL, PCL/P3ANA ve PCL/P3ANA-RGD nanofiberleri üzerinde büyütülen hücrelerin morfolojileri birbirine benzerlik göstermiş ve poligonal şekil sergilemiştir. BMP-2 ile işlevsel hale getirilen nanofiber üzerinde büyütülen hücreler osteosit benzeri morfoloji göstermiştir. Cam lamel, PCL, PCL/P3ANA, BMP-2/PCL/P3ANA ve PCL/P3ANA-RGD nanofiberleri üzerinde büyütülen Saos-2 hücrelerinin alkalin fosfataz (ALP) aktivetisi ve kalsiyum birikimi incelenmiştir. BMP-2 immobilize edilmiş nanofiberler üzerinde büyütülen hücreler, diğer nanofiber ve cam lamel üzerinde büyütülen hücrelere kıyasla en fazla ALP aktivitesi ve kalsiyum birikimine sahip olarak, en yüksek osteogenez derecesine sahip olmuştur.

Elektriksel uyarının kemik iliği mezenkimal kök hücrelerin kemik hücresine farklılaşmasına etkisi ve PCL/P3ANA nanofiberlerinin elektriksel sinyalleri hücrelere iletimi incelenmiştir. Hücrelerin elektriksel olarak uyarılması amacıyla, 0.5 kHz, 1 kHz, 5 kHz ve 10 kHz frekansta; 200 mV/mm, 400 mV/mm and 800 mV/mm elektrik alan (birim mesafede uygulanan voltaj) uygulanmıştır. En yüksek hücre canlılığı 1 kHz frekans uygulanması ile elde edilmiştir. 0.5 kHz ve 1 kHz frekansta en yüksek hücre canlılığı ise hücrelere 400 mV/mm elektrik alan uygulandığında gözlenmiştir. 800 mV/mm elektrik alan uygulandığında ise uygulanan frekanstan bağımsız olarak hücre canlılığı % 50 oranında düşmüştür. Yüksek frekans (5 kHz ve 10 kHz) hücre canlılık değerlerinin belirgin bir şekilde düşmesine neden olmuştur. Elektriksel uyarı varlığında PCL/P3ANA nanofiberleri üzerinde büyütülen hücreler, nanofiberler üzerine yayılarak çoğalmışlardır. 200 mV/mm ve 400 mV/mm voltaj uygulandığında kök hücreler, adherent hücrelerin sahip olduğu aktin uzantılarıyla birlikte osteosit benzeri morfoloji göstermişlerdir. Kemik iliği mezenkimal kök hücrelerinin osteojenik farklılaşmasını incelemek adına, hücreler ALP aktivetesi ve kalsiyum birikiminin gösterilmesi için boyanmıştır. Hücreler, çoğalma testinde görülen eğilime uygun olarak ALP aktivitesi ve kalsiyum birikimine sahip olmuştur. 800 mV/mm voltaj uygulanan hücreler ALP aktivitesi ve mineralizasyon göstermemiştir. Hücrelerin düşük osteogenez derecesinin, yüksek voltaj uygulanması ile hücre canlılığının azalması ile ilişkili olduğu görülmüştür. En fazla kalsiyum birikimi ve ALP aktivitesi hücreler 1 kHz frekansta 400 mV/mm voltaj ile uyarıldıklarında görülmüştür. Hücrelerin elektriksel uyarıya verdikleri cevabın incelenmesi ile, nanofiber yapısında bulunan P3ANA polimerinin, nanofiberler üzerindeki kemik iliği mezenkimal kök hücrelerine elektriksel sinyalleri iletebildiği gösterilmiştir.

1. INTRODUCTION

1.1 Purpose of Thesis

Tissue engineering (TE) is an important emerging filed in biomedical engineering, which implies the use of organ-specific cells for seeding on a scaffold that serves as a three-dimensional template for tissue regeneration (Bianco & Robey, 2001). The cells seeded onto scaffolds, proliferate, migrate and differentiate into the specific tissue while secreting the extracellular matrix components required creating the tissue (Sachlos & Czernuszka, 2003). The scaffold having an ideal surface chemistry and microstructure, serves as a mimic for the native extracellular matrix (ECM) and plays a pivotal role in tissue regeneration by providing temporary support for the cells during the formation of a more natural ECM by the cells. The scaffold plays a critical role in providing the appropriate chemical, morphological and structural cues to direct the cells towards a targeted functional outcome (Zhang, Reagan, & Kaplan, 2009). Therefore, the choice of scaffold is very important to enable the cells to behave in the required manner to produce tissues and organs of the desired shape and size. There are several characteristics such as biocompatibility and porostiy considered essential for scaffold design. Nanofibers are ideal scaffolds for tissue engineering applications thanks to their porosity with extremely high specific surface area due to their small diameters. The dimensions of nanofibers are similar to components in the extracellular matrix (ECM) and mimic its fibrillar structure, providing essential cues for cellular organization, survival and function (Nisbet, Forsythe, Shen, Finkelstein, & Horne, 2008; Spagnuolo & Liu, 2012). These unique characteristics plus the functionalities from the polymers themselves impart nanofibers with many desirable properties for Tissue engineering scaffolds (Nisbet et al., 2008; Woo, Chen, & Ma, 2003) (W. J. Li, Laurencin, Caterson, Tuan, & Ko, 2002). Electrospinning has recently emerged as a leading technique for generating nanofibers as biomimetic scaffolds made of synthetic and natural polymers for tissue engineering applications (M. Li et al., 2005). Among all polymeric materials, poly(ε-caprolactone) (PCL) and their copolymers or blends, has been the most extensively

studied nanofiber system for the regeneration of tissues. PCL nanofibers are biodegradable, cytocompatible and possess good mechanical properties for regeneration of tissues, in particular for bone tissue (Jang, Castano, & Kim, 2009). Despite the properties of nanofiber scaffolds, they are often unable to create the microenvironment necessary for complete tissue development. Chemical or physical factors are paramounts to stimulate tissue regeneration. Nanofibers can be modified chemically by immobilization of growth factors, known as biofunctionalization, to manipulate *in vitro* tissue growth to obtain scaffolds with improved biological functions. Bioactivity can be achieved via covalent attachment of biomolecules on to the nanofibers by using functional groups in polymer. Besides biofunctionalization, electrical stimulation as a physical factor, can initiate the transformation of cell into bone cells (Hronik-Tupaj, Rice, Cronin-Golomb, Kaplan, & Georgakoudi, 2011). For both biofunctionalization and electrical stimulation, there must be suitable support, which has functional groups for surface modification, and are able to deliver electrical signal directly to the cells cultured on the nanofiber. Conductive polymers (CPs) are good candidates for both purposes. There is a growing interest in CPs for tissue engineering applications (M. Li, Guo, Wei, MacDiarmid, & Lelkes, 2006). Polyaniline (PANI) and its derivatives are one of the most promising class due to their well-defined electrochemical properties. However, their processability is limited due to their low solubility (Dagli, Guler, & Sarac, 2015). Poly(m-anthranilic acid) (P3ANA) is a PANI derivative with modification of aniline monomer with carboxyl groups (-COOH) which makes it soluble in aqueous and non-aqueous solvents as well as other polar solvents. Therefore, in the current study, P3ANA was introduced into PCL nanofibers for not only providing (-COOH) groups for biofunctionalization but also obtaining an electroactive nanofiber scaffold for electrical stimulation. Bioactive-electroactive PCL/P3ANA nanofibers was fabricated by electrospinning and growth factors were incorporated into nanofiber scaffold by covalent attachement. These new nanofiber systems mimicked the ECM by containing growth factors and enabled manipulation of stem cell functions by enhancing differentiation and ossification processes.

1.2 Tissue engineering

Tissue and organ lose or failure is a major and costly health problem, which can even cause death of patient. Tissue engineering (TE) is emerging as a significant potential alternative or complementary solution to the traditional treatment options such as transplantation, surgical repair, artificial prostheses and mechanical devices. However, the success of these methods for organ and tissue replacement is limited because of potential immunologic reactions, shortages in supply, poor integration and failure of mechanical devices. The goal of tissue engineering is to surpass the limitations of conventional treatments by implanting natural, synthetic, or semisynthetic tissue and organ mimics that are fully functional from the start, or that grow into the required functionality (Sachlos & Czernuszka, 2003).

TE implies the cell seeding *in vitro* on to a scaffold that serves as a three dimensional template for tissue regeneration (Bianco & Robey, 2001). The cells then proliferate on to the scaffold, migrate and differentiate into the specific tissue while secreting the extracellular matrix components which is necessary for formation of the tissue (Sachlos & Czernuszka, 2003) (Figure 1.1).

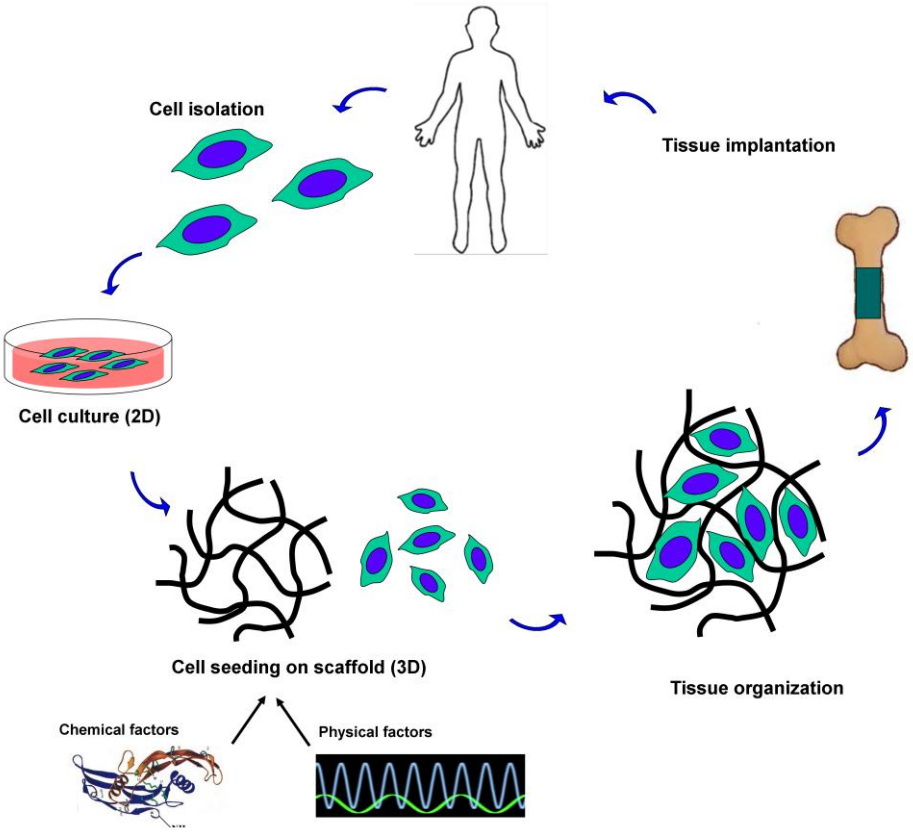

Figure 1.1 : Schematic representation of tissue engineering.

The components of TE can be classified as scaffolds, chemical or physical bioactive signals and cells (Laurencin & Nair, 2008).

1.2.1 Tissue engineering scaffolds

The scaffold serves as a mimic for the native extracellular matrix (ECM) and plays a pivotal role in tissue regeneration by maintaning temporary support for the cells. The scaffold provides the appropriate chemical, morphological and structural cues to direct the cells (Zhang et al., 2009). Scaffolds perform various functions such as creating a substrate for cells to attach, grow, proliferate, migrate and differentiate on; serving as a delivery vehicle for cells, facilitating the cell distribution; providing space for neotissue formation and remodeling; enabling the efficient transport of nutrients, growth factors and removal of waste material (Karande & Agrawal, 2008). Therefore, the choice of scaffold is very critical to enable the cells to behave in the required manner and to develop a cell-scaffold construct which can repair and regenerate tissue defects. Since the composition of the ECM of tissues varies from one to another, for each tissue engineering application, there is a need for selectrion of the scaffolds with spesific properties considering the spesific tissue morphologies. In order for scaffolds to perform these functions, they have to meet several essential characteristics. The first requirement is that the scaffold should be biocompatible, able to support appropriate cellular activity to optimize tissue regeneration without producing an unfavorable physiological response, such as rejection, inflammation or immune activation, in the host. Secondly, scaffolds is required to be biodegradable which is defined as ability to get broken down eventually and eliminated from the body via naturally occurring processes (Cheung, Lau, Lu, & Hui, 2007; Zhang et al., 2009). A highly porous scaffold with high surface area which allows maximum cell loading and cell–matrix interactions, is required to accommodate mammalian cells and guide their growth and tissue regeneration. Porous structure not only provides space for tissue in-growth, but also allows loading of bioactive molecules that manipulate cells in large amounts (Marx, Jose, Andersen, & Russell, 2011; Nisbet et al., 2008). Besides these parameters, the other important features scaffolds are the mechanical, surface and architectural properties. The mechanical properties such as strength, elasticity and toughness of the scaffold should match the host tissue in vivo. The porosity, interconnectivity of the pores and surface hydrophilicity affects the attachment and survival of the cells, since the cells must recognize the surface and

migrate through the scaffold. Also, the easy fabrication and processing of scaffolds are favorable in a reproducible manner (Karande & Agrawal, 2008).

Nanofibers are ideal candidates as tissue engineering scaffolds thanks to their porous structures with high specific surface area and pore interconnection (Woo et al., 2003). The morphological and surface properties of nanofibers are very similar to ECM and they can mimic fibrillar structure of ECM, provide essential cues for cellular organization, survival and function (Nisbet et al., 2008; Spagnuolo & Liu, 2012). The size of fibers is in the nanometer range, which is close to the size scale of the fibrous proteins found in the ECM, such as collagen. The size, structure and topography of nanofibers enhance the cell adhesion and proliferation (Flemming, Murphy, Abrams, Goodman, & Nealey, 1999). Nanofiber scaffolds have a very high surface available to interact with cells which enhance the cell-scaffold interaction and cell attachement (Sharma & Elisseeff, 2004). Porosity favors the transportation of nutrients trough the nanofiber scaffold.

Electrospinning has recently emerged as a leading technique for fabrication of nanofibers with desired properties, which allow their usage as a scaffold. Electrospining provides control over the physical, chemical and mechanical properties of nanofibers (M. Li et al., 2005; W. J. Li et al., 2002).

1.2.2 Electrospinning process

Electrospinning is a technique to form synthetic fibers with diameters ranging from tens of nanometers to a few micrometers, by using electrostatic forces. Electrospining utilizes a high voltage to inject charge of a certain polarity into a polymer solution or melt, which is then accelerated toward a collector of opposite polarity. When high voltage potential is applied to the polymer solution, electrostatic attraction between the oppositely charged polymer solution and collector increases. The charged ions in the polymer solution move in response to the applied electric field towards the electrode of opposite polarity by exceeding the surface tension of the solution. The fiber jet travels through the atmosphere allowing the solvent to evaporate, thus leading to the deposition of solid polymer fibers on the collector (Sill & von Recum, 2008). A schematic representation of electrospinning process is shown in Figure 1.2.

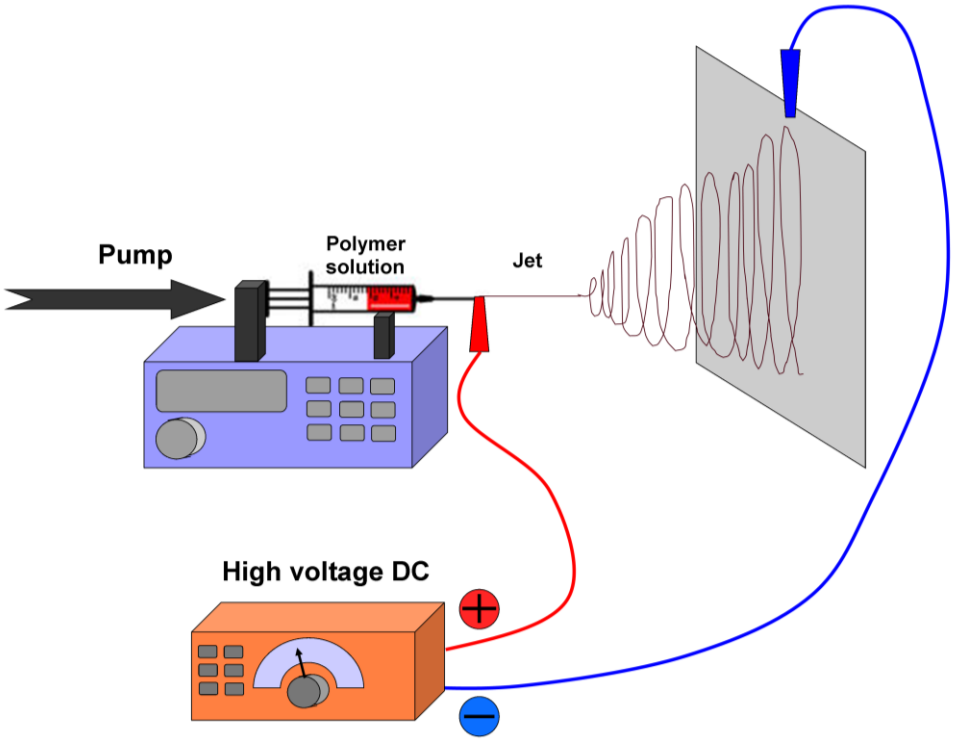

Figure 1.2 : Schematic representation of electrospinning setup.

The nanofiber morphology can be tuned by changing electrospinning parameters in which can be separated mainly in three groups such as system parameters (solution properties), process conditions (operational parameters) and ambient conditions. System parameters include the selection of a polymer with certain molecular weight and distribution and an appropriate solvent to obtain desired homogeneity in fiber diameter; polymer properties such as viscosity, surface tension, and conductivity, determine the nanofiber diameter and reduce the possibility of bead formation (M. Li et al., 2005). In relative order of their impact on the diameter and morphology of resulting nanofibers, system parameters include polymer concentration, solvent volatility and solvent conductivity (Sill & von Recum, 2008). The polymer solution must have a concentration high enough to cause polymer entanglements, yet not so high that the viscosity prevents polymer motion induced by the electric field (Qin, 2010). There is a relationship between resulting nanofiber diameter and polymer solution concentration, the nanofiber diameter increases with the increasing concentration of polymer solution. The same polymer concentration in different solvents can result different fiber morphologies, therefore the choice of solvent is also important. For sufficient solvent evaporation to occur between the capillary tip and the collector, solvent must be volatile. Dielectric constant of the solvent is also

changes the nanofiber diameter. The solvent having low dielectric constant result thinner fibers while low dielectric constant increases the fiber diameter (Wannatong, Sirivat, & Supaphol, 2004). Solution conductivity also affects the nanofiber diameter. Solutions with high conductivity will have a greater charge carrying capacity than solutions with low conductivity and thus the fiber jet of the first one will be subjected to a greater tensile. Charge accumulation on the solution jet results in strong electrostatic repulsion among the sprays which can overcome the surface tension of the jet to reduce diameters of the nanofibers (Giray, Balkan, Dietzel, & Sezai Sarac, 2013).

Process parameters include; flow rate of polymer (feed rate), distance between tip and of the capillary and the collector, and electric potential. Process parameters such as distance between capillary and metal collector determine the extent of evaporation of solvent from the nanofibers, and deposition on the collector, whereas motion of collector determines the pattern formation during fiber deposition (M. Li et al., 2005). High voltage helps to start nanofiber formation by inducing the charges in the polymer solution. The feed rate affects the nanofiber diameter since it determines the volume of solution which is used to fabricate nanofibers. Generally, too fast feeding rates cause bead formation. The distance between tip and collector changes the morphology of the nanofiber by changing the travel time of the electrospinning solution and the time for solvent evapotation. Nanofibers with cylindrical and straight morphology can be achieved by increasing the distance (Jalili, Hosseini, & Morshed, 2005).

Lastly, ambient conditions include humidity, airflow and temperature. High temperature can change the rigidity of the polymer and solution viscosity which can result thinner nanofibers. At high humidity, the polymer solution can absorb the ambient water resulting the formation of nanofibers with increased morphology (De Vrieze et al., 2009). Even tough, there are numbers of general relationships between electrospining parameters and fiber morphology, it is important to realize that the exact relationship will differ for each polymer/solvent system.

Due to the ability to control the nanofiber properties as well as the flexibility in material selection plus the functionalities from the polymers themselves, electrospun nanofibers have been used as scaffolds in various tissue engineering applications

(Nisbet et al., 2008; Woo et al., 2003) (W. J. Li et al., 2002). Besides the morphological properties of the scaffold, the choice of suitable material for a specific tissue engineering application is a critical consideration. Choices in materials include both natural and synthetic materials, as well as composites or blends of the two, which can provide an optimal combination of mechanical and biomimetic properties (Martina & Hutmacher, 2007; Sill & von Recum, 2008).

1.2.3 Natural and synthetic polymers

Natural polymers includes proteins such as collegen, fibrin, silk or gelatin (Rezwan, Chen, Blaker, & Boccaccini, 2006) and polysaccharides such as starch, alginate, chitin/chitosan and hyaluronic acid derivatives (Agarwal, Wendorff, & Greiner, 2008). Natural polymers favors cell attachment and their biocompatibility is higher compared to synthetic polymers, however their poor mechanical properties and differences in batch-to-batch/source property limit their usage in tissue engineering applications (Liang, Hsiao, & Chu, 2007).

The design and fabrication of synthetic scaffolds consists biodegradable polymers including polyglycolide (PGA), polylactides (PLA), poly- L -lactic acid (PLLA), poly- D , L –lactic acid (PDLA), polycaprolactone (PCL), which confer both degradation and mechanical property customization (Martina & Hutmacher, 2007). The impurities, mechanical or physical of properties, toxicity and degredation rate of these synthetic polymers can be controlled during synthesis by using well-known and simple constituent monomeric units (Rezwan et al., 2006). PCL as a biocompatible synthetic polymer is among the few synthetic polymers approved by the Food and Drug Administration (FDA) (Chen, Ushida, & Tateishi, 2000). Also, PCL was first suggested to be a degradable nanofiber matrix for the bone regeneration (Jang et al., 2009). PCL is a hydrophobic and semi-crystalline polymer which has low melting point (59–64 ºC), good solubility and blending compatibility. Compare to other synthetic polymers, the reological and viscoelestic properties of PCL are superior which make PCL easy to manufacture and manipulate into a large range of scaffolds (Woodruff & Hutmacher, 2010).

Conducting polymers (CPs) are a special class of polymeric materials with electronic and ionic conductivity (Ravichandran, Sundarrajan, Venugopal, Mukherjee, &

Ramakrishna, 2010) which make them an important class of materials for a wide range of applications. Compared to other polymers, CPs are relatively new to the tissue engineering (Bendrea, Cianga, & Cianga, 2011). However, there is a growing interest for CPs in tissue engineering applications, since they can be processed to form nanostructures such as nanofibers (Xiaofeng Lu, Zhang, Wang, Wen, & Wei, 2011) for cell growth. CPs are biocompatible (Schmidt, Shastri, Vacanti, & Langer, 1997) and have the ability to subject cells to an electrical stimulation (Ravichandran et al., 2010). Because, human body responds to electrical field and tissues including the brain, heart, muscle and bone are electrically responsive (Warren, Walker, Anderson, Rhodes, & Buckley, 1989; Yow, Lim, Yim, Lim, & Leong, 2011) which means cellular functions can be modulated under electric field.

Conductivity in CPs arises from the presence of conjugated double bonds, the bonds between the carbon atoms are alternatively single and double, along the backbone (Wise, Wnek, Trantolo, Cooper, & Gresser, 1998). CPs derived from hetero-aromatic monomers such as pyrrole, thiophene, aniline and their derivatives have been gaining interest in tissue engineering. Polyaniline (PAni) which has high stability and electroactivity, can be polymerized from aniline monomer (Wise et al., 1998). By comparison, PAni is one of the least studied CP as potential conductive substrates for tissue engineering applications (M. Li et al., 2006). It is only quite recently that PANi has been explored as a biocompatible polymer in vitro/in vivo and can be used as a scaffold in tissue engineering (Mattioli-Belmonte et al., 2003; Wei et al., 2004). However, the hydrophobicity, low processibility and solubility (Han, Song, Ding, Xu, & Niu, 2007) of PAni limits its adoption to tissue engineering. CPs have need for modifications to increase the biodegradability and cell adhesion (Bidez et al., 2006). Therefore, it is an essential to introduce solubility, biocompatibility, and biodegradability to conductive polymers, which are designed to be applied in tissue engineering. Cellular activities depends on the surface properties such as hydrophilicity/hydrophobycity, charge and roughness (C. Wang, Dong, Sengothi, Tan, & Kang, 1999). Different approaches have been applied to ensure good biocompatibility, including the use of monomers that contain hydrophilic chains (Cosnier, Dawod, Gorgy, & Da Silva, 2003). The carboxyl (–COOH) group substitution to the aniline monomer can increase the solubility and result hydrophilic polymer (Han et al., 2007). Poly(m-anthranilic acid) (P3ANA) which has carboxylic

acid group on the main aniline backbone can be polymerized from 2-amino benzoic acid (Khalil, Shaaban, Azab, Mahmoud, & Metwally, 2013). The chemical structure of P3ANA is represented in Figure 1.3. P3ANA has electrochemical activity in wide pH range, good mechanical and thermal properties (Shukla, Quraishi, & Prakash, 2008).

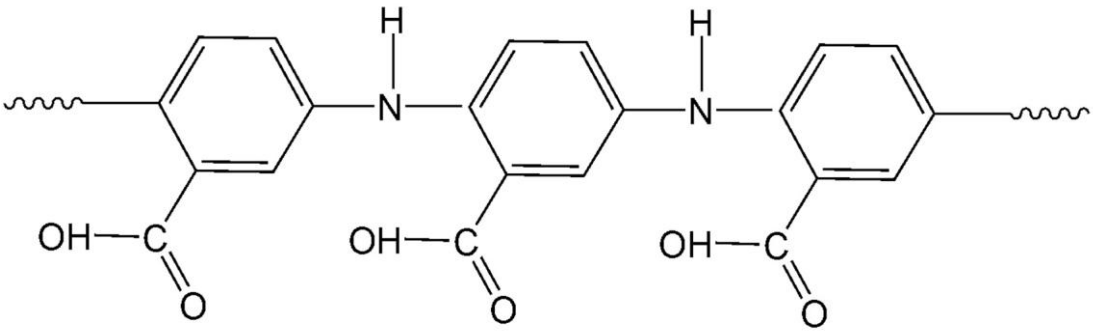

Figure 1.3 : The chemical structure of P3ANA.

In order to control the chemical composition, the mechanical properties, the degradation rate and the conductivity, polymer blends can be prepared with mixtures of synthetic and conducting polymers. This hybrid nanofiber scaffold can bring balance of biological and mechanical properties that promote cell survival (Annabi, Fathi, Mithieux, Weiss, & Dehghani, 2011). The synthetic PCL and conductive P3ANA polymers were blended in this study, in order to fabricate a conductive and bioactive nanofiber scaffold, which is capable of manipulating cellular functions with bioactive signals. Figure 1.4 represents the chemical structure of PCL/P3ANA and shows the interaction between partial positive charges of amine groups in P3ANA (Benyoucef, Huerta, Vázquez, & Morallon, 2005; Vacareanu, Catargiu, & Grigoras, 2012) and partially negative charges in PCL backbone (Khandanlou, Ahmad, Shameli, Saki, & Kalantari, 2014).

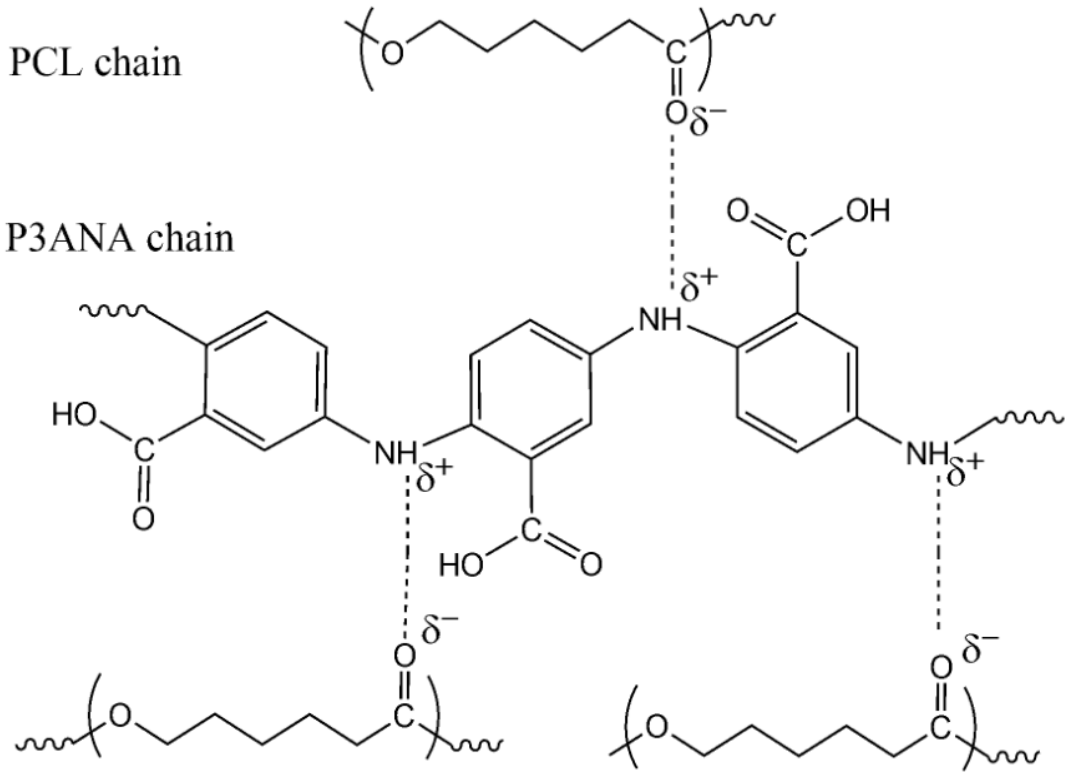

Figure 1.4 : The chemical structure of PCL/P3ANA.

Cellular functions can be regulated depending on the microenvironment which is provided by scaffold. Cells can attach, proliferate or differentiate into a certain fate in the presence of a chemical or physical stimulation. Chemical stimulations include the modification of the surface with a bioactive molecule. In the case of electroactive scaffolds, electrical field as a physical stimulation can be applied to the cell to control their functions and behaviors (Sill & von Recum, 2008; Yow et al., 2011). For these stimulations, there must be suitable scaffold which can provide functional groups for chemical modification and deliver the electrical signals to the cells. Thanks to carboxyl groups and conductivity of P3ANA, the PCL/P3ANA nanofibers scaffold is suitable for delivering both chemical or electrical bioactive signals.

1.3 Chemical and pyhsical bioactive signals

1.3.1 Surface functionalization with covalent biomolecule immobilization

The structural and morphological properties of nanofiber scaffolds affect the cell functions such as adhesion, proliferation, and migration (Sill & von Recum, 2008). However, due to the surface properties such as hydrophobicity, the initial cell adhesion to the scaffold can be limited. Therefore, the initial cell-scaffolds

interactions can be increased with bioactivation of scaffolds by surface modifications through attachment of bioactive molecules to the surface of the nanofibrous scaffold (Jang et al., 2009; T. G. Kim & Park, 2006; Sill & von Recum, 2008). Such modifications can be used to generate both physical and chemical guidance cues, which can be employed for the desired biomedical application. Surface modifications for incorporating biomolecules have been achieved by both physical and chemical modifications. Biomolecules can be incorporated physically to the scaffold via mixing (De Crombrugghe, Yunus, & Bertrand, 2008) or via chemical interactions such as covalent attachment (Wisse et al., 2011). Although mixing of biomolecule is simple, covalent attachment has the advantage of controlling the location and amount of attached biomolecule (Zheng, Zhang, & Jiang, 2010). In order to gain intended biological performance, the attached biomolecules should maintain their biological in a timely and proper manner. After physical attachment, biomolecules are weakly bounded and can rapidly diffuse from the application local and be rapidly degraded through endocytosis pathways(C.-H. Chang et al., 2015; Nakanishi, Sakiyama, Kumada, Imamura, & Imanaka, 2008). Covalent immobilization provides a prolonged availability for immobilized molecules to induce cellular functions [(Z. Guler & Sarac, 2016)].

Bioactivation of scaffolds through covalent immobilization can be achieved by using carboxylic acid groups in polymer backbone. The carbodiimide reagent offers a method for covalent bonding between carboxylic acid and amine groups, without itself being incorporated. The water-soluble and low toxic reagent, carbodiimide 1-ethyl-3-(3-dimethyl aminopropyl)carbodiimide (EDC) provides the formation of amide bonds between carboxylic acid groups and amino groups (Wisse et al., 2011). There EDC and N-hydroxysuccinimide (NHS) are used together to covalent attachment of biomolecules to polymers (Hronik-Tupaj et al., 2011). Covalent immobilization of biomolecules onto a -COOH group containing surface consists of preparation of a succinimidyl ester (-COOSuc)-terminated surface and its reaction with an amino ($-NH_2$) group on the biomolecule. This reaction is referred as surface "activation" which is conducted by reacting a surface bearing carboxyl end groups with NHS, in the presence of carbodiimide such as EDC (Staros, Wright, & Swingle, 1986). EDC/NHS activation of carboxylic acids has been widely applied to various kinds of substrates of polymers (Dai, Baker, & Bruening, 2006), silicon (Sam et al., 2010), nanotubes (Z.-G. Wang, Wang, Xu, Li, & Xu, 2009) or nanoparticles (C.

Wang, Q. Yan, H.-B. Liu, X.-H. Zhou, & S.-J. Xiao, 2011). In these studies, the concentrations of EDC and NHS strongly vary in a wide range (from M to the mM range) from one study to another (Voicu et al., 2004; Wissink et al., 2001; Z. Yang et al., 2010). In one study, they used 0.1 M NHS and 0.4 M EDC in order to activate silicon surface (Voicu et al., 2004). In another study, equal amounts of EDC and NHS (100 mM) were used for activation of carboxylic acid terminated self-assembled monolayers (Ducker, Montague, & Leggett, 2008). In another study, the surface of plasma-treated PCL nanofibers were activated by using approximately 25 mM EDC and 43 mM NHS (Zander, Orlicki, Rawlett, & Beebe, 2012). Electrospun collagen or gelatin nanofibers were activated by 30 mM EDC and 6 mM of NHS (Casper, Yang, Farach-Carson, & Rabolt, 2007). Very large concentrations of EDC or NHS result the formation of the byproducts at the surface which can prevent the formation of -COOsuc surface and affect the success of the surface activation. In the case of EDC and NHS concentrations are very low, then the surface activation reaction remains incomplete (Mohamad, Marzuki, Buang, Huyop, & Wahab, 2015). Therefore, the usage of optimum EDC/NHS concentration for surface activation is critical to increase the amount of immobilized biomolecule.

The activation of the carboxyl groups on the nanofiber scaffold can be achieved in several steps. The first step is the addition of the OH group of the carboxylic acid across one of the double bonds of the carbodiimide reactant, forming an O-acylurea adduct (Z. Guler & Sarac, 2016). Then, the surface O-acylurea can be transformed into succinimidyl ester (-COOSuc) product with a nucleophilic attack by NHS. Then, this product reacts with a primary amine and yield a peptide coupling through an amide bond (Figure 1.5).

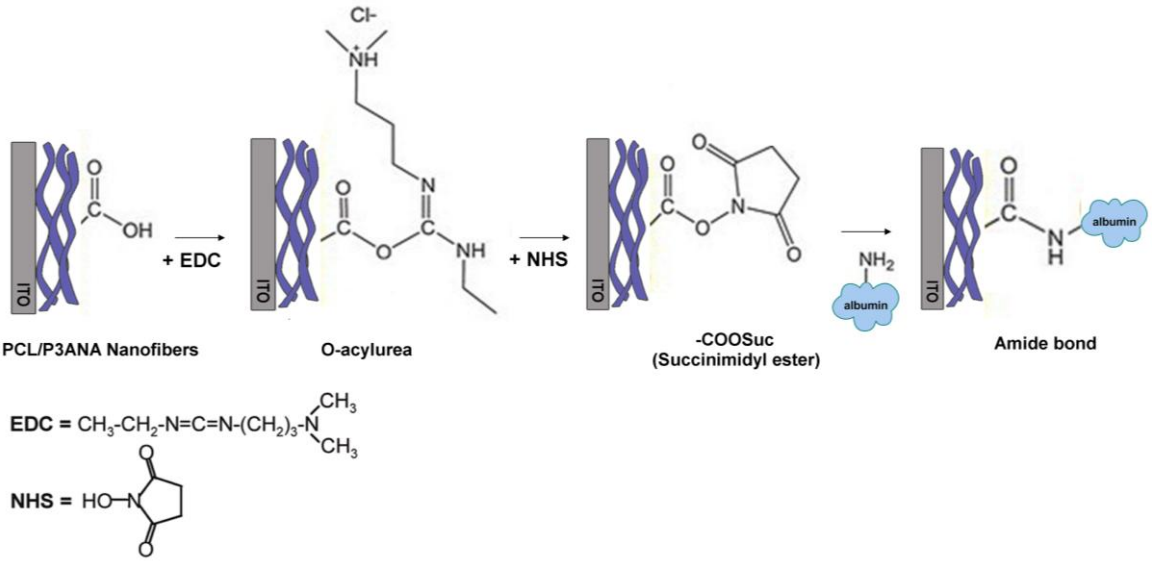

Figure 1.5 : Schematic representation of covalent immobilization of protein through EDC/NHS activation.

Growth factors provide to produce more biofunctional engineered tissues which facilitate the tissue repair at the site of injury and improve in vitro tissue growth. They enhance cellular processes such as attachment, proliferation or differentiation (Fromigue, Marie, & Lomri, 1998). Growth factors have been shown to modulate the healing response in slow-healing hard tissue such as bone by guiding the differentiation of stem cells (Volpato et al., 2012).

In bone tissue engineering, scaffolds biofunctionalized with bone-reactive growth factors tune the initial cell adhesion and growth, osteogenic differentiation (Jang et al., 2009). Growth factors for use in bone repair and regeneration such as bone morphogenetic proteins (BMPs), insulin-like growth factors (IGFs), platelet-derived growth factor (PDGF) and RGD peptide (R: arginine; G: glycine; D: aspartic acid) have the ability to induce significant bone formation (Lo, Ulery, Ashe, & Laurencin, 2012).

Among these growth factors BMP-2 and RGD peptide used for biofunctionalization of PCL/P3ANA nanofibers. Figure 1.6 represents the covalent protein (BMP-2) binding onto PCL/P3ANA nanofibers.

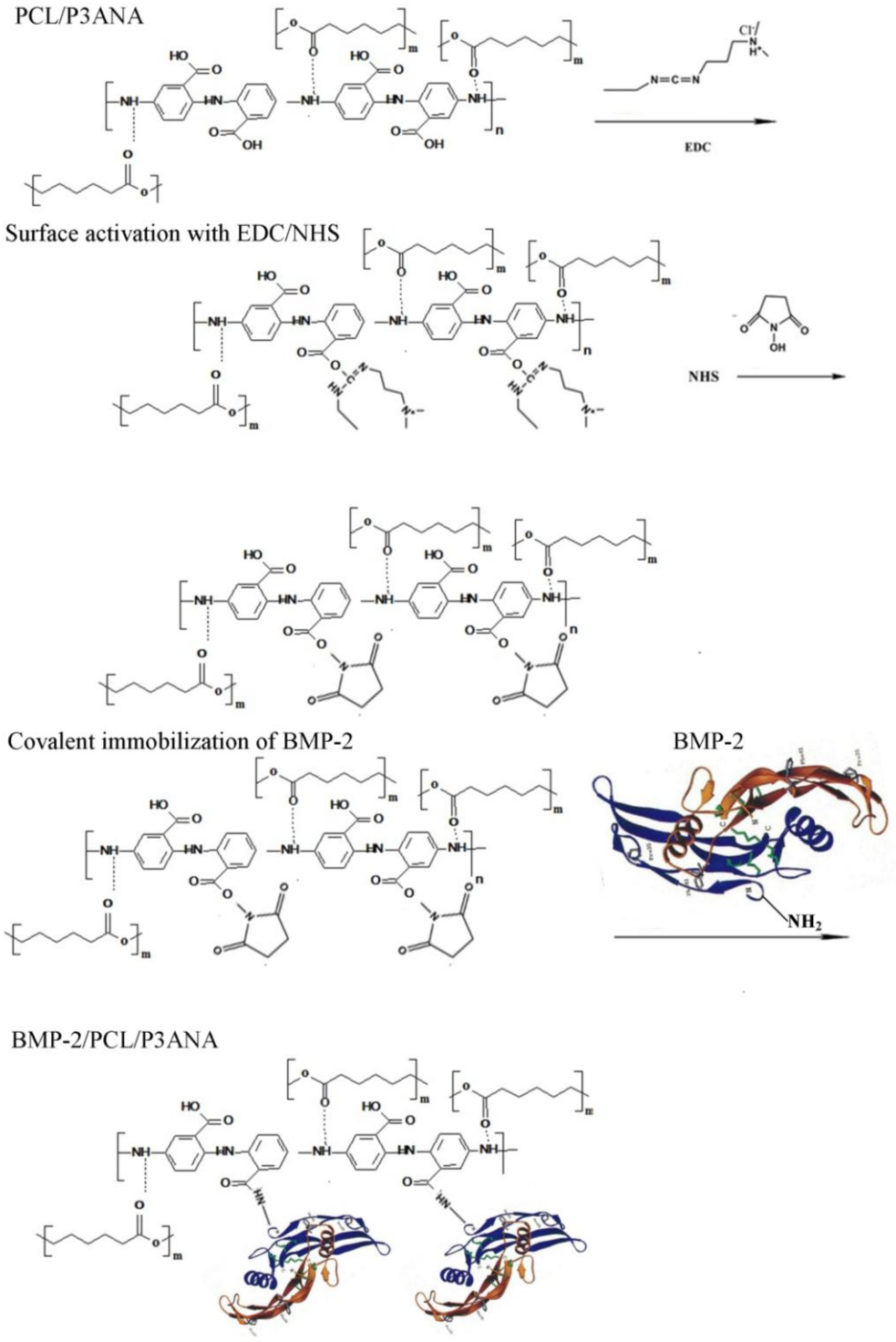

Figure 1.6 : Schematic representation of covalent immobilization of BMP-2 onto PCL/P3ANA nanofibers.

Bone morphogenetic proteins (BMPs) is a strong osteoinductive factors which have great potential to promote and enhance bone formation (Bae, Choi, Joung, Park, & Han, 2012). BMP family has over 20 members and at least 7 of them have

documented osteoinductive capacities. BMPs have been divided into separate subgroups depending on their their amino acid sequence homology. BMP-2/-4 group and the osteogenic protein-1 group (BMP-5 to -8) which both are the members of the transformation growth factor-β (TGF-β) superfamily except for BMP-1, which does not have the C-terminal sequence of the TGF-β family. BMPs found in the extracellular bone matrix and are synthesized by skeletal cells. Mesenchymal stem cells can be differentiate into the osteoblastic phenotype in vitro in the presence of BMPs (Kempen et al., 2010). BMP-2 has been immobilized onto different scaffold surfaces with either physical or chemical methods to assess the role of BMP-2 onto bone formation (L. Li et al., 2015; Prideaux et al., 2014). BMP-2 favors the osteoblastic phenotype that evidenced with increased ALP activity which is an osteoblastic marker.

The surface properties of scaffolds fabricated by synthetic polymers usually weak for supporting strong cell affinity, therefore adhesive proteins or peptides are used to improve the initial bone cell responses (Sill & von Recum, 2008). With respect to bone tissue engineering, one way to modify the surface chemically, is covalent immobilization of RGD peptide which enhances proliferation and osteoblastic differentiation of human mesenchymal stem cells (Paletta et al., 2010). RGD peptide fuctionalized scaffolds enhance cell attachement, spreading and proliferation of cells by enhancing the interactions between scaffold and cells(T. G. Kim & Park, 2006). RGD peptide accelerates and enhances the ingrowth of bone on synthetic biomaterials and even though the main role of RGD peptide is cell adhesion, it is also efficient in bone reconstruction (Beuvelot et al., 2009). Figure 1.7 represents the secondary structure of BMP-2 and RGD peptide.

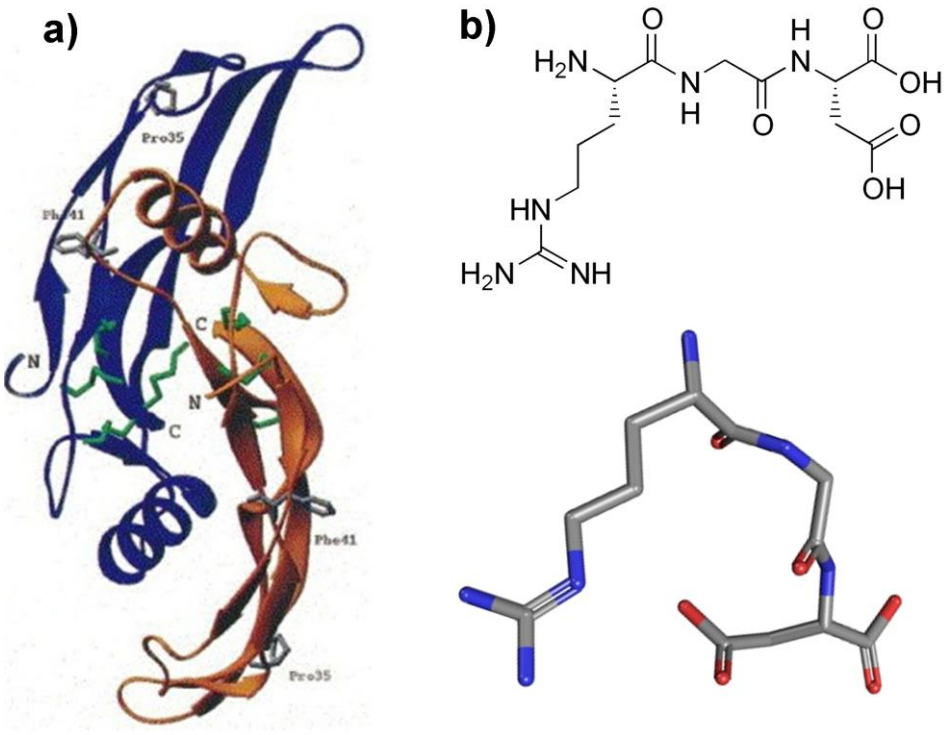

Figure 1.7 : The secondary structure of BMP-2 (a) (Scheufler, Sebald, & Hülsmeyer, 1999) and RGD peptide (b) (Balacheva et al., 2012).

1.3.2 Electrical stimulation

Controlling the functions, behaviors and differentiation of cells into assigned lineage is an ultimate goal for tissue engineering. Chemical and physical signals can provide such control over cells. Physical signals, electrical stimulation in particular, can manipulate cellular functions (Hronik-Tupaj et al., 2011). Human body generates biological electric field and current (Foulds & Barker, 1983; Zipse, 1993), which is inherent in wound healing. An endogenous electrical field (EF) is formed which guides cell migration directly toward the wound edge, after formation of a wound. The inhibition of EF results a slow wound healing process. A voltage gradient called "action potential" across cell membrane plays an important role on this process by triggering cells to transmit signals (McCaig, Rajnicek, Song, & Zhao, 2005). The cells are responsive to the exogenous electric field and their behaviours can be controlled through a manipulation of the cytoskeleton proteins using external physical stimuli such as EF (Mehedintu & Berg, 1997; Smith, McLeod, Liboff, & Cooksey, 1987). EF may serve as an efficient tool to control and to adjust cell and tissue functions such as adhesion, proliferation, differentiation, directional migration, as well as division. However, usage of this information in tissue engineering

applications is relatively more recent (Markx, 2008). The main application of electric field in tissue engineering is the formation of artificial tissues by the micromanipulation of the cells using electric fields. Usage of conducting polymers as tissue engineering scaffolds provides advantage of direct delivery of electrical signals to the cells. Conductive polymers were used to evaluate their functional and processible properties for biological purposes, especially in electrical stimulation. Electrical stimulation increases the adsorption of serum proteins on electrically conducting polymers for more favorable cellular interactions (Nisbet et al., 2008). When cultured on a conductive polymer containing scaffolds cells get the electrical signal from the scaffold rather than from the culture medium (Meng, Rouabhia, & Zhang, 2011). To date, mesenchymal stem cells, bone and cartilage cells, neuronal cells, and cardiac cells which are electrically responsive cells, have been used to study their responses to ES. To manipulate cell functions, DC or AC electric fields can be used. When a DC electric field is applied to cell suspension, cells can move by electrophoresis and their attachement can be controlled (Ozkan et al., 2003). However, the electric field that is needed to electrophorese cells is quite large and it elicits very high electric fields across the cell membrane, which can adversely affect cell viability. Also, it can cause heating problem near the electrodes (Markx, 2008). Due to these disadvantages, AC electric field is preferable over DC electrical fields. AC electric fields are dominated by dipole effects depending on the applied frequency. At high frequencies (MHz range) cell dipoles are dominantly formed by interfacial polarization effects at the cell membrane which has a much lower dielectric constant and much less conductivity than the culture medium and the cytoplasm. Therefore, charge accumulation occurs at the cell membrane and causing a large dipole moment in an externally applied electric field in this frequency range. The interaction between the dipole induced by the electric field and the electric field itself can lead to a variety of effects (Markx & Davey, 1999).

Cellular activities are regulated by distribution of soluble ions through membrane proteins, such as ion channels, pumps and transporters, which are sensitive to electrical field stimulations. These membrane proteins referred to as voltage-sensing proteins, sense and use the external electric field to regulate cellular functions. Cell membrane surface is negatively charged due to the predominance of negatively charged chemical groups in membrane proteins and glycans. Cell membrane has an

electrical potential gradient in the order of -100 mV which is stem from uneven distribution of ions on both sides of the membrane (Bezanilla, 2008). The potential difference, in the order of 100 mV between the two sides of the membrane, plays an important role in signal transduction processes (Aaron, Boyan, Ciombor, Schwartz, & Simon, 2004). Electrical field also affects the functions of gap junctions which enable efficient propagation of ions, nutrients, metabolites and small molecules under ~ 1,000 Da between adjoining cells (Stains & Civitelli, 2005). EF induces the movement of proteins and soluble ions towards the binding sites on cell membrane (Adey, 1993). Electrical field can change the density and distribution of receptors through polarizing membrane components, moving receptors, or alternating receptor conformation (Orr, Helmke, Blackman, & Schwartz, 2006). In bone tissue engineering, it is found that electrical field can increase the gene expression of TGF-β, collagen type-I, alkaline phosphatase (ALP) and bone morphogenetic proteins (BMPs) in osteoblastic cells (Meng, Zhang, & Rouabhia, 2011). The increased level of TGF-β in osteoblastic cells after electrical stimulation was associated with a mechanism involving calcium/calmodulin pathway (Zhuang et al., 1997). The calcium ion channel on the cell surface can detect the membrane potential and opens the channels and cause a change in cellular calcium ion concentration (Min et al., 2014). The previous studies showed that EF induced an increase in cytosolic Ca2+ via voltage-gated calcium channels, resulting in activated calmodulin, as well as an increase in TGF-β1 mRNA (Zhuang et al., 1997). In other study, it was found that electrical stimulation increased the calcium deposition which is an important indication of osteogenesis of bone-associated cells (Siggelkow et al., 2002).

Cell responses to electric stimulation differ depending on the cell type. In order to stimulate cells and control their behaviours, electrical stimulation parameters such as intensity, duration and frequency should be optimize depending on the cell type. The choice of the appropriate cell type is also a critical parameter in tissue engineering applications.

1.3.3 Cells

Bone tissue engineering offers a new and promising approach for bone repair and regeneration. Bone tissue engineering applications involve the use of scaffolding materials in combination with biological cues and cells (Ehrbar, Lütolf, Rizzi,

Hubbell, & Weber, 2008). The choices of cell type and source are important parameters to restore lost tissue and functions. An ideal cell source should be easily expandable to higher passages, non-immunogeneic and have a protein expression pattern similar to the tissue to be regenerated. The isolated cells from patients biopsies can be considered as a good choice due to their nonimmunogenicity. However, this a time consuming process which provides limiting the number of cells with low expansion rate. (Salgado, Coutinho, & Reis, 2004). Because of these limitations, the usage of stem cells emerge as a promising solution for tissue engineering applications. Stem cells are undifferentiated cells that have the capacity both to self-renew and to differentiate into one or more types of specialized cells including differentiated cells (Blau, Brazelton, & Weimann, 2001; Mezey, Chandross, Harta, Maki, & McKercher, 2000). The sources of stem cells for tissue engineering include embryos and adult donors (Vats, Tolley, Bishop, & Polak, 2005). Embryonic stem cells (ESCs) are commonly derived from the inner cell mass of a blastocyst, an early (4–5 days) stage of the embryo. They can differentiate into every cell lineage and eventually develop into every tissue and organ, including bone marrow, peripheral blood, umbilical cord, and adipose tissue. However, the use of human embryos and ESCs for research purposes remains a major ethical issue. Besides, the long-term biological consequence of ESCs at the implant site, as well as issues of cell plasticity, remains largely unknown (Heliotis et al., 2009). On the other hand, adult stem cells (ASCs) are much easier to obtain from bone marrow or other tissues, such as adipose tissue and dental pulp. ASCs are found in tissues after birth and have been found to differentiate into a narrower range of cell types, primarily those phenotypes found in the originating tissue (Ahsan, Doyle, & Nerem, 2009). Under appropriate conditions, they have the potential to develop into various cell phenotypes such as osteoblasts . Hematopoietic stem cells (HSCs) and mesenchymal stem cells (MSCs) are two groups of adult stem cells. MSCs found in adult bone morrow and contribute to the regeneration of mesenchymal tissues, such as bone, cartilage, muscle, ligament, tendon, adipose, and stroma (Haynesworth, Goshima, Goldberg, & Caplan, 1992). Figure 1.8 represents the classification of stem cells. MSCs can differentiate into osteoblasts, chondrocytes, adipocytes and other myocytes like cardiac muscle cells. Therefore, MSCs are widely used in bone tissue engineering applications.

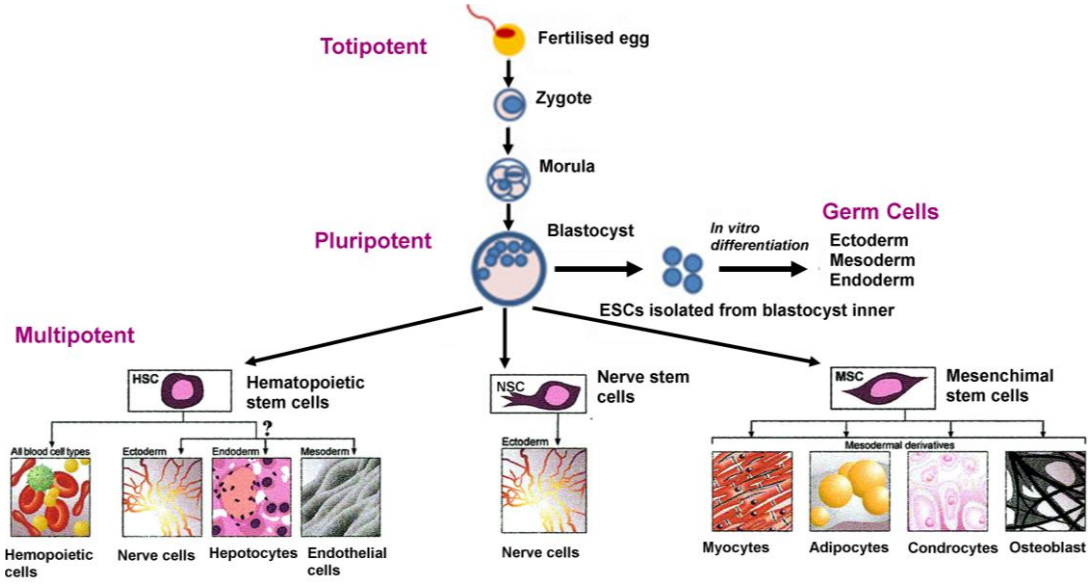

Figure 1.8 : Schematic representation of stem cell types.

Stem cell functions such as self-renewal or differentiation depend on the culture microenvironment. They are responsive to biochemical and physical cues (Haider, Gupta, & Kang, 2014; Hwang, Varghese, Zhang, & Elisseeff, 2006). MSCs cultured on scaffolds with different properties can display different behaviors in terms of cell proliferation and phenotype expression (Gigante et al., 2008). Under stimulation, MSCs undergo osteogenic differentiation, acquiring osteoblastic markers and secreting extracellular matrix and calcium crystals (Jang et al., 2009; Pittenger et al., 1999). The differentiation of stem cells into into osteoblasts and other phenotypes can be promoted by electrical stimulation (Meng, Rouabhia, et al., 2011). Therefore, bone morrow mesenchymal stem cells (BMSCs) are good candites for investigation of effects of electrical stimulation on the differentiation of BMSCs into osteogenic fate (Engler, Sen, Sweeney, & Discher, 2006{Yow, 2011 #108).

Stem cells have some drawbacks (Vats et al., 2005), such as being difficult to obtain and liimited continuous culture, immortalized cell lines instead of stem cells are also used in tissue engineering applications. They are easier to procure and maintain, better characterized, and less prone to phenotypic drift than their primary cell counterparts. However, a suitable immortalized cell line must be chosen considering their behaviors may change along with the desired immortality (Kilpadi, Sawyer, Prince, Chang, & Bellis, 2004). Saos-2 osteosarcoma cell line possesses several osteoblastic features. Osteoblasts, which are active in bone development and bone remodelling as bone-forming cells, have the ability to synthesize and secrete collagen

type I and glycoproteins (osteopontin, osteocalcin), cytokines, and growth factors into the unmineralized matrix (osteoid) between cell body and mineralized regions (Kartsogiannis & Ng, 2004). Saos-2 cells can be used in bone tissue engineering to model behaviors of osteoblast-like cells such as attachment, spreading, proliferation, and differentiation in response to various bone-compatible biomaterials and surface treatments (Degasne et al., 1999; Mayr-Wohlfart, Fiedler, Günther, Puhl, & Kessler, 2001). Saos-2 cell have been used as a model in a large number of studies on osteoblasts growth and mineralization (Beuvelot et al., 2009; J. Y. Lim et al., 2008; Manjubala, Ponomarev, Wilke, & Jandt, 2008; Sofia, McCarthy, Gronowicz, & Kaplan, 2001). Microenviromental conditions induce the differentiation of Saos-2 cells into osteoblastic lineage in culture, and, favor their mineralization. When they stimulated with chemical cues, Saos-2 cells synthesize mineral deposits and express the key bone enzyme, alkaline phosphatase; the cytokine, bone morphogenetic protein 2 (BMP-2); and the major extracellular fibrillar structural molecule, collagen type I (Müller et al., 2011; X. Wang et al., 2014).

2. MATERIALS AND METHODS

2.1 Materials

Poly(ε-caprolactone) (Mw = 80000 g/mol), 3-aminobenzoic acid (m-anthranilic acid), albumin (M w ~ 66 kDa), N-(3-dimethy-laminopropyl)-N'-ethylcarbodiimide hydrochloride (EDC), N-hydroxysuccinimide (NHS), 2-morpholinoethane sulfonic acid (MES, low moisture content, ≥99), bone morphogenetic protein-2 (BMP-2), RGD peptide, *in vitro* toxicology assay kit [3-(4,5- dimethyl-2-thiazolyl)-2,5-diphenyltetrazolium bromide-MTT], the bicinchoninic acid (BCA) Protein Quantitation Kit, McCoy's 5A medium and Naphthol AS-MX Phosphate were purchased from Sigma Aldrich (St Louis, MO, USA). StemPro human Bone marrow mesenchymal stem cells (BMSCs) (A15652) and phosphate buffer saline (PBS) were obtained from Gibco Gibco (Carlsbad, CA). Resazurin sodium salt and Alizarin red S sodium salt were purchased from Alfa Aesar (Germany). Fetal bovine serum (FBS), penicillin/streptomycin and DAPI (40,6-diamidino-phenyindol) were purchased from Life Technologies (USA). Acti-stain™ 555 Fluorescent Phalloidin fluorescence dye was purchased from Cytoskeleton, Inc. (USA). Saos2 osteoblast-like cell line was purchased from ATCC (HTB 85). Dimethyl formamide (DMF Analytical Grade) and Tetrahydrofurane (THF Analytical Grade) (109731) were supplied from Merck (Darmstadt, Germany).

2.2 Synthesis of Poly(m-anthranilic acid)

3-aminobenzoic acid (0.043 mol) has been dissolved in 90 mL of 0.5 M NaOH. Equal mole of ammonium persulfate in water (30 mL) has been added drop wise to this solution and the mixture stirred at room temperature for 24 h. The precipitated polymer collected by filtration, washed with 1.2 M HCl and water until the filtrate became colourless and dried in vacuum at 60°C for two days. This polymer recovered in 70% yield as a brown powder. Molecular weight of the polymer was measured by GPC and found 7028 g/mol.

2.3 Characterization of Poly(m-anthranilic acid)

The synthesized P3ANA was characterized FTIR-ATR spectrophotometer (Spectrum One, with a universal ATR attachment with a diamond and a ZnSe crystal) (Perkin Elmer, Massachusetts, USA). All FTIR-ATR spectra were collected with 12 scans in the 600–4000 cm^{-1} spectral region at 4 cm^{-1} resolution. The effect of the P3ANA on the PCL/P3ANA nanofibers were also characterized by UV–Visible (Perkin Elmer, Lambda 45) spectrophotometry**.**

2.4 Fabrication of Poly(m-anthranilic acid)/ Poly(ε-caprolactone) Nanofibers

Poly(m-anthranilic acid) in increasing amounts were dissolved in THF and DMF mixture (1/1 v/v) containing poly(ε-caprolactone). The obtained polymer blends were stirred for 3 h at room temperature to obtain homogeneous solution for optimum electrospinning conditions. The PCL/P3ANA electrospinning solutions contects are shown in Table 2.1.

Table 2.1 : Contents of PCL/P3NANA electrospinning solutions.

PCL amount (g)	P3ANA amount (g)	Sample code
0.5	-	PCL
0.5	0.050	PCL/P3ANA(10)
0.5	0.075	PCL/P3ANA(15)
0.5	0.100	PCL/P3ANA(20)
0.5	0.125	PCL/P3ANA(25)

Electrospinning solutions were placed inside a plastic syringe with a blunt needle (23 gauge) connected to a high-voltage direct current (DC) power supply (ES 30 Model Gamma High Voltage Inc., Florida, USA). The PCL/P3ANA nanofibers were obtained onto round cover glasses with 12 mm diameter and ITO-PET (NV Innovative Sputtering Technology, Zulte, Belgium, PET 175 lm, Coating ITO-60) substrate with dimensions of 0.5x2.5 mm for cell culture studies and electrochemical measurments, respectively. Electrospun fibers were obtained at 15 kV driving voltage at a collection distance of 15 cm and the flow rate of 1 mL/h which was controlled by a syringe pump (NE-500 Model, New Era Pump Systems, Inc. New York, USA).

2.5 Characterization of Poly(m-anthranilic acid)/ Poly(ε-caprolactone) Nanofibers

2.5.1 Spectroscopic characterization of PCL/P3ANA nanofibers

The structure of PCL/P3ANA nanofibers which contains increasing amounts of P3ANA was determined by FTIR-ATR spectrophotometer (Spectrum One, with a universal ATR attachment with a diamond and a ZnSe crystal) (Perkin Elmer, Massachusetts, USA). All FTIR-ATR spectra were collected with 12 scans in the 600–4000 cm^{-1} spectral region at 4 cm^{-1} resolution. The effect of the P3ANA on the PCL/P3ANA nanofibers were also characterized by UV–Visible (Perkin Elmer, Lambda 45) spectrophotometry**.**

2.5.2 Morphological characterization of PCL/P3ANA nanofibers

The morhological properties of PCL/P3ANA nanaofibers were determined by scanning electron microscopy (SEM) (QUANTA 400 F) (FEI, Oregon, USA) and Atomic force microscopy (AFM) (Nanosurf EasyScan2). SEM analyses were performed with 10kV accelerating voltage after nanofiber mats were coated with gold by Ion Sputter Metal Coating Device (MCM-100 Model). The average nanofiber diameters were determined using Image J by randomly measuring the diameters of 20 individual fibers shown in SEM images with 3 μm magnification. AFM images were taken in non-contact mode using Al coated high resonance frequency silicon tips Nanosensors NCRL tips (40 μm width, 225 μm length). Root-mean-square (RMS) roughness values of nanofibers were calculated *via* Easy Scan 2 Software™ (version 3.0.2.4) by selecting raw data**.**

2.5.3 Characterization of surface properties of PCL/P3ANA nanofibers

The surface area of nanofibers was determined through the Brunauer–Emett–Teller (BET) surface area from nitrogen physical adsorption-desorption isotherms at 77 K obtained with the ASAP2420 M instrument (Micromeritics, USA). Before the analysis, all samples were dried at 50 °C at least for 12h in vacuo (1 Pa).

2.5.4 Mechanical characterization of PCL/P3ANA nanofibers

Mechanical properties of PCL/P3ANA nanofibers were determined by Dynamic Mechanical Analyser (DMA) (TA Q800 Dynamic Mechanical Analyser). The tensile properties of each nanofiber mat were determined. The scaffolds were cut into rectangular strips and the thicknesses of the mats were measured at 3 different positions and the average thickness was taken to calculate the cross sectional area of the specimen. Each mat was loaded into the tensile testing fixture of a dynamic mechanical analyzer and subjected to a load of 18N in the ramp force mode and a ramp force of 0.1 N/min was applied. The stress - strain curve was generated and the Young modulus was determined from the initial 10% strain at the linear regime for each specimen. The Young's modulus, toughness, ultimate strength and ultimate strain were determined trough stress-strain curve. The Young's modulus of nanofibers was determined from the initial slope of the linear region of stress-strain curve (Phipps et al., 2011). The toughness of was measured from the area under the stress–strain curve (Ma, Xie, Jiang, Shuler, & Bartlett, 2013).

2.5.5 Electrochemical impedance spectroscopic characterization of PCL/P3ANA nanofibers

EIS measurements were performed by using potentiostat 2263 Electrochemical Analyser (Princeton Applied Research, Tennessee, USA) in PBS (0.1 M, pH 7.4) with frequency range between 0.01 Hz and 100 kHz and AC voltage of 10 mV. Three-electrode system, consisting of nanofiber mats on ITO-PET as working electrode, platinum wire as counter electrode, and silver wire as pseudo reference electrode, was used. The pseudo-reference was calibrated externally using a 5 mM ferrocene solution in the electrolyte ($E_{1/2}$ (Fc / Fc^{+}) = +0.51 V vs. silver wire in 0.1 M $NaClO_4$ / ACN). All measurements were repeated three times for confirmation. The measured impedance spectra were analyzed in terms of electrical equivalent circuits using the analysis program ZSimpWin V.3.10 (Princeton Applied Research, Tennessee, USA**).**

2.6 Optimization of Biofunctionalization of PCL/P3ANA nanofibers with covalent protein immobilization

Bioactivation of the nanofibers was achieved with the reaction between amino (–NH_2) group on the proteins and (–COOSuc)-terminated surface of the nanofibers. This was formed through the carboxyl group (–COOH) of P3ANA on the nanofibers by using (EDC)/ (NHS) activation. In order to optimize the biofunctionalization process, the -COOH groups available on the surface of the PCL/P3ANA nanofiber mat, the appropriate concentrations (5/0.5, 0.5/5, 5/5 and 50/50 mM) of EDC and NHS solutions were prepared with cold water. In order to investigate the influence of EDC and NHS concentrations during activation of carboxyl -COOH groups in nanofibers, PCL/P3ANA nanofiber mats on ITO-PET substrates were treated by shaken gently with 5 mL of the EDC/NHS solutions for 2h at room temperature [24]. Activated mats were then washed twice with water. Activated mats were treated with 1 mL of albumin dissolved in MES buffer (pH 5.7) with the concentration of 2 mg/mL. Albumin was selected as model protein to covalently immobilizee to the activated nanofibers, due to its low price and availability in large amounts. Nanofiber mats were incubated with albumin for 2h at +4°C, being shaken gently. Finally, mats were taken out, washed twice again with water and dried for characterization. Initial albumin solutions as well as the residual solutions of each consecutive washing step were collected for further characterization.

2.6.1 Spectroscopic and morphological quantification of protein amount on the nanofiber mats

The activation of carboxylic acid groups on PCL/P3ANA nanofibers and the gradual change in the amount of immobilized protein depending on the EDC and NHS concentrations in the activation procedure was determined by FTIR-ATR spectrophotometer. The surface activation yield were estimated by calculation of the FTIR peak ratios of the formed succinimidyl ester and O-H stretching of carboxylic acid group by using Beer-Lambert law (C. Wang, Q. Yan, H. B. Liu, X. H. Zhou, & S. J. Xiao, 2011). SEM/EDX analyses were performed before and after albumin immobilization. The influence of EDC and NHS concentrations on the structure and composition of the albumin immobilized PCL/P3ANA nanofibers were analyzed by detection of elemental concentrations for nitrogen and oxygen with EDX. The

distribution of immobilized albumin on the surface of nanofiber mats was examined by EDX-mapping. The amount of immobilized albumin on the activated nanofiber mats was determined by BCA protein assay by subjecting the initial and residual solutions from albumin immobilization. As a control, albumin immobilization was carried out on non-activated PCL/P3ANA nanofibers under the same experimental conditions. The total protein content in each sample was calculated by comparing the means of absorption values with a standard curve of bovine serum dilutions (between 0 and 2mg/mL). The samples were incubated with BCA working solution at 37°C for 30 minutes and the absorbance was followed at 562 nm by UV-Vis spectrophotometer (Lambda 45) (Perkin Elmer, Massachusetts, USA) (Ficen et al., 2013). AFM images of PCL/P3ANA and albumin immobilized nanofibers after activation with 5/0.5, 0.5/5, 5/5 and 50/50 mM of EDC and NHS, were taken in non-contact mode and Root-mean-square (RMS) roughness values of nanofibers were calculated *via* Easy Scan 2 Software™ (version 3.0.2.4) by selecting raw data.

2.6.2 Electrochemical impedance spectroscopic measurements of albumin immobilized nanofibers

The effect of the concentrations of the EDC and NHS reactants on the activation reaction and on the amount of immobilized protein was investigated by Electrochemical Impedance Spectroscopy (EIS). EIS measurements were performed in PBS (0.1 M, pH 7.4) using potentiostat 2263 Electrochemical Analyser (Princeton Applied Research, Tennessee, USA) with frequency range between 0.01 Hz and 100 kHz and AC voltage of 10 mV. Three-electrode system, consisting of nanofiber mats after albumin immobilization as working electrode, platinum wire as counter electrode, and silver wire as pseudo reference electrode, was used. All measurements were repeated three times for confirmation. The measured impedance spectra were analyzed in terms of electrical equivalent circuits using the analysis program ZSimpWin V.3.10 (Princeton Applied Research, Tennessee, USA).

2.7 Biofunctionalization of PCL/P3ANA nanofibers with BMP-2 and RGD peptid

PCL/P3ANA nanofibers were biofunctionalized with either BMP-2 or RGD peptide by the activation of the carboxyl groups (–COOH) available on the surface of the nanofiber mats. Nanofibers were activated with EDC and NHS (50/50 mM) solution. PCL/P3ANA nanofiber mats were treated by shaking gently with 5 mL of the EDC/NHS solution prepared in cold water for 2 h at room temperature (Z. Guler & Sarac, 2016). Activated mats were then washed twice with water. Then, nanofiber mats were treated with 1 mL of BMP-2 (50 ng/mL) or 1 mL of RGD peptide (5µg/mL) dissolved in MES buffer (pH 5.7) for 2h at +4°C, being shaken gently. Finally, mats were taken out, washed twice again with water and dried for characterization. BMP-2 immobilized nanofibers were coded as PCL/P3ANA/BMP-2. Initial BMP-2 solution as well as the residual solutions of each consecutive washing step was collected for further characterization.

2.7.1 Characterization of BMP-2/PCL/P3ANA and PCL/P3ANA-RGD nanofibers

The structures of PCL/P3ANA/BMP-2 and PCL/P3ANA-RGD nanofibers were determined by ATR-FTIR spectrophotometer. The immobilization of proteins onto nanofibers was examined with Electrochemical Impedance Spectroscopy (EIS). The amounts of covalently bound BMP-2 or RGD peptide onto nanofibers were determined by BCA protein assay by subjecting the initial and residual solutions from protein immobilization. As a control, BMP-2 immobilization was carried out on non-activated PCL/P3ANA nanofibers under the same experimental conditions. After BMP-2 immobilization SEM/EDX analyses were performed and the elemental concentrations for nitrogen and oxygen atoms after BMP-2 immobilization and the distribution of immobilized BMP-2 onto PCL/P3ANA nanofibers were determined by EDX-mapping. Contact angle measurements were performed at room temperature using a CAM101 The surface properties and hydrophilicity of PCL/P3ANA/BMP-2 and PCL/P3ANA-RGD nanofibers were investigated by the contact angle measurements which were performed at room temperature using a CAM101 Optical

Contact Angle and Surface Tension Meter from KSV Instruments (Helsinki, Finland).

2.8 Cell culture studies on BMP-2/PCL/P3ANA and RGD/PCL/P3ANA nanofibers

2.8.1 Cell culture

The effects of immobilized BMP-2 and RGD peptide on cell behaviour were investigated by using a human osteosarcoma cell line (Saos-2). Saos-2 cells were used as an *in vitro* model since they can differentiate into osteocyte-like cells under mineralizing conditions (Prideaux et al., 2014). The nanofibers on cover glasses were placed inside teflon cups of 8 mm inner diameter. Nanofibers were sterilized with 70% ethanol, washed several times with PBS and washed once with culture medium. Nanofiber mats in teflon cups were then placed in 24-well culture plates. Saos-2 cells were seeded onto nanofibers at a density of 2 x 10^4 cells/cm^2 and maintained with McCoy's 5A, supplemented with 10 % FBS and penicillin/streptomycin, at 37 °C with 5% CO_2 in a humidified environment. Each experimental condition had 3 samples and was repeated 3 times.

2.8.2 Cytotoxicity of nanofibers

The viability of the Saos-2 cells on electrospun PCL/P3ANA and PCL/P3ANA/BMP-2 or PCL/P3ANA-RGD nanofibers was investigated by *in vitro* MTT toxicity assay. Cells cultured on the tissue culture plate were used as reference. At day 1 of culture, cells were washed with PBS, and 100 µl 0.3mg/ml MTT solution in culture medium was added to each well. Cells were incubated for 4 h in 5% CO_2 incubator at 37ºC. Then, MTT-containing medium was removed and 100 µl of MTT solubilization solution was added to dissolve the purple coloured formazan crystals. Absorbance was measured at 570 nm by NanoDrop Spectrometer (NanoDrop Technologies, Wilmington, DE, USA) (Polat, Güler, Balkan, & Sarac, 2016).

2.8.3 Cell proliferation

Cell proliferation was determined via resazurin reduction assay. Proliferation of Saos-2 cells on nanofiber mats was assessed by resazurin dye (7-hydroxy-3H-

phenoxazin-3-one 10-oxide) after 9 days of culture by reading absorbance of resazurin (600 nm) and its reduced form, resorufin (570 nm) (Borra, Lotufo, Gagioti, Barros Fde, & Andrade, 2009). The reduction of resazurin to resorufin correlates with the number of live organisms. The absorbance was measured using a microplate reader (Biotek ELX800UV). Proliferation of cells was monitored with scanning electron microscope (SEM) after 9 days culture.

2.8.4 Immunofluorescence staining

At day 3 of culture, supernatants were removed and cells on nanofiber mats were washed with PBS and fixed with 4 % paraformaldehyde (PFA) for 15 min at room temperature. Fixed cells were permeabilized with buffer (5% Triton X-100 in PBS) and stained for F-actin using Acti-Stain 555 Phalloidin for 30 min in the dark at room temperature, followed by DAPI for 2.5 min as a nuclear counterstain. After washing with PBS, the stained cells on nanofiber mats were imaged using a fluorescence microscope (Nikon Eclipse Ti).

2.8.5 Alkaline phosphatase activity

Alkaline phosphotase (ALP) activity of Saos-2 cells was determined after 9 days of culture in order to investigate the osteoblastic phenotype of cells. Cells were fixed with 4% paraformaldehyde and washed with PBS three times. Fixed cells were treated with ice cold acetone for 5 minute and incubated with ALP working solution (Tris buffer-pH 8.74, distilled water and naphthol AS-MX phosphate/DMF solution) for 15 min. Cells were washed with PBS and ALP positive cells were visualized as pink with an optical microscope

2.8.6 Mineralization Assay

The mineralization and calcium deposits on Saos-2 cells were assessed by staining with alizarin red S after 9 days of culture. Cell were fixed with 4% PFA and washed with PBS. Fixed cells were treated with 1% alizarin red solution (pH 4.2) for 3 min at room temperature and observed with an optical microscope.

2.9 Electrical stimulation of BMSCs on PCL/P3ANA nanofibers

Capacitive coupled method in which there is no current passing between the electrodes. was used for stimulating the cells. The capacitive coupled stimulation is similar to a capacitor which contains two electrodes bearing opposite charges and the electric field is between the electrodes. The electrical field effect on to the differentiation of BMSCs into bone feature was studied by using a cell culture electrical stimulation setup which was built in-house. The cover lid of a 24-well culture plate was removed and slits of size 0.3 mm on the lid were drilled. Rectangular platinum (Pt) strips with dimensions 3 mm × 0.1 mm × 4 mm were placed through the slits. The cover plate with the Pt strips was checked with a multimeter to make sure that the Pt strips were firmly in place with no gaps between the strips and the slits. Pt wires were used to connect the Pt strips with opposite charges in parallel to each other and in series to the wells. The setup checked with the signal generator and a multimeter to make sure there were no loose or disconnected wires and Pt strips. Figure 2.1 shows the schematic representation and of the electrical stimulation setup. The cover lid was sterilized by soaking in 70% ethanol overnight and left to dry in a biosafety cabinet before use. The modified 24-well culture plate was connected to the function generator (AWG1000 Series Function Waveform Generator) and stimulated in the cell culture incubator (Şekil 2.1-b). In order to stimulate cell electrically, BMSCs were seeded onto PCL/P3ANA nanofibers at a density of 2 x 10^4 cells/cm^2 and maintained with alpha-MEM with L-Glutamine (Gibco, 41061037), supplemented with 10 % FBS and penicillin/streptomycin, at 37 °C with 5% CO_2 in a humidified environment. Each experimental condition had 3 samples and was repeated 3 times. Eletrical stimulation was applied to the cells on 48-hour culture, for 4 h with the electric field (voltage difference per unit distance) of 200 mV/mm, 400 mV/mm and 800 mV/mm at frequency of 0.5 kHz, 1 kHz, 5 kHz and 10 kHz. The cells grown without any applied voltage was used as a control. The effect of applied voltage and frequency on to the viability of cells and proliferation was determined. The osteogenic activity of cells under electrical stimulation was determined by staining for ALP and Ca deposits.

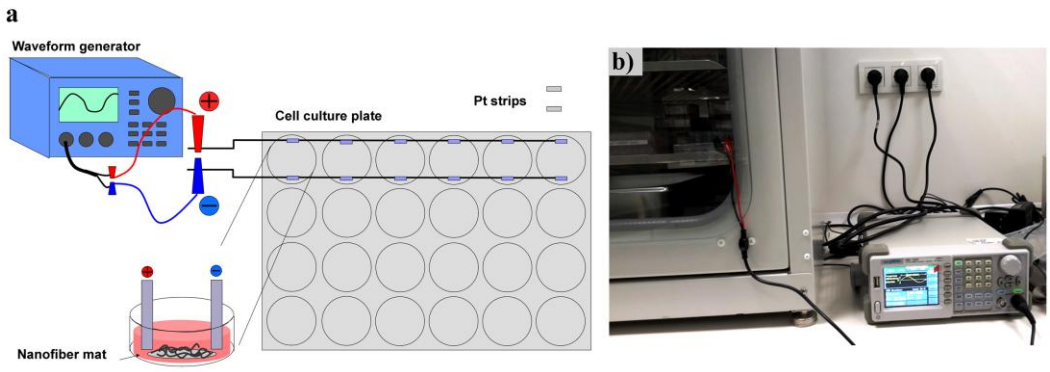

Figure 2.1 : Schematic representation of electrical stimulation setup (a). Electical stiumaltion of cell cultured in the cell culture incubator (b).

2.9.1 Cell viability after electrical stimulation

The viability of the BMSCs on PCL/P3ANA nanofibers was investigated by *in vitro* MTT toxicity assay after culturing cells 2 days and applying electrical stimulation on the third day. Cells cultured on the nanofibers without electrical stimulation were used as reference. Cells were washed with PBS, and 100 µl 0.3mg/ml MTT solution in culture medium was added to each well. Cells were incubated for 4 h in 5% CO_2 incubator at 37ºC. Then, MTT-containing medium was removed and 100 µl of MTT solubilization solution was added to dissolve the purple coloured formazan crystals. Absorbance was measured at 570 nm by NanoDrop Spectrometer (NanoDrop Technologies, Wilmington, DE, USA) (Polat et al., 2016).

2.9.2 The effect of electrical stimulation on cell proliferation

Cell proliferation was determined via resazurin reduction assay. The effect of electical stimulation on to the proliferation of BMSCs was assessed by resazurin dye after appliying AC current. The absorbance of resazurin (600 nm) and its reduced form, resorufin (570 nm) was measured (Borra et al., 2009) using a microplate reader (Biotek ELX800UV).

2.9.3 Morphology of the BMSCs after electrical stimulation

The spreading, proliferation and morphology of the cells were investigated by SEM and fluorescence staining at culture day 14. For fluorescence staining mediums were removed and cells on nanofiber mats were washed with PBS and fixed with 4 % paraformaldehyde (PFA) for 15 min at room temperature. Fixed cells were permeabilized with buffer (5% Triton X-100 in PBS) and stained for F-actin using

Acti-Stain 555 Phalloidin for 30 min in the dark at room temperature, followed by DAPI for 2.5 min as a nuclear counterstain. After washing with PBS, the stained cells on nanofiber mats were imaged using a fluorescence microscope (Nikon Eclipse Ti).

2.9.4 The effect of electrical stimulation on alkaline phosphatase activity

Alkaline phosphotase (ALP) activity of BMSCs was determined after applying AC current for 9 days. Cells were fixed with 4% paraformaldehyde and washed with PBS three times. Fixed cells were treated with ice cold acetone for 5 minute and incubated with ALP working solution (Tris buffer-pH 8.74, distilled water and naphthol AS-MX phosphate/DMF solution) for 15 min. Cells were washed with PBS and ALP positive cells were visualized as pink with an optical microscope.

2.9.5 The effect of electrical stimulation on mineralization assay

The mineralization and calcium deposits on BMSCs were assessed by staining with alizarin red S after applying AC current for 9 days. Cell were fixed with 4% PFA and washed with PBS. Fixed cells were treated with 1% alizarin red solution (pH 4.2) for 3 min at room temperature and observed with an optical microscope.

2.10 Statistical analysis

The results are expressed as average ± standard deviation (SD) (n= 3). Statistical comparisons were performed by using Student's t-test. The statistical significance was considered at *$p<0.05$ and **$p<0.01$.

3. RESULTS AND DISCUSSION

3.1 Characterization of Poly(m-anthranilic acid)

Synthesized P3ANA were characterized by FTIR-ATR spectrotometer and UV-vis spectrophotometer. The characteristic peaks of P3ANA were represented on the FTIR-ATR spectrum (Figure 3.1). P3ANA have wide band between 3750 and 1800 cm^{-1} , and also the peaks 3200 cm^{-1} and 3034 cm^{-1} are attributed to O-H stretching and C-H stretching of P3ANA. The peaks at 1690 cm^{-1}, 1570 cm^{-1}, 1507 cm^{-1}, 1251 cm^{-1} and 1103 cm^{-1} were assigned to C=O stretching, C=C stretching, N-H stretching and C-N stretching, respectively. The out of plane C-N stretching peaks of P3ANA were observed at 821 cm^{-1} , 753 cm^{-1} , 679 cm^{-1} (Dash, Tripathy, Sasmal, Mohanty, & Nayak, 2010; Patra & Munichandraiah, 2005).

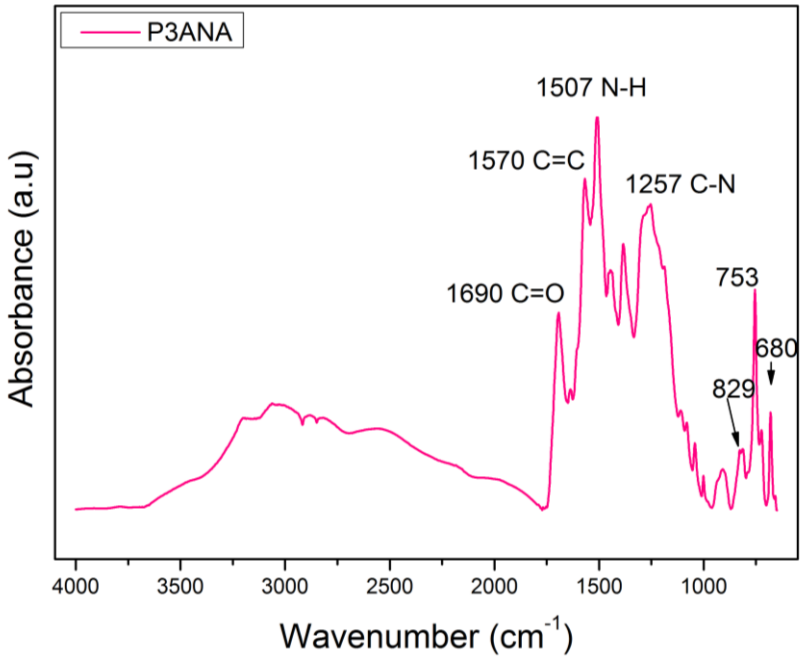

Figure 3.1 : FTIR-ATR spectrum of synthesized P3ANA.

Figure 3.2 shows the UV-vis spectrum of synthesized P3ANA. UV-vis spectra shows the characteristic peaks for P3ANA. The absorption at 340–380 nm, corresponding

to p – p * transition in benzene ring of poly(m-anthranilic acid). The broad absorption band extended from 480 nm to 600 nm due to the existence of polaron bands (Giray et al., 2013).

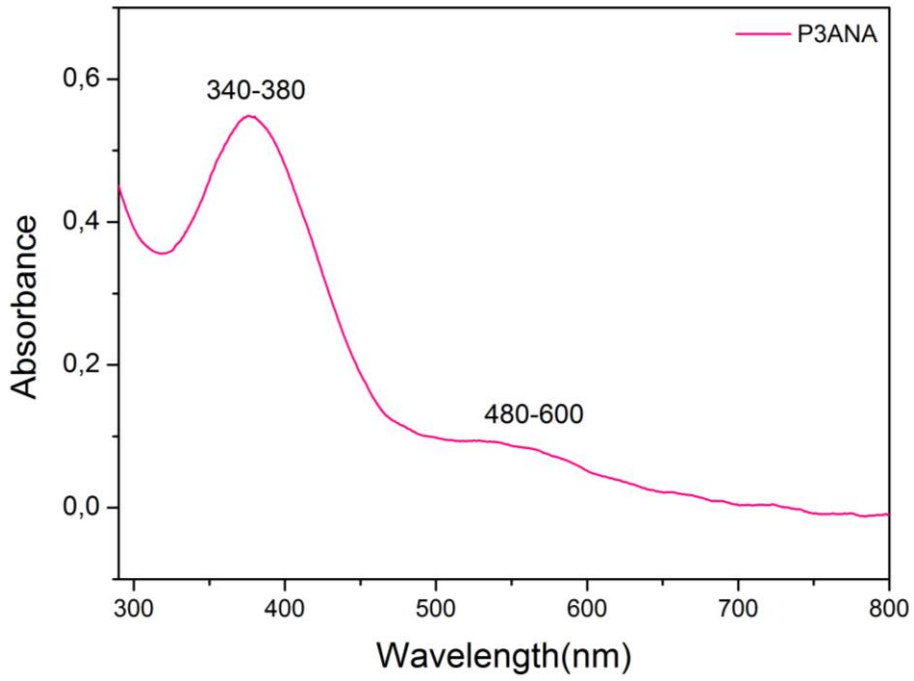

Figure 3.2 : UV-vis spectrum of synthesized P3ANA.

3.2 Characterization of Poly(m-anthranilic acid)/ Poly(ε-caprolactone) Nanofibers

3.2.1 Spectroscopic characterization of PCL/P3ANA nanofibers

Incorporation of P3ANA into PCL/P3ANA nanofibers was followed by UV–Visible spectroscopy following to dissolving the nanofibers are dissolved in DMF/THF (1/1, v/v) solution with the final concentration of 1 mg/mL. Solutions were diluted 10 times before measurement (Figure 3.3). UV-Vis spectra of PCL and PCL/P3ANA nanofibers dissolved in DMF/THF are given in Figure 3.4. PCL nanofibers showed an increase of the absorption intensity around 300 nm, related to carbonyl groups (Campos & Franchetti, 2005). PCL/P3ANA nanofibers exhibited new bands which are characteristic to P3ANA. The peak at 340–380 nm corresponds to π–π* transition in benzene ring of poly(m-anthranilic acid). The broad band in the range of 480-650 nm results due to the existence of polaron bands, which depends on the overall

oxidation state of the polymer (Giray et al., 2013). These new bands in the UV spectra of PCL/P3ANA nanofibers confirm the incorporation of P3ANA into the nanofiber structure. The absorbances of characteristic peaks of P3ANA were increased with the increasing amount of P3ANA in the nanofibers.

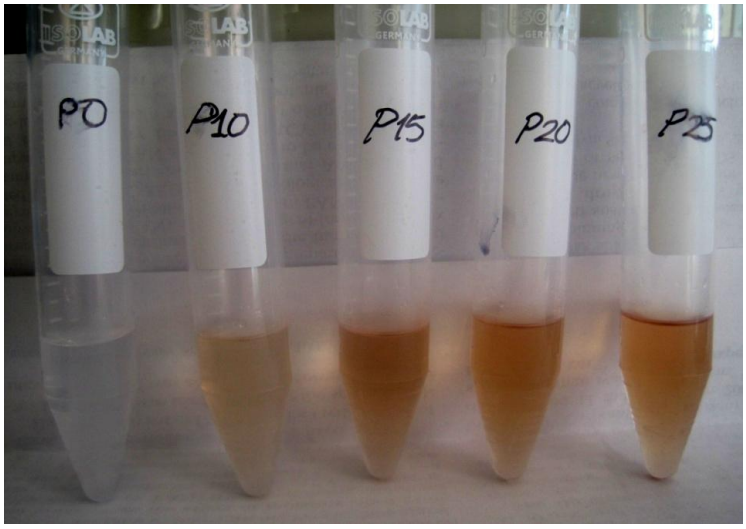

Figure 3.3 : Solutions of PCL and PCL/P3ANA nanofibers dissolved in DMF/THF.

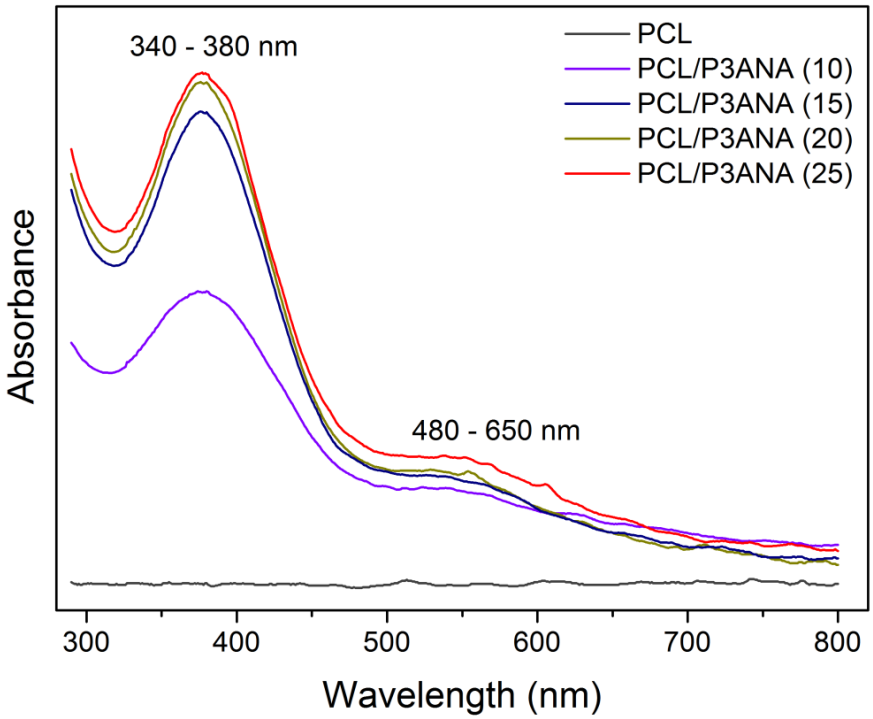

Figure 3.4 : UV-vis spectra of PCL and PCL/P3ANA nanofibers with increasing P3ANA content, which were dissolved in DMF/THF.

UV-Vis spectrophotometric data, which confirm the incorporation of P3ANA polymer into PCL/P3ANA nanofiber, was further supported by subsequent FTIR-ATR analysis. FTIR spectra of PCL and PCL/P3ANA nanofibers which contain 10 wt%, 15 wt%, 20 wt% and 25 wt% of P3ANA are given in Figure 3.5. The peaks observed at 1730 cm^{-1} and 1165 cm^{-1}were attributed to C=O stretching vibration and C-O stretching of PCL (Ducker et al., 2008). P3ANA in the PCL/P3ANA nanofibers displays the peaks at 1690, 1580 and 1510 cm^{-1} which were attributed to C=O stretching, C=C stretching and N-H stretching, respectively (Sophia, Gopu, & Vedhi, 2012). The intensity of C=C and N-H stretching peaks of P3ANA were increased with the increase in amount of P3ANA in the nanofiber structure (Figure 3.5-inset and Figure 3.6).

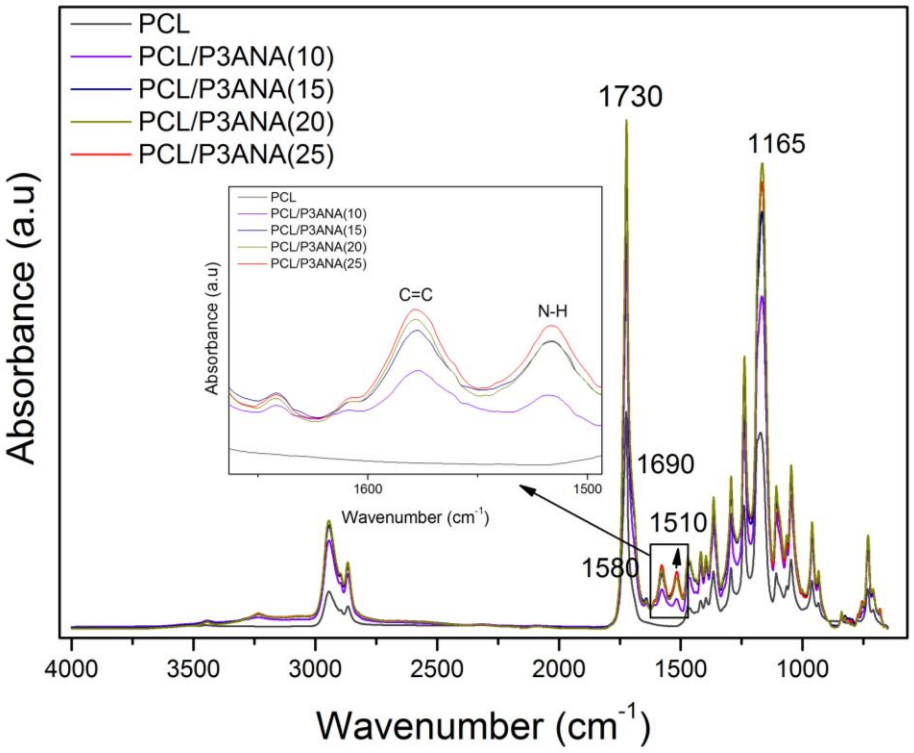

Figure 3.5 : FTIR-ATR spectra of PCL, PCL/P3ANA nanofibers with increasing P3ANA content. C=C and N-H stretching peaks of P3ANA (inset).

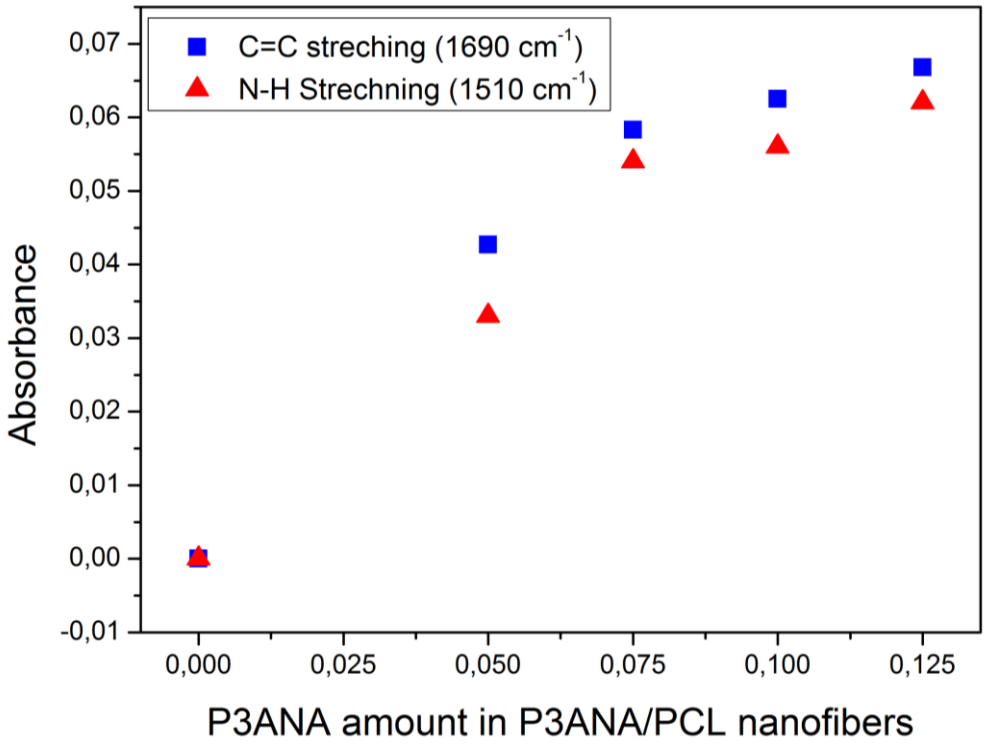

Figure 3.6 : Increase of peak intensities at 1690 cm^{-1} and 1510 cm^{-1} of P3ANA.

3.2.2 Morphological characterization of PCL/P3ANA nanofibers

The morphology PCL and PCL/P3ANA nanofibers which contain increasing amount of P3ANA was investigated by SEM (Figure 3.7) and AFM (Figure 3.8). SEM images showed that PCL and PCL/P3ANA nanofibers exhibited no bead formation. The average diameters of PCL nanofibers were determined as 101±12 nm. The average diameter of PCL/P3ANA nanofibers which contain contain 10 wt%, 15 wt%, 20 wt% and 25 wt% of P3ANA relative to PCL were determined as 99±15 nm, 95±11 nm, 90±14 nm and 89±16 nm, respectivly. The diameter of nanofibers was slighly decreased which correlates with change in the volatility of the solvent and the conductivity of the polymer solution due to P3ANA addition. The aminocarboxyl groups in the backbone of P3ANA results an increase in the charge density of the polymer solutions and promotes a large charge accumulation. During electrospinning, the high electrical field generates stronger elongation forces on the jet due to the self-repulsion of these excess charges. Therefore, this repulsive force easily overcomes the surface tension, in turn, results in reduction of the diameters of the nanofibers (Dagli et al., 2015; Giray et al., 2013; Yu et al., 2012).

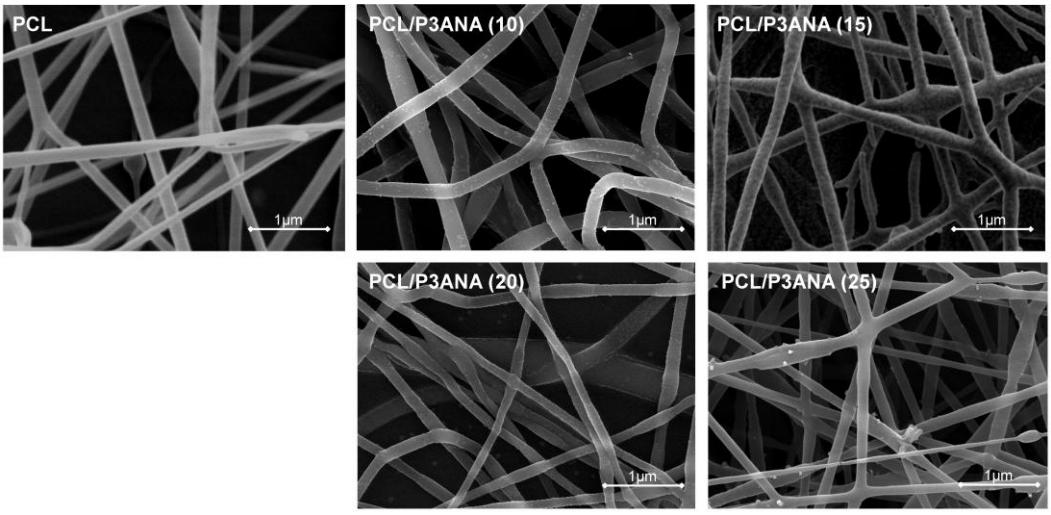

Figure 3.7 : SEM images of PCL and PCL/P3ANA nanofibers with increasing P3ANA content.

The surface roughness values of PCL and PCL/P3ANA nanofibers which contain contain 10 wt%, 15 wt%, 20 wt% and 25 wt% of P3ANA relative to PCL, were 122.7 nm, 130.2 nm, 135.7 nm, 142.1 nm, and 150.3 nm, respectively. The surface roughness was increased with the decrease in fiber diameter. Higher surface roughness enhances the interaction between cells and the nanofibers (Wan et al., 2015), thus the PCL/P3ANA nanofibers with the highest P3ANA content not only provides active sides for biofunctionalization but also increases the cell attachement.

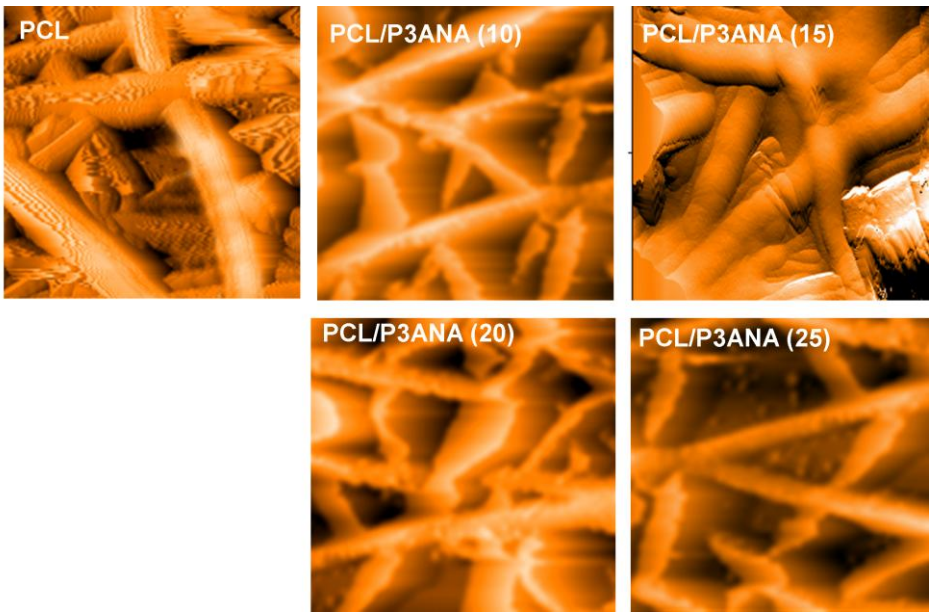

Figure 3.8 : AFM images of PCL and PCL/P3ANA nanofibers with increasing P3ANA content.

3.2.3 Characterization of surface properties of PCL/P3ANA nanofibers

BET is the most frequent method for determination of specific surface area of porous materials (Jakub et al., 2012). The BET surface area of PCL and PCL/P3ANA nanofibers which contains 10 wt%, 15 wt%, 20 wt% and 25 wt% of P3ANA was calculated from N_2 adsorption/desorption isotherms is 1.32 m^2/g, 1.34 m^2/g, 2.23 m^2/g, 2.9 m^2/g and 3.58 m^2/g, respectively (Table 3.1). The surface area of nanofibers increased with the increasing P3ANA content in the nanofibers. The increase in surface area after incorporation of P3ANA into the nanofiber can be related with fiber diameter. The addition of conductive polymer into nanofiber structure leads to a decrease in fiber diameter due to enhancement of electrostatic repulsion force on the surface of the jet during electrospinning. The decrease in fiber diameter results increase of BET surface area (Matsumoto & Tanioka, 2011). The large surface area of nanofibers can provide available sites for RGD-peptide binding and thus enhance the interaction between cells and nanofibers (Wan et al., 2015). Specific surface area of nanofibers plays an important role on initial cell adhesion and on the following cell proliferation. Nanofibers with high surface area provide more sites for cell attachment after seeding (Murphy, Haugh, & O'Brien, 2010). Therefore, addition of P3ANA into nanofiber structure can contribute to the interaction between cells and nanofiber mat by increasing the surface area.

Table 3.1 : BET surface area of PCL and PCL/P3ANA nanofibers.

Sample	S_{BET} (m^2/g)
PCL	1.32
PCL/P3ANA(10)	1.34
PCL/P3ANA(15)	2.23
PCL/P3ANA(20)	2.97
PCL/P3ANA(25)	3.58

3.2.4 Mechanical characterization of PCL/P3ANA nanofibers

The mechanical properties of PCL and PCL/P3ANA nanofibers were determined by obtaining the stress-strain graph (Figure 3.9). The Young's modulus, toughness, ultimate strength and ultimate strain were determined trough stress-strain curve and the obtained values are given in Table 3.2. The mechanical properties of electrospun nanofibers can influence cellular behaviors and regulate cell response. The mechanical properties of electrospun nanofibers can be tailored by varying the

composition with using different types of polymers and polymer blends, and by adjusting the size of individual nanofibers (Ma et al., 2013). The Young's modulus of nanofibers was determined from the initial slope of the linear region of stress-strain curve (Phipps et al., 2011). The toughness of was measured from the area under the stress–strain curve (Ma et al., 2013). The Young's modulus of PCL nanofibers was 3.57 MPa and it is increased to 5.5 MPa, 8.2 MPa, 8.89 MPa and 11.7 MPa for PCL/P3ANA nanofibers which contains 10 wt%, 15 wt%, 20 wt% and 25 wt% of P3ANA. The increase in P3ANA amount in the nanofiber structure were resulted an increase in Young's modulus and toughness of nanofibers. The toughness values of PCL and PCL/P3ANA nanofibers which contains 10 wt%, 15 wt%, 20 wt% and 25 wt% of P3ANA, were 29.63 MPa, 19.41 MPa, 21. 7 MPa, 23.79 MPa and 43.73 MPa. The ultimate strenght of nanofibers were increased with the addition of increasing amounts P3ANA into nanofiber structure. Mechanical properties of electrospun nanofibers, including tensile strength and Young's modulus are mainly affected by their nanostructured surface. The mechanical properties of PCL/P3ANA nanofibers changed due to P3ANA amount which changed the structural properties of the nanofibers. As stated earlier, the decrease in fiber diameter results increase of BET surface area, in addition it can cause higher modulus and strength (Ma et al., 2013). The addition and increase of P3ANA in the nanofibers enhanced the mechanical properties of PCL/P3ANA nanofibers by resulting higher Young's modulus, and ultimate stress and smaller strain.

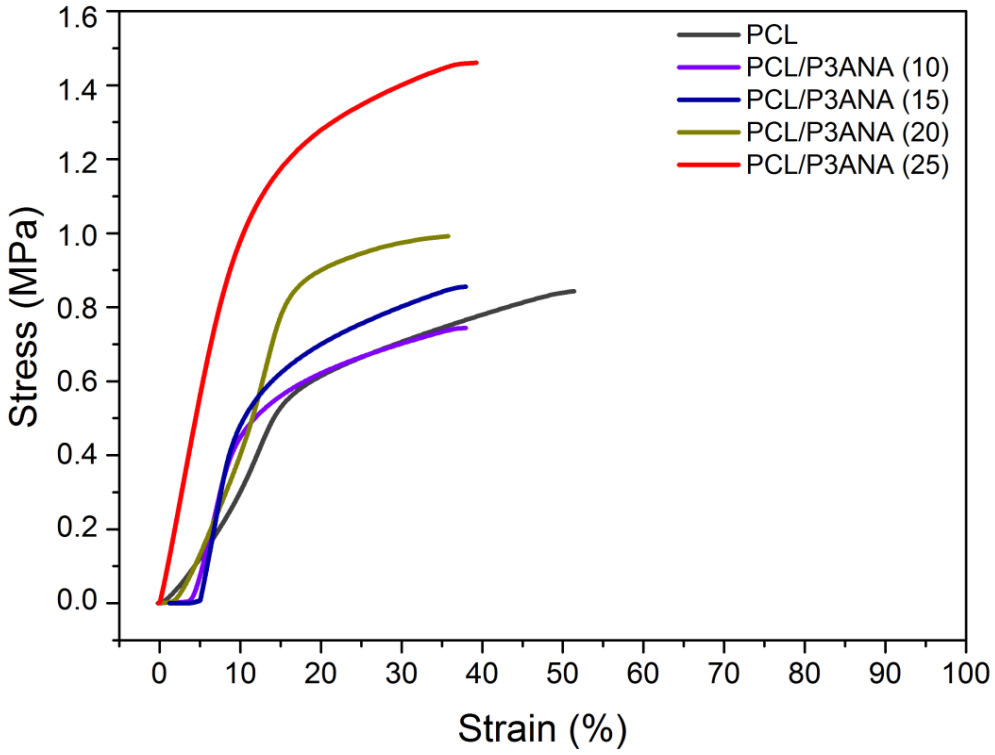

Figure 3.9 : Stress-strain curves of PCL and PCL/P3ANA nanofibers which contain 10 wt%, 15 wt%, 20 wt% and 25 wt% of P3ANA.

Table 3.2 : Mechanical properties of PCL and PCL/P3ANA nanofibers which contain 15 wt%, 20 wt% and 25 wt% of P3ANA.

	Young modulus (MPa)	Ultimate Tensile strength (MPa)	Toughness (MPa)	Ultimate strain
PCL	3.6	0.9	29.6	51.6
PCL/P3ANA (10)	5.5	0.8	19.4	37.8
PCL/P3ANA (15)	8.2	1.0	21.7	37.1
PCL/P3ANA (20)	8.9	1.0	23.8	35.7
PCL/P3ANA (25)	11.7	1.4	43.7	39.6

The functionalization of PCL/P3ANA can be acheived by obtaining succinimidyl ester (-COOSuc)-terminated surface by reacting carboxyl groups (-COOH) of P3ANA with N-hydroxysuccinimide (NHS) in the presence of N-ethyl- N-(3-(dimethylamino)propyl) carbodiimide (Z. Guler & Sarac, 2016). The addition of P3ANA into nanofiber structure with increasing amount resulted higher (-COOH) group which is evidenced by the increase of the absorbance peak of C=O streching of P3ANA at 1690 cm^{-1}. Moreover, it resulted higher surface area and therefore

enhaced mechanical properties which enhance protein loading capacity and cell attachment. The surface and mechanical properties depending on the P3ANA amount are represented in Figure 3.10. Therefore, the nanofiber mat which contain higher amount of P3ANA was chosen for functionalization with proteins in the course of this thesis.

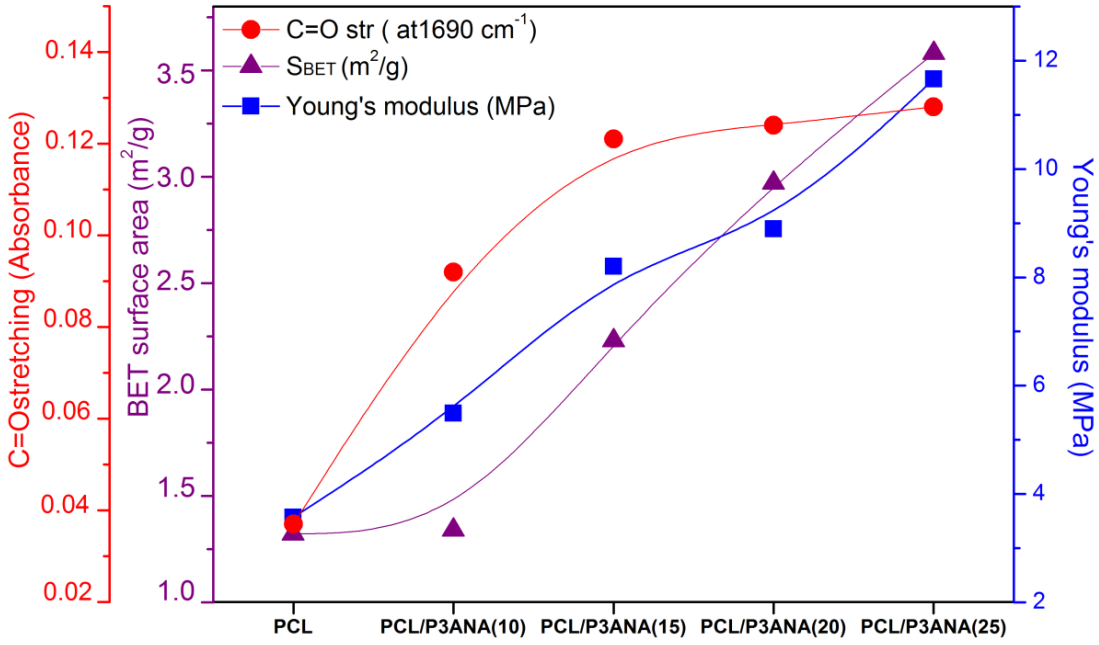

Figure 3.10 : Relationship among the P3ANA amount with surface (BET) and mechanical (Young's modulus) properties of nanofibers.

3.2.5 Electrochemical impedance spectroscopic characterization of PCL/P3ANA nanofibers

The electrical properties of PCL/P3ANA nanofibers which contains 10 wt%, 15 wt%, 20 wt% and 25 wt% of P3ANA relative to PCL was investigated by EIS. During EIS measurements, PCL/P3ANA nanofibers exhibited electroactivity and stability, without any deformation or decomposition. The Nyquist, Bode phase and Bode Magnitude plots of the nanofibers were recorded by applying AC signal of 10 mV amplitude in the frequency range 0.01 Hz to 100 kHz. Significant differences in the impedance spectra of nanofibers were observed depending on the P3ANA content in the nanofiber structure. The diameter of the semicircle of Nyquist plot which corresponds to the charge transfer resistance (R_{ct}) (Golshaei, Guler, & Sarac, 2016; Zainudin, Hairul, Yusoff, Tan, & Chong, 2014), decreased with an increase of P3ANA content in the nanofibers (Figure 3.11). Figure 3.12 represents the Bode phase plots of nanofibers. At higher frequency domain, a change in maximum phase

angle value of PCL/P3ANA nanofibers was observed depending on the P3ANA content. At higher frequency, Bode phase values for PCL/P3ANA nanofibers which contain 10 wt%, 15 wt%, 20 wt% and 25 wt% of P3ANA, were 5 °, 11 °, 1.8 ° and 1.4 °, respectively. The maximum Bode phase was shifted to higher frequencies which indicates addition of capacitive elements on the nanofiber surface and electronic behavior of nanofibers (Zeliha Guler, Erkoc, & Sarac, 2015). The Bode plot of magnitude in which the absolute values of impedance are plotted against the frequency obtained for the nanofibers (Figure 3.13). In low frequency region, Bode magnitude plots of nanofibers showed linear behavior with low-slope which indicates slightly capacitive behavior (Randles, 1947). The addition of P3ANA into the nanofiber structure decreased the absolute impedance $|Z|$ of the nanofibers, resulting that P3ANA addition enhanced the capacitive behavior of the PCL/P3ANA nanofibers. The EIS data were fitted with an equivalent circuit in order to characterize the electrochemical properties of the nanofibers and to describe the physical properties of the system. The impedance spectra for PCL/P3ANA nanofibers is described by the equivalent circuit R(CR)(QR)W in shorthand. Table 3.3 represents the fitting parameters for the equivalent circuit elements by modeling of the impedance spectra. First R in the circuit represents the solution resistance (Rs) of the electrolyte corresponds to the Ohmic resistance due to the presence of the electrolyte on the nanofiber and in solution (Sam et al., 2010) and of electrical contacts (Zehani, Dzyadevych, Kherrat, & Jaffrezic-Renault, 2014). R_s values for PCL/P3ANA nanofibers were decreased with the increase in P3ANA content in the nanofibers. Addition of P3ANA into naofiber structrure result more positively charged nanofibers. In PBS buffer wherein the EIS measurments were performed, the total positive charge concentration is greater that the total negative charge concentration (Birner, Uhl, Bayer, & Vogl, 2008). The alignment of positively charged solvated ions along the surface of nanofibers containing higher P3ANA, may decrease compared to the surface of nanofibers with low P3ANA content. Therefore the decrease in R_s value can be associated with P3ANA amount in the PCL/P3ANA nanofibers. The second resistance in both circuits represents the charge transfer resistance (R_{ct}) which corresponds to diameter of the semicircle in the Nyquist plot. The charge transfer resistance R_{ct} values were 777.2 Ω, 746.5 Ω, 213.7 Ω and 210 Ω for PCL/P3ANA nanofibers which contain 10 wt%, 15 wt%, 20 wt% and 25 wt% of P3ANA, respectively. The decrease in R_{ct} vaues is related with

enhancement in impedance behavior of nanofiber due to amino benzoic acid structure. C in the circuit was attributed to double layer capacitance (C_{dl}) arise from alignment of solvated counter ions along nanofiber surface. The electron transfer through electrode occurs by overcoming activation barrier, charge transfer resistance and solution resistance (J.-Y. Park & Park, 2009). No significant difference was observed in double layer capacitance (C_{dl}) along the surface of PCL/P3ANA nanofibers. Q was applied in the equivalent circuit as a constant phase element (CPE) for the simulation of the impedance data in order to take into account the non homogeneity of the conductance (Giray et al., 2013) and the electrode (Zehani et al., 2014). The impedance of a non-ideal electrode is defined by the formula ($Z_{CPE} = T_{CPE}(jw)^{-n}$) where TCPE and n are frequency-independent constants; w is the angular frequency (Gu, Su, & Loh, 2005), n is a parameter describing the deviation from an ideal capacitor and arises from the slope of the log Z versus log f plot. The values for n vary from 0 to 1. n = 1 subscribes to an ideal capacitor, while n=0 and 0.5 denotes a resistance and Warburg behavior, respectively (Xiangjun Lu et al., 2012). The n values for PCL/P3ANA nanofibers were increased with the increase in P3ANA content indicating more capacitive behavior. W represents the Warburg impedance and it is attributed to the diffusion of counter-ions. Once the electron transfer begins, the electrode kinetics determined by Warburg impedance (W) due to the mass transport (J.-Y. Park & Park, 2009). Rp represents the pore resistances of the nanofiber layer (Ohmic resistances of the electrolyte in the pores) (Panić, Dekanski, Mišković-Stanković, & Nikolić, 2009). W and Rp values for PCL/P3ANA nanofibers were increased due to the increase in P3ANA content. These increase in pore resistance and Warburg impedance can be related with the changes in nanofiber structure (Pauliukaite, Ghica, Fatibello-Filho, & Brett, 2010). The surface roughness and surface area of nanofibers were increased after the amount of P3ANA in the nanofibers increased (Z. Guler & Sarac, 2016). The electrochemical properties of PCL/P3ANA nanofibers were enhaced with the addition of P3ANA in higher amounts. The nanofiber with 25% wt of P3ANA amount relative to PCL, was chosen for cell culture studies since the higher electrical properties are advantegous delivering electrical signal to the cells.

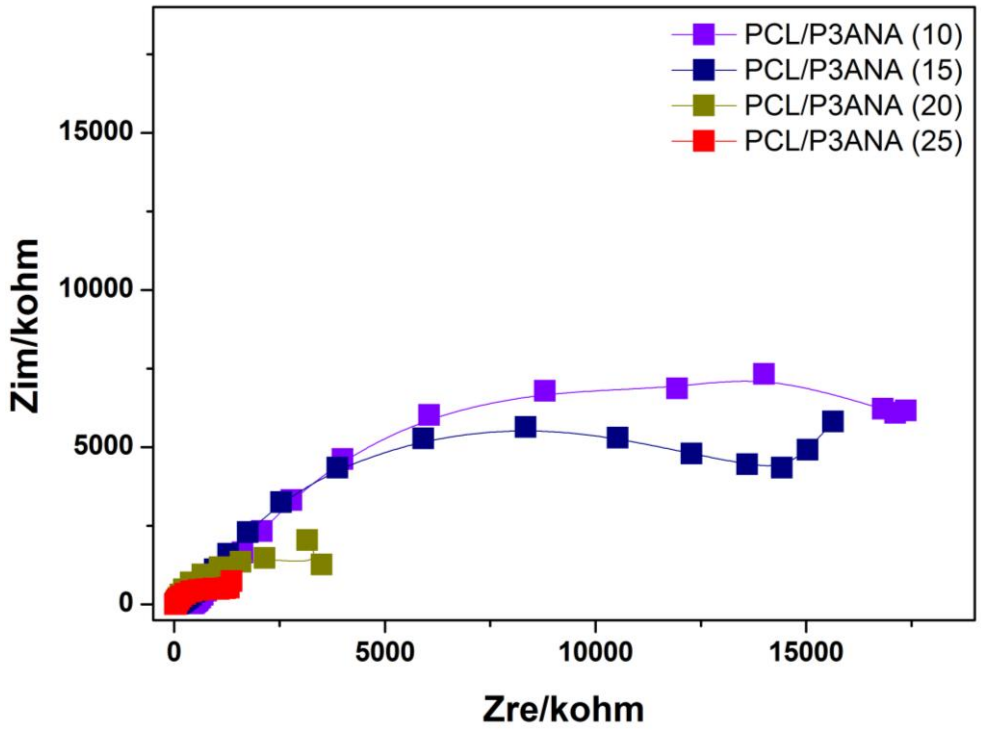

Figure 3.11 : Nyquist Nyquist plots of PCL/P3ANA nanofibers which contain 15 wt%, 20 wt% and 25 wt% of P3ANA.

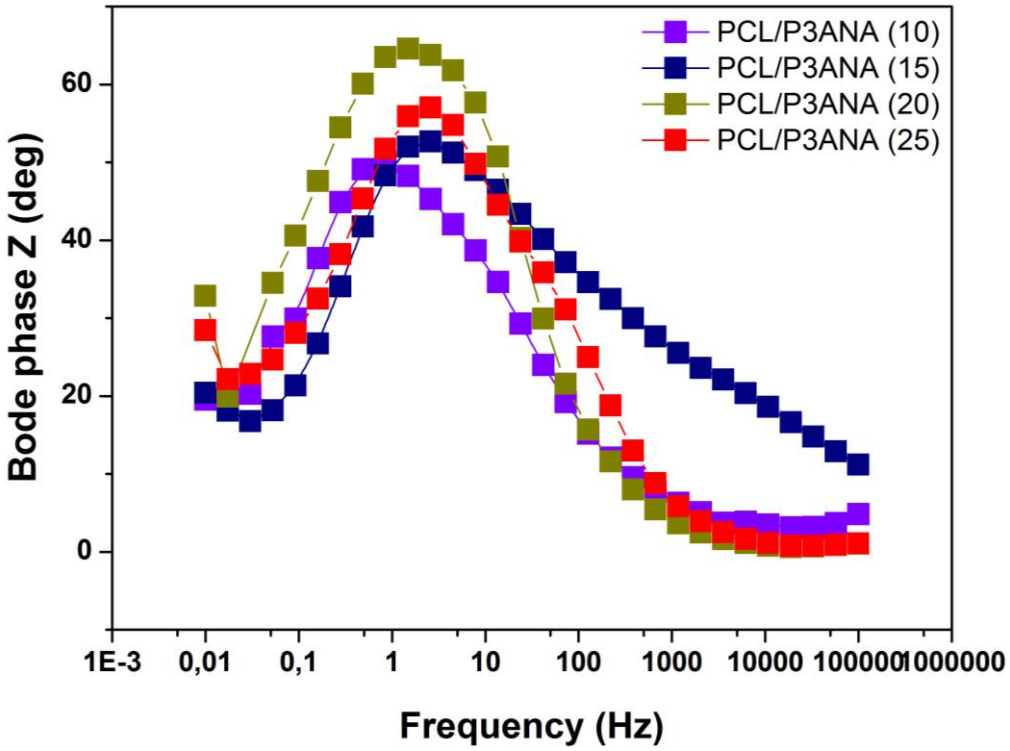

Figure 3.12 : Bode phase plots of PCL/P3ANA nanofibers which contain 15 wt%, 20 wt% and 25 wt% of P3ANA.

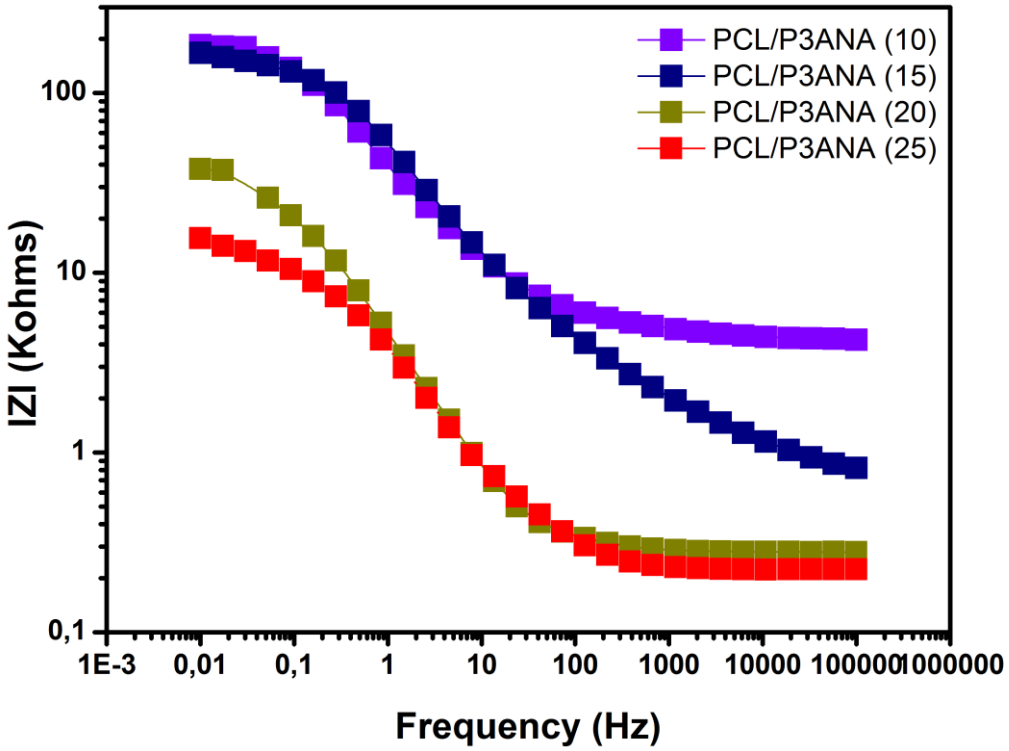

Figure 3.13 : Magnitude plots of PCL/P3ANA nanofibers which contain 15 wt%, 20 wt% and 25 wt% of P3ANA.

Table 3.3 : Fitting values for the equivalent circuit elements by the simulation of the impedance spectra of PCL/P3ANA nanofibers.

	Rs(Ω)	C_{dl} (μF)	R_{ct} (Ω)	Q(CPE) (10^{-7})(Ω^{-1})	Rp(kΩ)	W(10^{-5}) ($Ssec^5/cm^2$)	n	Chi-squared error (10^{-4})
PCL/P3ANA (10)	4309	12.23	777.2	0.16	0.71	1.42	0.56	1.87
PCL/P3ANA (15)	6320	14.58	746.5	0.22	0.81	1.67	0.80	1.75
PCL/P3ANA (20)	2800	12.34	213.7	0.49	1.35	2.51	0.81	1.92
PCL/P3ANA (25)	2771	13.04	210	0.19	2.87	3.05	0.85	3.83

3.3 Optimization of Biofunctionalization of PCL/P3ANA nanofibers with covalent protein immobilization

Covalent immobilization of biomolecules onto a -COOH group containing surface consists of preparation of a succinimidyl ester (-COOSuc)-terminated surface and its reaction with an amino ($-NH_2$) group on the biomolecule. This reaction is referred as surface "activation" which is conducted by reacting a surface bearing carboxyl end

groups with N-hydroxysuccinimide (NHS), in the presence of carbodiimide such as 1-ethyl-3-(dimethyl-aminopropyl) carbodiimide hydrochloride (EDC) (Staros et al., 1986). The studies in which EDC/NHS activation of carboxylic acids has been used, the concentrations of EDC and NHS strongly vary in a wide range (from M to the mM range) from one study to another (Voicu et al., 2004; Wissink et al., 2001; Z. Yang et al., 2010). Based on the EDC/NHS concentrations used in the literature, for the activation of carboxyl groups of PCL/P3ANA nanofibers, it was decided to use equal amounts of EDC/NHS (EDC/NHS=5/5 mM and EDC/NHS=50/50 mM), excess amount of EDC over NHS (EDC/NHS=5/0.5 mM) and excess amount of NHS over EDC (EDC/NHS=0.5/5mM). These concentrations were selected since very large concentrations of EDC or NHS result the formation of the byproducts at the surface which can prevent the formation of -COOsuc surface and affect the success of the surface activation. In the case of EDC and NHS concentrations are very low, then the surface activation reaction remains incomplete (Mohamad et al., 2015). Although the EDC/NHS activation has been widely used, the details of EDC/NHS activation of carboxyl groups of a semiconducting nanofiber and of the following amidation of NHS-ester for protein immobilization have not been reported. The optimum EDC/NHS concentration for surface activation of PCL/P3ANA nanofibers was throughly investigated by spectroscopy and electrochemical impedance spectroscopy before PCL/P3ANA nanofibers bioactivated with BMP-2 and RGD peptide**.**

3.3.1 Spectroscopic and morphological quantification of protein amount on the nanofiber mats

FTIR-ATR spectra of PCL/P3ANA nanofibers were obtained after activation procedure in order to reveal the influence of NHS and EDC concentrations (Figure 3.14). P3ANA in the PCL/P3ANA nanofibers displays the peaks at 2615, 1690, 1580 and 1510 cm^{-1} which were attributed to O-H stretching, C=O stretching, C=C stretching and N-H stretching, respectively. The peaks at 1250 and 1070 cm^{-1} were attributed to C-N stretching (Giray et al., 2013; Sophia et al., 2012). The carboxyl groups on P3ANA provide active sites for albumin binding through forming succinimidyl ester (-COOSuc) by reacting with NHS, in the presence of EDC (Mohamad et al., 2015). The attachment of a succinimidyl ester termination to PCL/P3ANA nanofibers can be evidenced by the triplet in the spectral range of the

C=O stretching vibrations. The activation can be observed in some spectra by a shoulder or an asymmetry of the 1772 cm^{-1} peak ascribed to the contribution of the C=O stretching mode (Sam et al., 2010). The Figure 3.14-B shows the C=O stretching vibrations of PCL/P3ANA nanofibers activated with different concentrations of EDC and NHS. When comparing the succinimidyl ester absorbance at 1772 cm^{-1} shown in Figure 3.14-B (inlet), at low concentrations (0.5 mM or 5 mM) of EDC and NHS, the activation reaction was incomplete. Compare to lower concentrations the activation was more successful when EDC=NHS=50 mM, since the peak absorbance at 1772 cm^{-1} was increased when the activation was performed by 50/50 mM of EDC/NHS (Figure 3.14B-inlet).

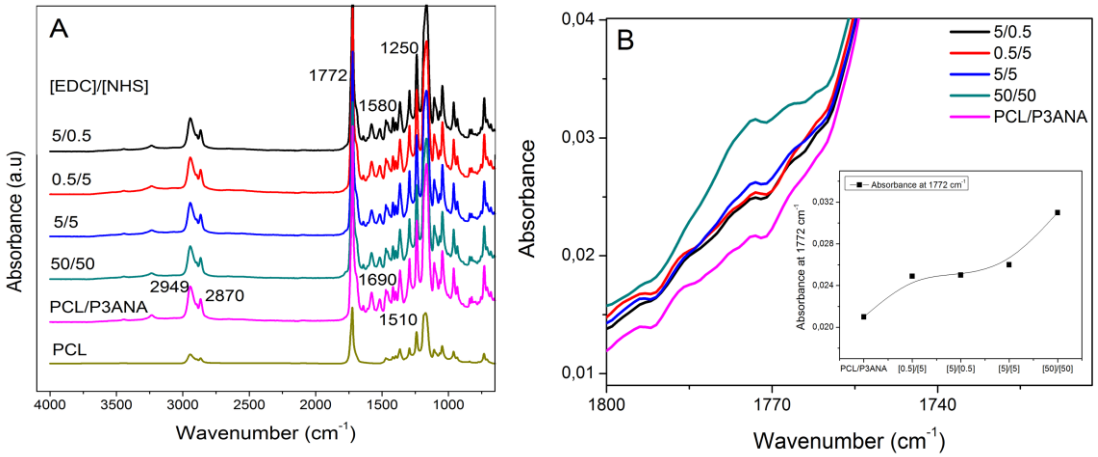

Figure 3.14 : FTIR-ATR spectra of PCL, PCL/P3ANA and PCL/P3ANA nanofibers activated with EDC/NHS mixtures of various concentrations (A), succinimidyl ester absorbance (B) and the increase in absorbance (B-inlet) after activation.

The surface activation yield (Figure 3.15) was estimated by calculation of FTIR peak ratios of the formed succinimidyl ester and O-H stretching of carboxylic acid group by using Beer-Lambert law. The relative percentages of surface species can be derived from their corresponding absorption bands by means of the Beer-Lambert law ($A = \varepsilon bc$), where A is the absorbance, ε the extinction coefficient, c the concentration and b is the length of the sample layer which was the same for all nanofiber mats. For calculation, the peaks at 1772 cm^{-1} and 2615 cm^{-1} were used for succinimidyl ester and O-H stretching of carboxylic acid, respectively. To estimate the reaction yield, peak height was measured to represent the absorbance (A) and the linear relationship among the individual extinction coefficients of succinimidyl ester and acid groups was 1:2 (C. Wang et al., 2011). Activation yield for each

PCL/P3ANA nanofibers activated with different amounts of EDC and NHS, was calculated as follows (3.1):

$$yield = \frac{\left(A_{1772}/\varepsilon_{\text{succinimidyl ester}}\right)}{\left(A_{1772}/\varepsilon_{\text{succinimidyl ester}} + A2615/\varepsilon_{\text{carboxylic acid}}\right)100\%}$$

(3.1)

The activation yield of carboxylic acid groups on PCL/P3ANA nanofibers activated with 5/0.5, 0.5/5, 5/5 and 50/50 mM of EDC and NHS was 71%, 72%, 73% and 82%.

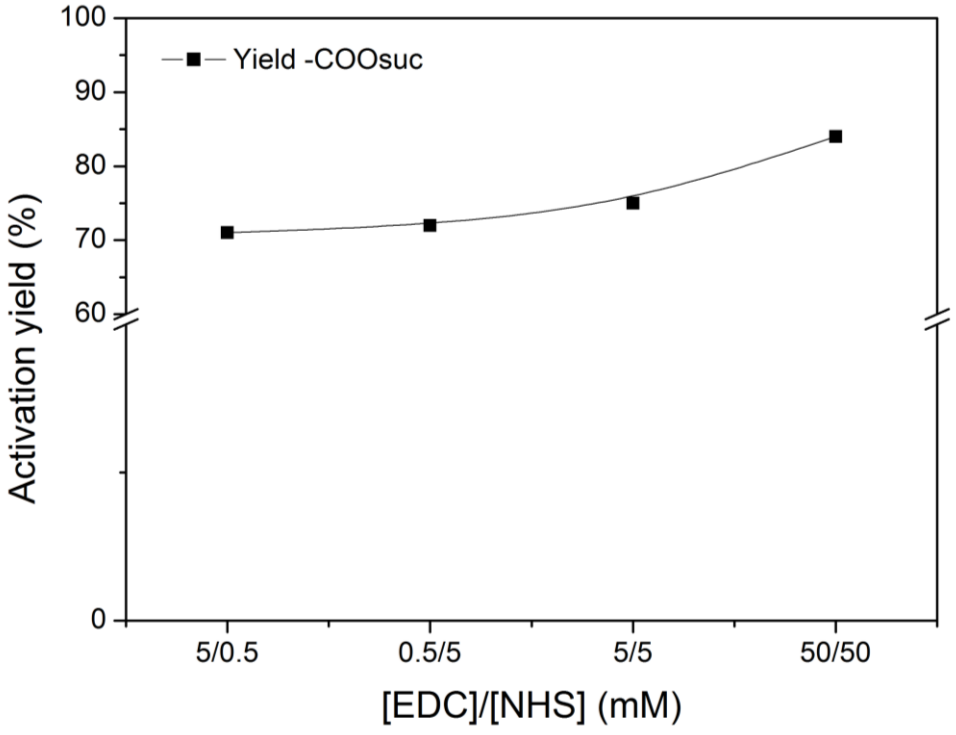

Figure 3.15 : Surface activation yields of carboxylic acid groups on PCL/P3ANA nanofibers depending on the EDC/NHS concentrations used.

Albumin immobilization was performed on the PCL/P3ANA nanofibers after activation with different concentrations of EDC and NHS (Figure 3.16). When compared to the PCL/P3ANA nanofibers which were not treated with albumin solution and nanofibers activated with lower concentration (0.5 and 5 mg) of EDC and NHS, there were no significant changes on FTIR spectra. On the contrary, after albumin immobilization onto nanofibers activated with 50/50 mM of EDC/NHS a broad peak was observed between 3000 cm^{-1} and 3600 cm^{-1}. The absorption in this

region can be influenced by the contribution of water but in proteins the N-H groups are generally in greater numbers than O-H groups (Grdadolnik & Maréchal, 2001). Also other albumin immobilized nanofibers showed no absorption at this region. The broad peak observed between 3000 cm^{-1} and 3600 cm^{-1} region of FTIR spectrum of nanofibers activated with 50/50 mM of EDC/NHS was attributed to the N-H stretching vibration of albumin (Bouhekka & Bürgi, 2012). FTIR data (Figure 3.16) showed that PCL/P3ANA nanofibers were activated successfully only when [EDC]=[NHS]=50 mM, therefore covalent binding of albumin was achieved on this nanofiber mat.

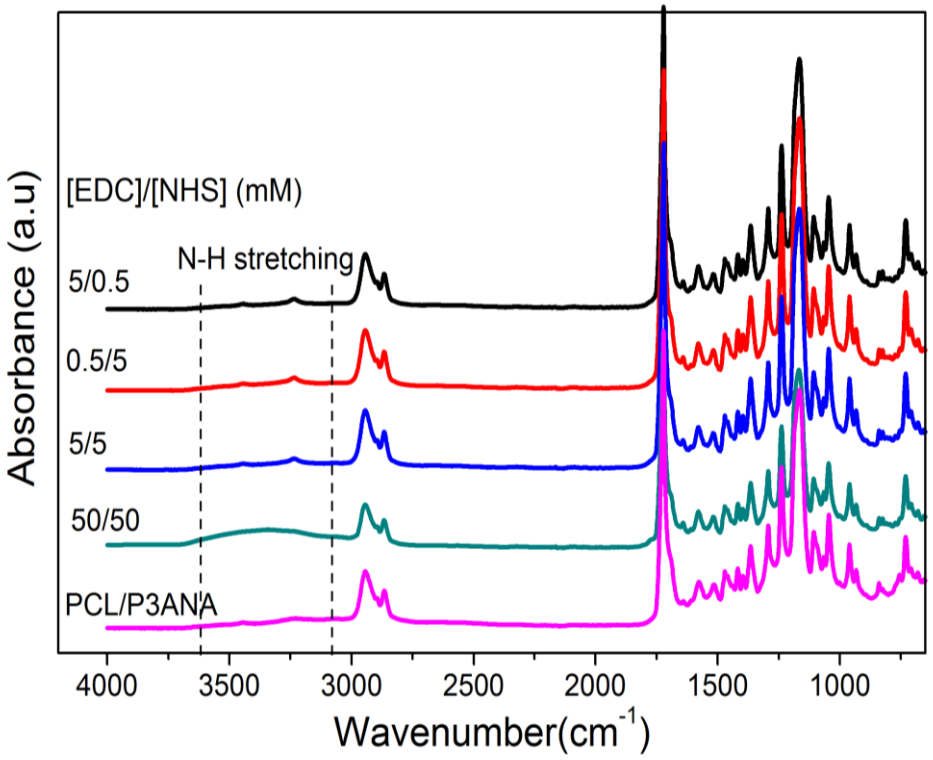

Figure 3.16 : FTIR-ATR spectra of albumin immoblized PCL/P3ANA nanofibers activated with EDC/NHS mixtures of various concentrations.

In order to determine the amount of covalently bound albumin onto nanofibers, the amount of bound protein on both non-activated and activated nanofibers was determined by BCA protein assay. After each reaction step, the nanofiber mats were taken out and washed with PBS to remove any residual albumin on the nanofiber mats. They were then reintroduced into a fresh reaction medium, and the albumin amount was detected. Figure 3.17 shows the amount of covalently bound albumin onto nanofibers after each immobilization step. 2 mg/mL of albumin was incubated

with non-activated PCL/P3ANA nanofibers (control) and PCL/P3ANA nanofibers which were activated by EDC/NHS at different concentrations. After incubation with albumin, albumin amount of the remaining solutions (cyan) were decreased. The difference between albumin amounts of the initial solutions (2 mg/mL) and solution obtained after binding step indicates that some of the protein is attached onto nanofibers. The highest amount of albumin (~1.85 mg) was atteched onto nanofibers activated with 50/50 mM of EDC/NHS. In control or orher samples activated with lower concentrations of EDC and NHS, the residual albumin amounts in the solutions obtained after binding step were similar to each other. Two washing steps were applied in order to remove physically absorbed protein. The amounts of washed albumin from non-activated nanofibers or nanofibers activated with lower concentrations of EDC/NHS were higher compared to amount of albumin washed from PCL/PANA nanofibers activated by 50/50 mM of EDC/NHS. This result indicates that the attachment was mostly physical on the nanofibers activated with lower concentrations of EDC/NHS. On the other, there was only 0.012 mg protein in the solution remained from PCL/PANA nanofibers activated by EDC/NHS at 50/50 mM concentration after two washing steps. In correlation with the FTIR-ATR data, albumin immobilization onto PCL/P3ANA nanofibers activated with 50/50 mM of EDC/NHS was achieved with covalent binding, since the attached albumin cannot be removed with washing steps. The amount of albumin bound covalently (purple) was the highest (~1.78 mg/mL), when nanofibers were activated with 50/50 mM of EDC/NHS.

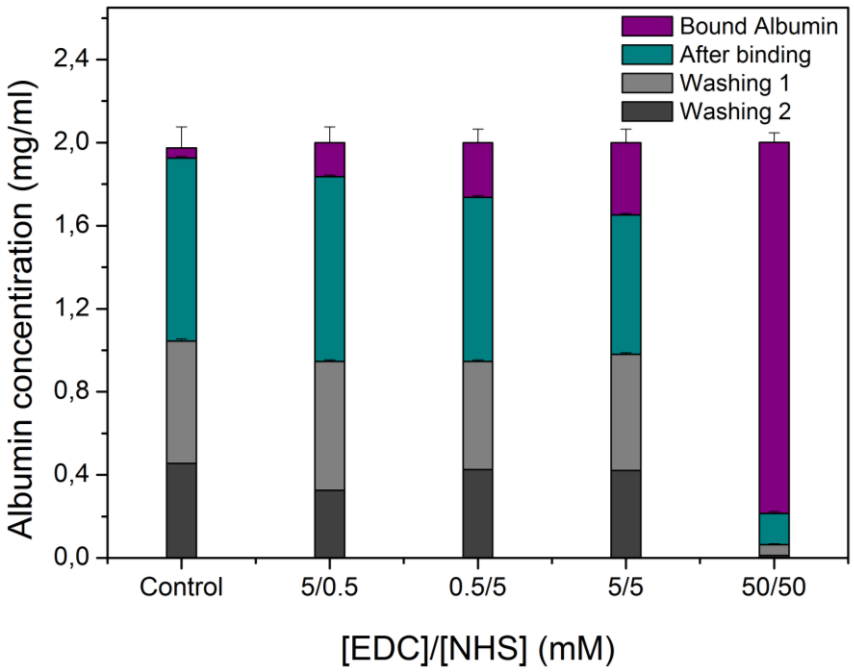

Figure 3.17 : Amount of initial and residual albumin after each immobilization step.

The morphology (Figure 3.18, Figure 3.19) and elemental composition (Figure 3.20, Table 3.4) of albumin immobilized PCL/P3ANA nanofibers activated by different concentrations of EDC/NHS were investigated. The average diameter of albumin immobilized PCL/P3ANA nanofibers activated with 5/0.5, 0.5/5, 5/5 and 50/50 mM of EDC/NHS were determined as 86±19 nm, 75±16 nm, 87±21 nm and 96±19 nm, respectively. The average fiber diameter of PCL/P3ANA before activation was determined as 89±16 nm. There is no significant change in diameter upon the binding of albumin onto PCL/P3ANA nanofibers activated with different concentration of EDC and NHS. AFM images of PCL/P3ANA and albumin immobilized nanofibers were represented in Figure 3.19. The surface of PCL/P3ANA nanofibers retained its topography after covalent immobilization of albumin indicating the EDC and/or NHS were not assembled or remained on the surface after washing steps (Sargeant, Rao, Koh, & Stupp, 2008). PCL/P3ANA nanofibers have RMS roughness of 150.3 nm. The surface roughness was slightly increased after albumin immobilization. The RMS roughness values of albumin immobilized nanofibers which were pre-activated with 5/0.5, 0.5/5, 5/5 and 50/50 mM of EDC and NHS, were 176.2 nm, 193.2 nm, 208.9 nm and 226.69 nm, respectively. This increase in roughness indicates the immobilization on albumin on the surface of activated PCL/P3ANA nanofibers (Cho et al., 2014; Zeliha Guler et

al., 2015). In correlation with FTIR-ATR, EDX and BCA, AFM images also indicates that the highest amount of albumin bound to nanofibers activated with 50/50 mM of EDC/NHS.

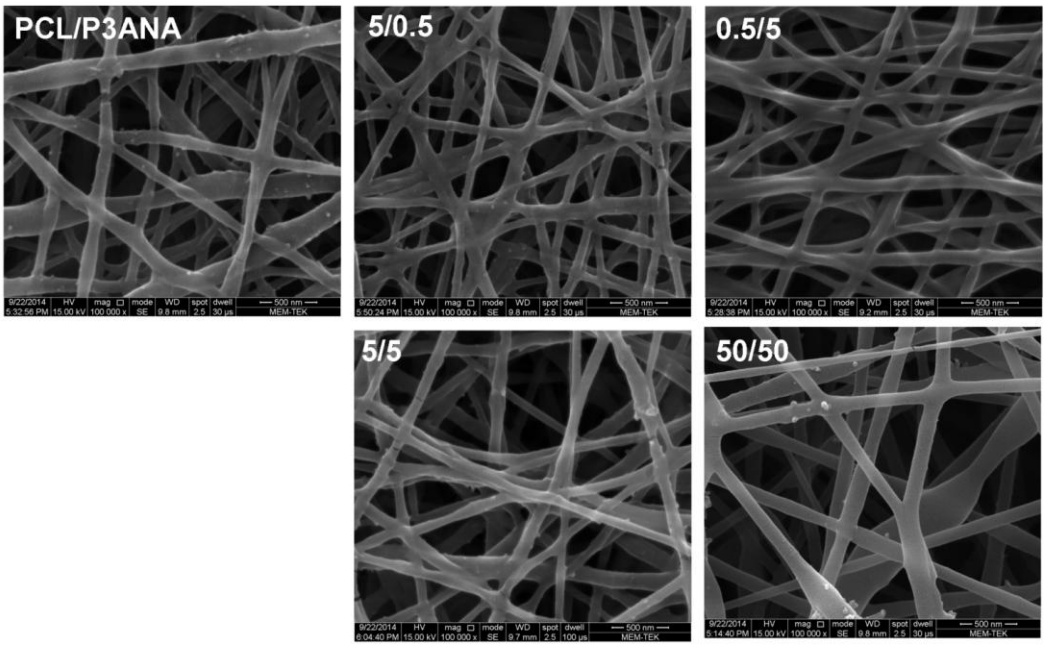

Figure 3.18 : SEM images of PCL/P3ANA and albumin immobilized PCL/P3ANA nanofibers activated with 5/0.5, 0.5/5, 5/5 and 50/50 mM of EDC/NHS.

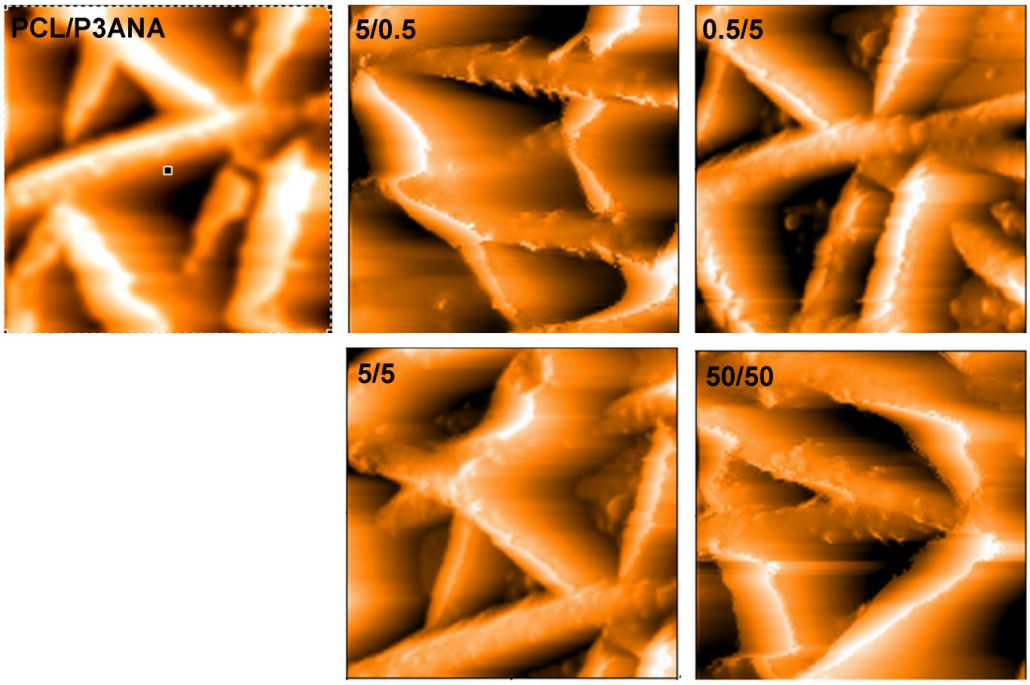

Figure 3.19 : Topography AFM images (6 µm x 6 µm) of PCL/P3ANA and albumin immobilized PCL/P3ANA nanofibers activated with 5/0.5, 0.5/5, 5/5 and 50/50 mM of EDC/NHS.

EDX analyses were performed to confirm the presence of the albumin onto nanofibers. The structure and composition of the albumin immobilized nanofibers were analyzed by detection of elemental concentrations for nitrogen (N) with EDX [31, 32]. In addition, the distribution of immobilized albumin on the surface was investigated by EDX-mapping of PCL/P3ANA nanofiber mats (Figure 3.20). P3ANA has N atoms in its backbone, as well as albumin. The distribution of nitrogen atoms on PCL/P3ANA nanofiber mat seems to be random. It can be explained by the porous structure of nanofiber mat which affects the penetration depth of electrons during EDX analysis (Rabiller-Baudry & Gouttefangeas). It is known that depending on the polymer chemical nature and porosity of mat, a loss of X-rays can be occured (Otto, Habicht, Dinjus, & Zimmerman, 2012). Also, P3ANA and PCL blended in a weight ratio of 25% w/w between two polymers. Since both PCL and P3ANA contains oxygen atoms on their backbones, the amount of O atoms (wt %) was 91.49 while N atom amounts (wt %) was 8.81 on the surface of PCL/P3ANA nanofibers. The amount of N (wt %) on the surface of PCL/P3ANA and of the nanofiber mats activated with 5/0.5, 0.5/5 and 5/05 mM of EDC/NHS were approximately the same. However, when nanofibers were activated with increasing (50/50 mM) amounts of EDC and NHS, the amount of N (wt %) on the surface were increased (10.97 wt %) which indicated that the N atoms were introduced to the structure of nanofibers through covalent binding of the albumin. The compositions of included atoms (nitrogen and oxygen) in the structure are given in Table 3.4. EDX-mapping images of albumin immobilized nanofibers showed the distribution of the immobilized albumin. EDX-mapping images indicate that the distribution of the albumin on the surface of nanofibers is affected by the distribution of activated functional groups -COOH of P3ANA. SEM/EDX results have been complementary with FTIR-ATR, BCA protein assay and able to verify the covalent immobilization of albumin onto PCL/P3ANA nanofibers activated with higher and equal concentrations of EDC and NHS.

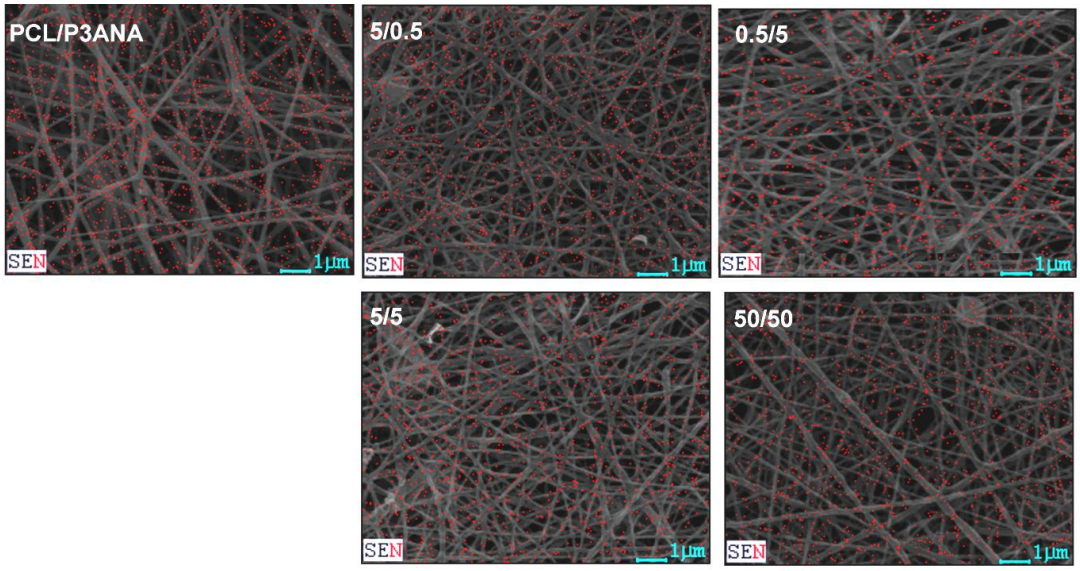

Figure 3.20 : EDX-mapping of nitrogen (red) atoms on the surface of PCL/P3ANA and albumin immobilized PCL/P3ANA nanofibers activated with 5/0.5, 0.5/5, 5/5 and 50/50 mM of EDC/NHS.

Table 3.4 : Elemental concentrations for nitrogen and oxygen atoms in PCL/P3ANA nanofibers and albumin immobilized nanofibers after activation with EDC/NHS.

Samples	Elements (wt %)	
[EDC]/[NHS] (mM)	N	O
PCL/P3ANA	08.51	91.49
[5]/[0.5]	08.80	91.20
[0.5]/[5]	08.48	91.52
[5]/[5]	08.91	91.09
[50]/[50]	10.97	89.03

3.3.2 Electrochemical impedance spectroscopic measurements of albumin immobilized nanofibers

Electrochemical impedance spectroscopy (EIS) measurements were performed on albumin immobilized PCL/P3ANA nanofibers on ITO-PET in order to understand the influence of NHS and EDC concentrations on the amount of bound albumin. The EIS data provide information about the nature of electrochemical process occurring at the electrode/electrolyte interface (Gu et al., 2005). EIS data were obtained on PCL/P3ANA and on albumin immobilized nanofibers which were activated with different concentrations of EDC and NHS. A significant difference in the impedance spectra was observed depending on the covalent immobilization of albumin onto nanofibers and the concentrations of the EDC and NHS used in activation. In

Nyquist plot (Figure 3.21), albumin immobilized PCL/P3ANA nanofibers exhibited a semi-circle while PCL/P3ANA nanofibers showed a linear behaviour. The diameter of the semicircle of Nyquist plot represents the charge-transfer resistance (R_{ct}) (Giray et al., 2013) and linear line with high-slope indicates capacitive behavior (Feng et al., 2015). Nanofibers became resistive after treated with albumin and the charge-transfer resistance of the albumin immobilized nanofibers was increased. PCL/P3ANA nanofibers activated with 50/50 mM of EDC/NHS had the largest diameter of the semicircle of the Nyquist plot indicated that the highest amount of albumin bound onto these nanofibers (Rodríguez-Sevilla, Ramírez-Silva, Romero-Romo, Ibarra-Escutia, & Palomar-Pardavé, 2014). This result was in correlation with the data obtained from FTIR-ATR, SEM/EDX and BCA.

The measured impedance spectra were analyzed in terms of electrical equivalent circuits to evaluate the kinetics of the systems using the analysis program ZSimpWin. The circuits for PCL/P3ANA nanofibers and on albumin immobilized nanofibers which were activated with different concentrations of EDC and NHS, which describe the physical properties of the system and provide a good fit to the measured data with a reasonable number of circuit elements, were chosen. The calculated and measured data were fitted well together with the chosen equivalent circuits (Figure 3.21). The impedance spectra for nanofibers (PCL/P3ANA) described by the equivalent circuit of R(CR)(QR)W (Figure 3.22) in short hand. For albumin immobilized PCL/P3ANA, the equivalent circuit of R(CR)(CR)(QR)W were selected since there are additional electrical components (resistance and capacitance) arising from immobilized albumin. Table 3.5 represents the fitting parameters for the equivalent circuit elements by modeling of the impedance spectra.

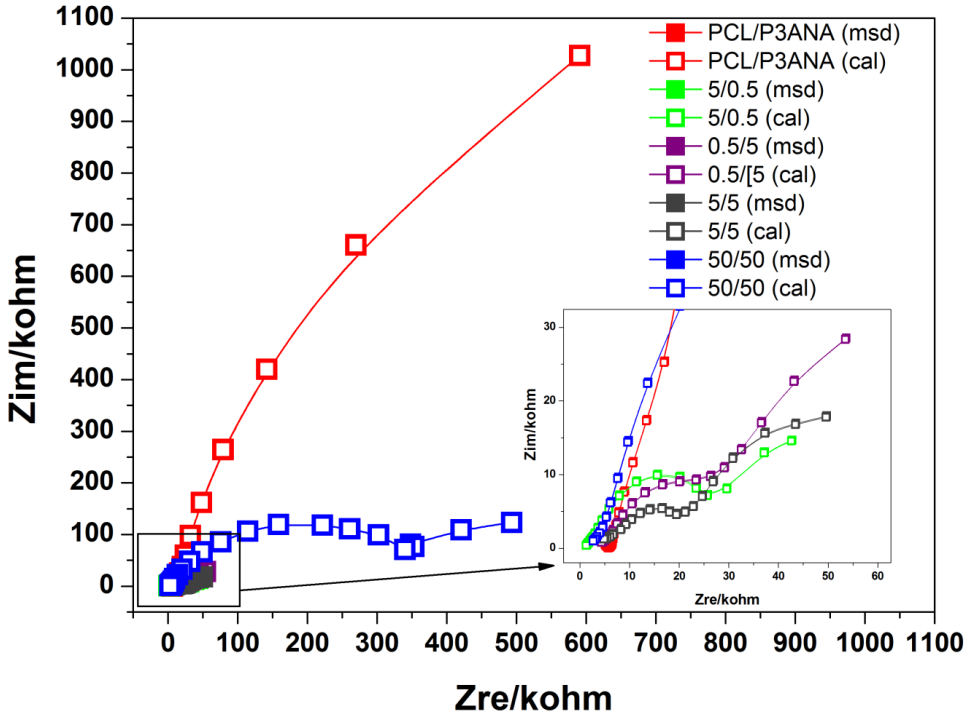

Figure 3.21 : Measured (msd) and calculated (cal) Nyquist plots of PCL/P3ANA and albumin immobilized PCL/P3ANA nanofibers activated with 5/0.5, 0.5/5, 5/5 and 50/50 mM of EDC/NHS.

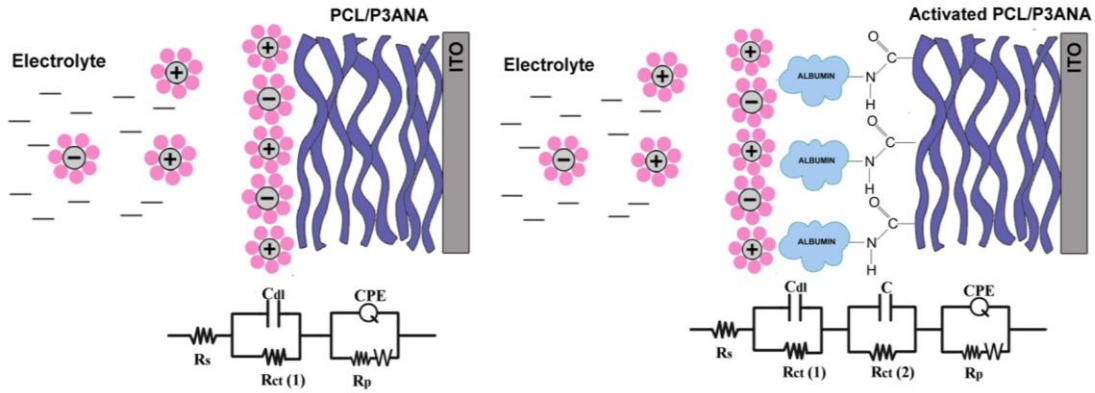

Figure 3.22 : Equivalent circuits for the simulation of the EIS spectra of PCL/P3ANA (top) and albumin immobilized PCL/P3ANA nanofibers activated with EDC/NHS nanofibers (bottom).

Table 3.5 : Fitting values for the equivalent circuit elements by the simulation of the impedance spectra.

[EDC]/[NHS] (mM)	Rs(Ω)	C_{dl} (μF)	$R_{ct}(1)$ (Ω)	C (μF)	$R_{ct}(2)$ (kΩ)	Q(CPE) $(10^{-7})(\Omega^{-1})$	Rp(kΩ)	$W(10^{-5})$ $(Ssec^5/cm^2)$	n	Chi-squared error (10^{-4})
PCL/P3ANA R(CR)(QR)W	2771	13.04	210	-	-	0.19	2.87	3.05	0.85	3.83
[5]/[0.5] R(CR)(CR)(QR)W	1108	0.08	1209	5.54	22.90	4.65	26.49	2.98	0.62	4.23
[0.5]/[5] R(CR)(CR)(QR)W	3403	0.09	1331	2.16	33.06	3.99	25.15	1.65	0.67	5.48
[5]/[5] R(CR)(CR)(QR)W	1143	0.08	4725	4.94	16.47	0.10	32.07	3.46	0.33	5.00
[50]/[50] R(CR)(CR)(QR)W	974.1	0.06	52790	12.59	202.60	0.13	693.50	1.14	0.30	1.39

Rs, the first component of two circuits, represents the solution resistance of the electrolyte corresponds to the Ohmic resistance due to the presence of the electrolyte on the nanofiber and in solution (Sam et al., 2010) and of electrical contacts (Zehani et al., 2014). Rs values for PCL/P3ANA nanofibers, albumin immobilized nanofibers activated with 5/0.5, 0.5/5, 5/5 and 50/50 mM of EDC and NHS were 2771 Ω, 1108 Ω, 3403 Ω, 1143 Ω and 974.1 Ω, respectively. The Rs values correspond to the behavior of the electrolyte, filling pores of nanofibers (Radecka, Wierzbicka, & Rekas, 2004). The second resistance in both circuits represents the charge transfer resistance (R_{ct}) between the solution and the surface of the PCL/P3ANA nanofibers or albumin immoblized nanofiber electrode surface. The charge transfer resistance $R_{ct}(1)$ of 210 Ω of PCL/P3ANA nanofibers increased to $R_{ct}(1)$ of 1209 Ω, 1331 Ω, 4725 Ω and 52790 Ω after albumin immobilization onto nanofibers activated with 5/0.5, 0.5/5, 5/5 and 50/50 mM of EDC/NHS, respectively. The increase in R_{ct} value is attributed to the formation of a new layer at the interface between solution and nanofibers (Sophia et al., 2012). First C in the circuits was attributed to double layer capacitance (C_{dl}) arise from alignment of solvated counter ions along nanofiber surface. The electron transfer through electrode occurs by overcoming activation barrier, charge transfer resistance and solution resistance (J.-Y. Park & Park, 2009). Double layer capacitance (C_{dl}) along the surface of PCL/P3ANA nanofibers was decreased after albumin immobilization. The decrease in C_{dl} is attributed to increase

in thickness of electronic double layer depending on the albumin immobilization (Sophia et al., 2012).

For albumin immobilized nanofibers, additional circuit elements of capacitance (C) and resistance (R) are connected in parallel to first ones in order to describe the capacitance and the charge transfer resistance between immobilized albumin molecules and PCL/P3ANA nanofibers, respectively. When PCL/P3ANA nanofibers were activated with 50/50 mM of EDC/NHS, the capacitance (C) occurring at the interphase between immobilized albumin and nanofibers increased as well as the charge transfer resistance of R_{ct} (2). The difference between capacitance values of albumin immobilized nanofibers can be explained by the different interfacial structures, assuming different structures or sizes (Kityakarn et al., 2012). PCL/P3ANA nanofibers are porous electrodes and they provide large surface areas which forms interfaces between electrodes and electrolytes, resulting in high capacitances. The immobilization of albumin onto the surface of nanofibers induces higher R_{ct} values (B.-Y. Chang & Park, 2010; Zainudin et al., 2014). The increase in R_{ct} values can be explained by the formation of a new layer at the interface between solution and nanofibers was formed after attachment of albumin onto surface (Sophia et al., 2012). The different interfacial structure between protein layer and nanofibers can cause higher R_{ct} values. Also, EIS measurements were performed in PBS buffer at pH 7.4 where albumin become negatively charged (Tribet, Porcar, Bonnefont, & Audebert, 1998). In PBS buffer, the total positive charge concentration is greater that the total negative charge concentration (Birner et al., 2008). After attachment of albumin on the surface, the negative charge on the surface of nanofibers was increased and this resulted in the alignment of positively charged solvated ions along the nanofiber surface and increase in R_{ct} values. Moreover, negatively charged ions can be repulsed by albumin on the surface and the transfer of positively charged and relatively big ions into positively charge nanofibers become challenging (Dagli et al., 2015). Q represents the constant phase element (CPE) which was applied in the equivalent circuit for the simulation of the impedance data, since CPE takes into account the non homogeneity of the conductance (Giray et al., 2013) and the electrode (Zehani et al., 2014). The impedance of a non-ideal electrode is defined by the formula ($Z_{CPE} = T_{CPE}(jw)^{-n}$) where TCPE and n are frequency-independent constants; w is the angular frequency (Gu et al., 2005), n is a parameter describing the deviation from an ideal capacitor and arises from the slope of the log Z versus log

f plot. The values for n vary from 0 to 1. n = 1 subscribes to an ideal capacitor, while n=0 and 0.5 denotes a resistance and Warburg behavior, respectively (Xiangjun Lu et al., 2012). The n value of PCL/P3ANA nanofibers was 0.85 and it is significantly reduced up to 0.30 with albumin immobilization. The values for n=0 indicates a resistance while n=0.5 denotes Warburg behavior. W represents the Warburg impedance and it is attributed to the diffusion of counter-ions. Once the electron transfer begins, the electrode kinetics determined by Warburg impedance (W) due to the mass transport (J.-Y. Park & Park, 2009). Rp represents the pore resistances of the nanofiber layer (Ohmic resistances of the electrolyte in the pores) (Panić et al., 2009). Rp values for PCL/P3ANA nanofibers were increased after albumin immobilization. These differences in Rp can be explained by the fact that covalent immobilization of albumin by EDC/NHS activation forms a different nanofiber mat structure (Pauliukaite et al., 2010). The highest value of 693.50 Ω of Rp was observed on nanofibers activated with 50/50 mM of EDC and NHS. AFM images indicated that surface roughness increased after albumin immobilization onto nanofibers activated with 50/50 mM of EDC and NHS, the increase in pore resistance value of PCL/P3ANA nanofibers (50/50 mM of EDC/NHS) can be related with the increase in surface roughness. EIS and equivalent circuit modeling indicated that 50/50 mM of EDC/NHS were the most effective concentration on the activation of carboxylic acid groups on PCL/P3ANA nanofiber.

FTIR-ATR analyses of the PCL/P3ANA nanofibers which were treated with different concentrations of EDC and NHS showed that, 50/50 mM of EDC/NHS were the effective concentration to activate the nanofibers. Also, the success of covalent immobilization of the albumin is directly depending on the efficiency of the activation procedure. The subsequent analyses (FTIR-ATR, EDX, BCA and EIS) performed on albumin immobilized nanofibers indicated that the highest amount of albumin was bound onto nanofibers activated with 50/50 mM of EDC/NHS. Figure 3.23 represents the relationship between the surface activation and albumin immobilization. The concentrations of nitrogen (N) atoms at the surface and the charge transfer resistance of albumin immobilized nanofibers were increased as the activation of the nanofibers were achieved represented by the increase in the absorbance (1772 cm-1) of the succinimidyl ester. During the activation procedure, the formation of the byproducts at the surface results a kinetic competition between

different reactions (Sam et al., 2010). In the case of EDC concentration is lower than NHS concentration (0.5/5 mM), the formation of O-acylurea become very slow resulting a slow succinimidyl ester formation. When EDC concentration is higher than NHS concentration (5/0.5 mM) O-acylurea formation become relatively fast however succinimidyl esters form very slow and byproducts of Anhydride and N-acylurea can be formed at the surface (Douarche, Cortès, De Villeneuve, Roser, & Braslau, 2008). When NHS and EDC concentrations are equal to each other and both low (5/5 mM) then slow kinetics for whole reaction are expected. On contrary, when the concentrations of both EDC and NHS increased to 50 mM, great balance between formation of O-acylurea and transformation of it into succinimidyl ester product can be obtained. The obtained data revealed that the highest amount of albumin bound to nanofibers activated with 50/50 mM of EDC/NHS which was found to be the optimum concentration for the activation of PCL/P3ANA nanofibers.

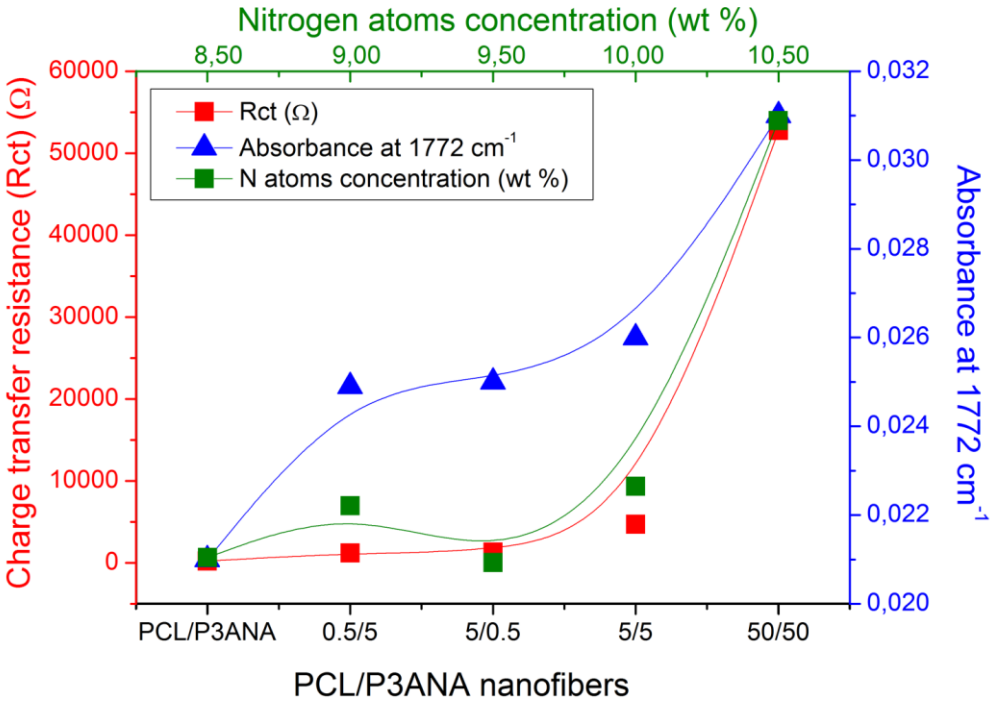

Figure 3.23 : The relationship among charge transfer resistance (R_{ct}) from EIS, succinimidyl ester absorbance from FTIR-ATR and N atoms concentrations from EDX data of activated PCL/P3ANA nanofibers.

3.4 Characterization of BMP-2/PCL/P3ANA and PCL/P3ANA-RGD nanofibers

3.4.1 Spectroscopic characterization of BMP-2/PCL/P3ANA and PCL/P3ANA-RGD nanofibers

The FTIR-ATR spectra of PCL, P3ANA and BMP-2/PCL/P3ANA nanofibers are shown in Figure 3.24. In the ATR-FTIR spectrum of PCL/P3ANA nanofibers, PCL exhibits peaks for C=O stretching vibration at 1733–1725 cm^{-1}, C-O stretching at 1160 cm^{-1}, C-H bending at 1397 cm^{-1}, C-H stretching at 2856 cm^{-1} (Elzubair, Elias, Suarez, Lopes, & Vieira, 2006). The characteristic peaks of P3ANA are observed at 2615, 1580 and 1510 cm^{-1} which are attributed to O–H stretching, C=C stretching and N–H stretching, respectively. The peaks at 1250 and 1070 cm^{-1} are attributed to C–N stretching of P3ANA (Z. Guler & Sarac, 2016). The absorption band at 1690 cm^{-1} is due to stretching vibration of C=O of –COOH groups of P3ANA. ATR-FTIR spectrum of PCL/P3ANA nanofibers indicated that P3ANA was successfully incorporated in the nanofiber structure. The carboxyl groups on P3ANA provide active sites for covalent immobilization of BMP-2 in the presence of EDC and NHS (Z. Guler & Sarac, 2016; J.-S. Lim et al., 2014). After biofunctionalization of PCL/P3ANA nanofibers with BMP-2, new peaks are observed in the FTIR spectrum of nanofibers (Figure 3.24-inset). The most sensitive region of FTIR spectrum for protein structural components is the 1700-1600 cm^{-1} region, which is mostly related with the C=O stretch vibrations of the peptide linkages. The peak at 1640 cm^{-1} is attributed to bending modes of N-H bond (Gilde et al., 2012). In the 1630 – 1680 cm^{-1} region, the FTIR spectrum presents the peaks for secondary structure of BMP-2. The peaks at 1645 cm^{-1}, 1652 cm^{-1} and 1670 cm^{-1} are attributed to unordered, α-helix and β-turn structures of BMP-2, respectively (Zeliha Guler et al., 2015). BMP-2 molecules binds to PCL/P3ANA nanofibers through the carboxyl group (–COOH) of P3ANA which shows an absorption band at 1690 cm^{-1} in the FTIR spectrum. After BMP-2 immobilization, the peak at 1690 cm^{-1} shifted to 1700 cm^{-1} and a new peak which is attributed to secondary structure of BMP-2 formed. ATR-FTIR spectrum of BMP-2 immobilized nanofibers indicates that BMP-2 is covalently attached onto PCL/P3ANA nanofibers.

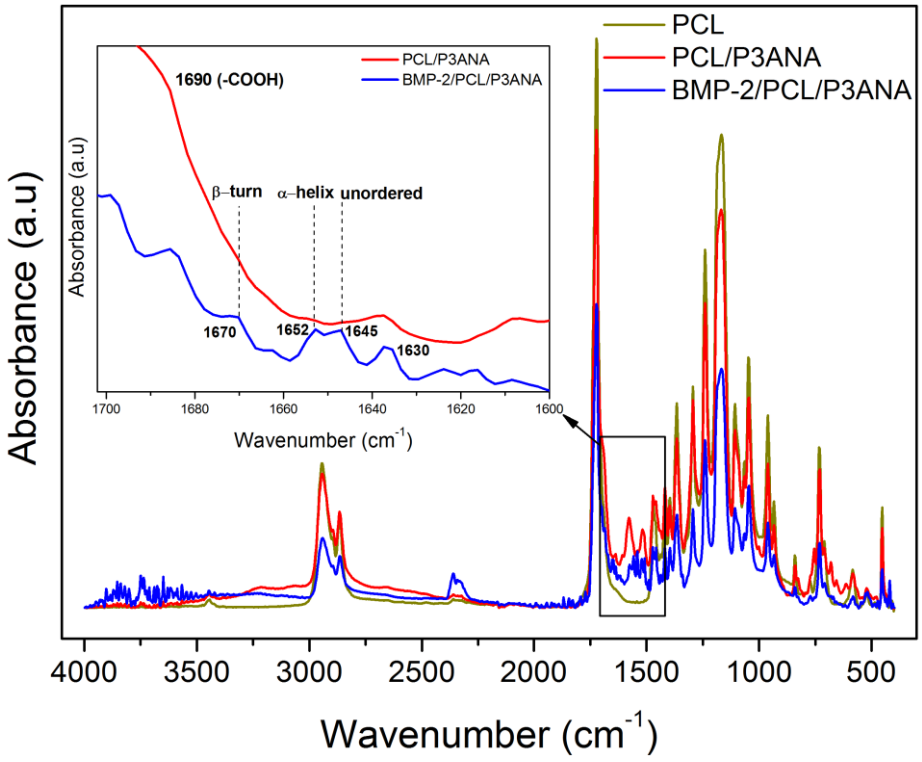

Figure 3.24 : ATR-FTIR spectra of PCL, PCL/P3ANA and BMP-2/PCL/P3ANA nanofibers. Inset: ATR-FTIR region for secondary structure of BMP-2/PCL/P3ANA.

FTIR-ATR spectra of PCL/P3ANA and RGD peptide immobilized nanofibers were represented in Figure 3.25. After RGD peptide immobilization, new peaks appeared in the spectrum of nanofibers. As stated earlier, the most sensitive region of FTIR spectrum for protein structural components is the 1700-1600 cm^{-1} region, which is mostly related with the C=O stretch vibrations of the peptide linkages (J.-S. Lim et al., 2014). The peak at 1560 cm^{-1} in the spectrum of PCL/P3ANA-RGD is attributed to bending modes of N-H bond of RGD (Ho et al., 2005). The peaks at 1740 cm^{-1}, 1650 cm^{-1} and 1540 cm^{-1} were attributed to the C=O stretching in ester group, C=O stretching of Amide I and N-H deformation of Amide II of RGD peptide (Figure 3.25-inset) (Yamazaki, 2007). RGD peptide binds to PCL/P3ANA nanofibers through the C=O in the carboxyl group (–COOH) of P3ANA which shows an absorption band at 1690 cm^{-1} in the FTIR spectrum. In the spectrum of PCL/P3ANA-RGD, the peak intensity of C=O streching was decreased. covalently attached onto PCL/P3ANA nanofibers.

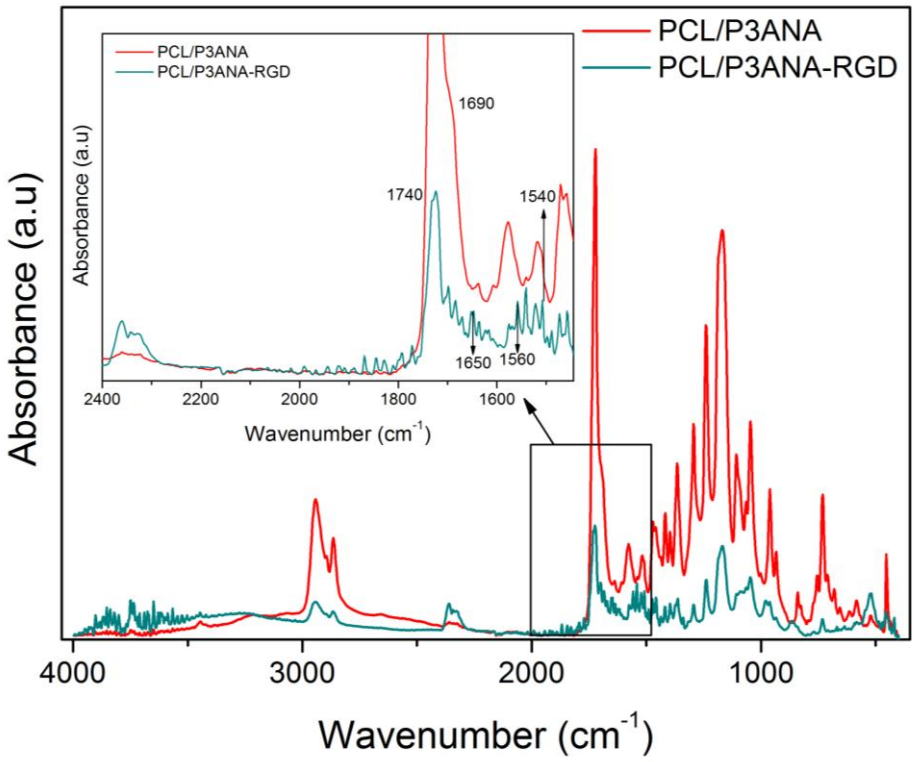

Figure 3.25 : PCL/P3ANA nanofibers and RGD-peptide immobilized nanofibers.

3.4.2 Determination of the amount of the covalently bound RGD and BMP-2

The amount of covalently bound BMP-2 onto nanofibers was determined by BCA protein assay (Figure 3.26). The initial BMP-2 amount was 50 ng/mL and after nanofibers treated with BMP-2 solution the amount of protein in the remaining solution decreased, since some protein attached physically or covalently to nanofibers. Approximately 42.6 ng of BMP-2 attached to PCL/P3ANA nanofibers activated with EDC/NHS. After two washing steps, physically adsorbed protein was removed from nanofibers and the amount of washed BMP-2 from non-activated nanofibers was higher compared to amount of BMP-2 washed from activated nanofibers. This result indicates that the attachment was physical on the non-activated nanofibers. On contrary, ~39 ng of BMP-2 remained attached to PCL/P3ANA nanofibers since attachment was covalent and achieved by EDC/NHS activation.

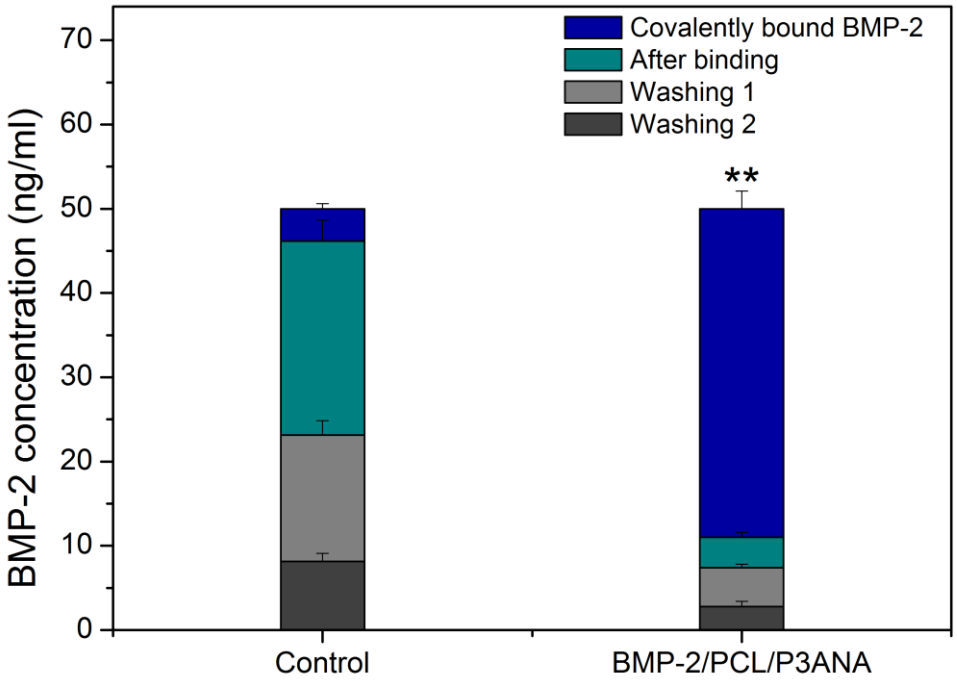

Figure 3.26 : Amount of initial and residual BMP-2 after each immobilization step. The asterisks indicate significant differences (** $p<0.01$).

The amount of immobilized RGD was determined by BCA protein assay (Figure 3.27). Activated nanofibers were treated with 5 μg/mL of RGD peptide solution and the concentration of RGD in the remaining solution after binding step (grey). This decrease indicates that RGD peptide was attached on the nanofibers via physical or chemical (covalent) interactions. In order to remove the physically attached RGD peptide, nanofibers were washed twice and the amount of RGD in the remainin solutions was determined. Great amount of RGD peptide was washed from non-activated nanofibers which indicated that RGD peptide was physically bounded onto the nanofibers. After two washing steps, the amount of RGD was 0.04 μg/mL and it was found that 4.08 μg/mL remained covalently attached onto the PCL/P3ANA nanofibers since the nanofibers were activated by EDC/NHS. BCA protein assay indicated that RGD peptide was covalently attached onto the nanofibers with the succes of ~80%.

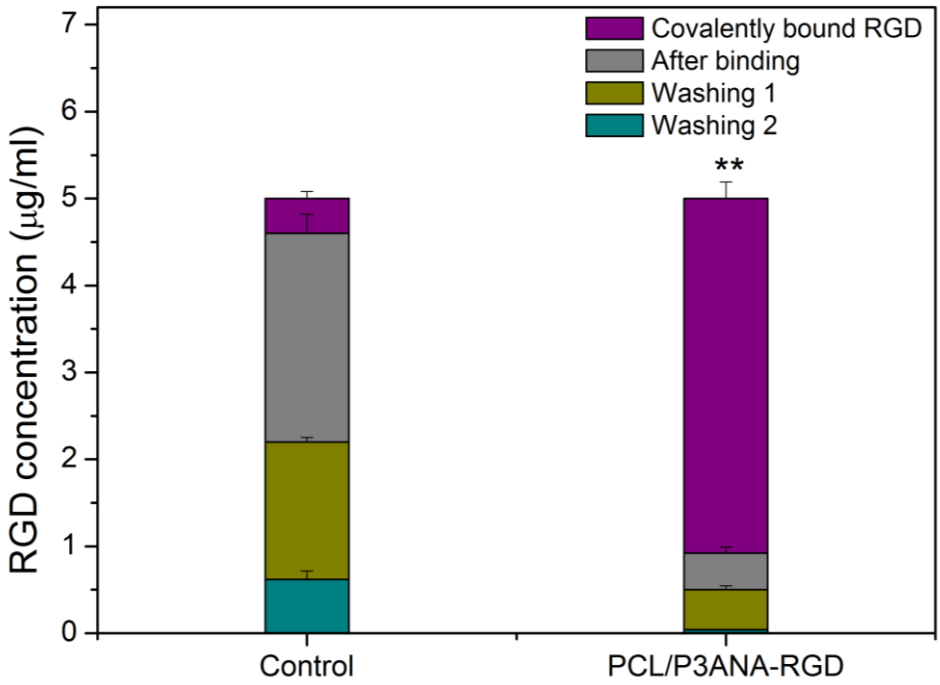

Figure 3.27 : Amount of initial and residual BMP-2 after each immobilization step. The asterisks indicate significant differences between covalently bound RGD amount on control and PCL/P3ANA nanofibers. (** $p<0.01$).

The presence and the distribution of the BMP-2 and RGD peptide on nanofibers were confirmed by EDX analyses. The morphology and elemental composition (Figure 3.28) of BMP-2 and RGD peptide immobilized PCL/P3ANA nanofibers were investigated by SEM/EDX. The average diameter of PCL/P3ANA, BMP-2/PCL/P3ANA and PCL/P3ANA-RGD nanofibers were 86±19 nm, 87±21 nm and 93±17, respectively. The elemental concentrations for nitrogen (N) and oxygen (O) were detected (Table 3.6) since BMP-2 and RGD peptide have nitrogen atoms in its structure. P3ANA has N atoms in its backbone, as well as BMP-2. Before biofunctionalization, the amount of O atoms (wt %) was 91.09 while N atom amounts (wt %) was 8.91 on the surface PCL/P3ANA nanofibers. The amount of N (wt %) on the surface of PCL/P3ANA increased to 9.80 wt% and 11.2 wt% after BMP-2 and RGD immobilization on nanofibers, respectively. EDX data indicates that the N atoms were introduced to the structure of nanofibers through covalent binding of the BMP-2 and RGD peptide.

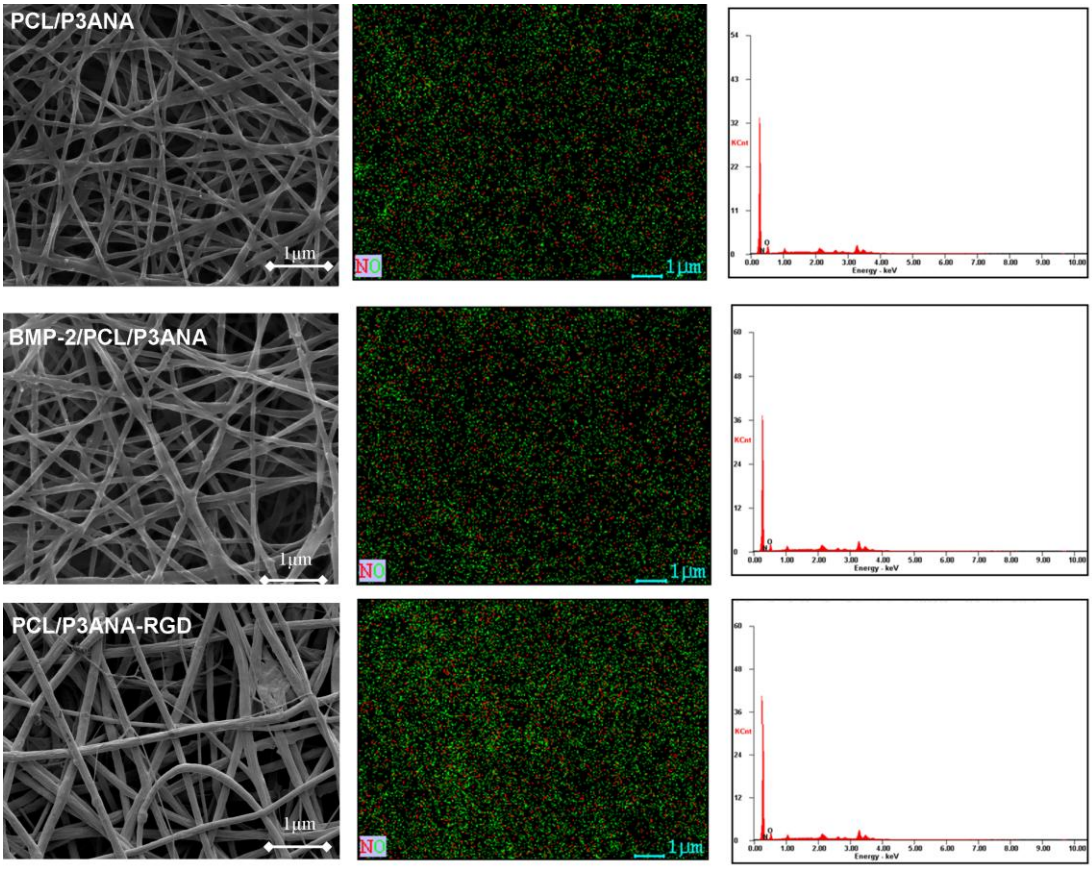

Figure 3.28 : SEM and EDX-mapping of PCL/P3ANA, BMP-2/PCL/P3ANA and PCL/P3ANA-RGD nanofibers.

Table 3.6 : Elemental concentrations of nitrogen and oxygen atoms in PCL/P3ANA nanofibers and BMP-2 immobilized nanofibers.

Samples	Elements (wt %)	
	N	O
PCL/P3ANA	8.91	91.09
BMP-2/PCL/P3ANA	9.80	90.20
PCL/P3ANA-RGD	11.20	88.80

3.4.3 Contact Angle Measurements of BMP-2/PCL/P3ANA and PCL/P3ANA-RGD nanofibers

The contact angles of PCL nanofibers decreased gradually with addition of P3ANA and BMP-2 or RGD peptide immobilization which point to a decrease in hydrophobic nature. PCL nanofibers had water contact angle of 133.6±0.4 °, which indicates a hydrophobic surface (Gomez, Alekseev, Aleksandrova, Brady, & Terzic, 1997; Safaeijavan, Soleimani, Divsalar, Eidi, & Ardeshirylajimi, 2013). After

addition of P3ANA to PCL nanofibers, the contact angle decreased to 108.2 ±2.7 °, which can be attributed to the presence of the carboxylic acid groups on P3ANA. The moderate hydrophobicity of PCL/P3ANA nanofibers is expected to favor cell attachment (Mohamad et al., 2015). BMP-2 immobilized nanofibers had the lowest contact angle (63.3±0.1 °) and BMP-2/PCL/P3ANA nanofibers were hydrophilic (Figure 3.29). RGD peptide immobilized nanofibers exhibited a contact value of 61.4±0.2 ° and resulted a hydrophilic nanofiber surface. This dramatic increase in contact angle value of nanofibers after RGD peptide immobilization proves the surface modification of nanofibers. Hydrophilicity of a surface is an important factor to enhance the interaction between cells and nanofibers by creating a favorable interface between them (Elzubair et al., 2006).

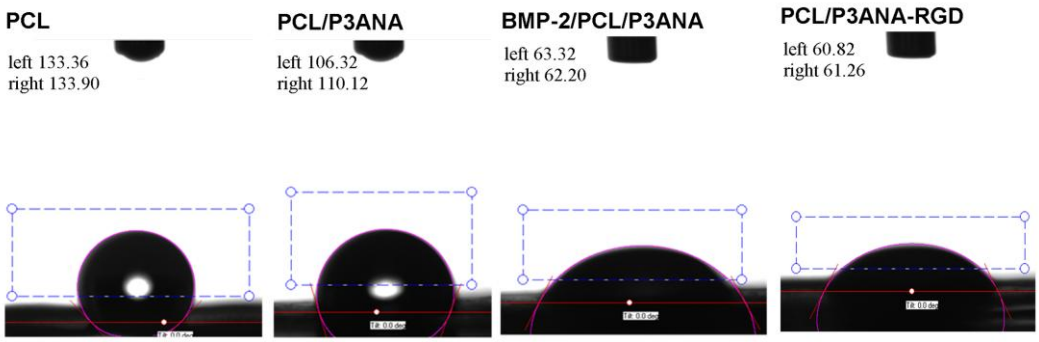

Figure 3.29 : Contact angles of PCL, PCL/P3ANA, BMP-2/PCL/P3ANA and PCL/P3ANA-RGD nanofibers.

3.4.4 EIS Measurements of BMP-2/PCL/P3ANA and PCL/P3ANA-RGD nanofibers

BMP-2 immobilization was also evidenced by electrochemical impedance spectroscopy (EIS) since it is a very sensitive method for detection of surface modification with a biomolecule (Gu et al., 2005; Z. Guler & Sarac, 2016). A significant difference in the impedance spectra between BMP-2/PCL/P3ANA and PCL/P3ANA nanofibers was observed due to the covalent immobilization of BMP-2 on nanofibers. In Nyquist plot (Figure 3.30), PCL/P3ANA nanofibers exhibited an almost linear behaviour before biofunctionalization. After covalent attachment of BMP-2 onto nanofibers, they had a semi-circle in their Nyquit plot. The linear line with high-slope in the Nyquist plot is related with capacitive behavior while the diameter of the semicircle of the plot represents the charge-transfer resistance (R_{ct}) (Golshaei et al., 2016; Zainudin et al., 2014). The measured impedance spectra were

analyzed in terms of electrical equivalent circuits to describe the physical properties of the system. The impedance spectra for PCL/P3ANA nanofibers is described by the equivalent circuit R(CR)(QR)W (Figure 3.30A) in shorthand. For BMP-2 immobilized PCL/P3ANA, the equivalent circuit R(CR)(CR)(QR)W (Figure 3.30B) was selected since there are additional electrical components (resistance and capacitance) arising from the immobilized protein. Fitting values for the equivalent circuit elements by the simulation of the impedance spectra of BMP-2/PCL/P3ANA and PCL/P3ANA-RGD nanofibers were given in Table 3.7. The electrochemical properties of the nanofibers and circuit elements before and after protein immobilization were explained in detail in the section "3.3.2. Electrochemical impedance spectroscopic measurements of albumin immobilized nanofibers". Charge transfer resistance of the PCL/P3ANA nanofibers was 12 kΩ and it increased to 40 kΩ with the covalent immobilization of BMP-2 onto the nanofibers. Covalent attachment of BMP-2 onto nanofibers caused an increase in charge transfer resistance since a layer at the interface between electrolyte and nanofiber surface was formed due to immobilized BMP-2 (Pauliukaite et al., 2010; Sophia et al., 2012). Also, the increase in charge transfer resistance in the BMP-2/PCL/P3ANA nanofibers can be explained by the different interfacial structures, assuming different structures or sizes of protein and nanofibers (Y. Wang et al., 2009).

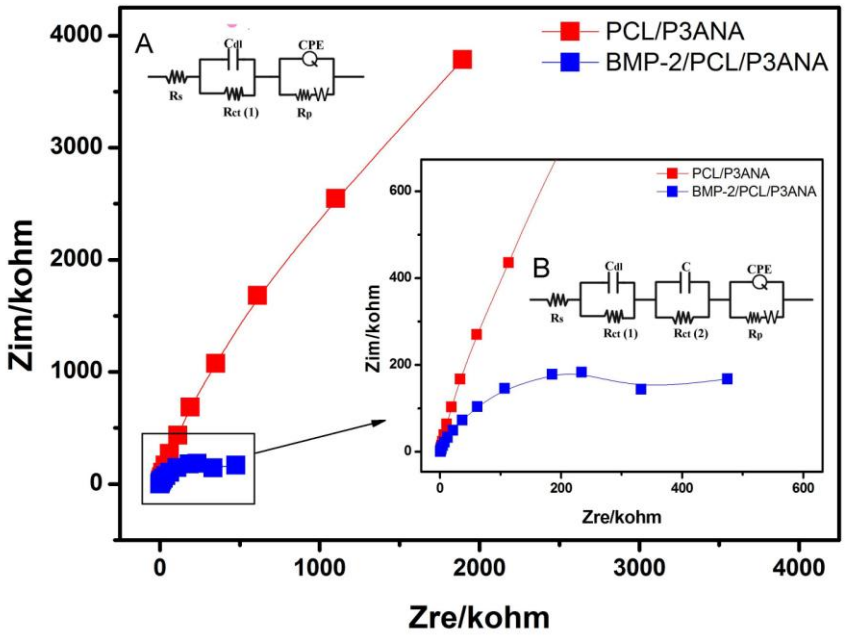

Figure 3.30 : Nyquist plots of PCL/P3ANA and BMP-2/PCL/P3ANA nanofibers. The equivalent circuits used for the simulation for EIS data of PCL/P3ANA (A) and BMP-2/PCL/P3ANA (B) nanofibers.

The Nyquist plot for PCL/P3ANA-RGD showed significantly different behavior from unfunctionalized nanofibers and additional components were added to the circuit to describe the resistance and capacitance arising from the immobilized protein. The R_{ct} of PCL/P3ANA (12 kΩ) was dramatically increased to 61.3 kΩ after RGD peptide immobilization due to the differences in sizes or structures of the nanofibers and RGD peptide (Pauliukaite et al., 2010). Also, as supported with contact angle measurements (Figure 3.31), the RGD peptide immobilization modificated the surface of nanofibers probably by forming an additional layer. This additional protein layer on the nanofiber surface lead to an increase in R_{ct} and a decrease in double layer capacitance (C_{dl}) values. The decrease in C_{dl} is attributed to increase in thickness of electronic double layer depending on the RGD immobilization (Sophia et al., 2012).

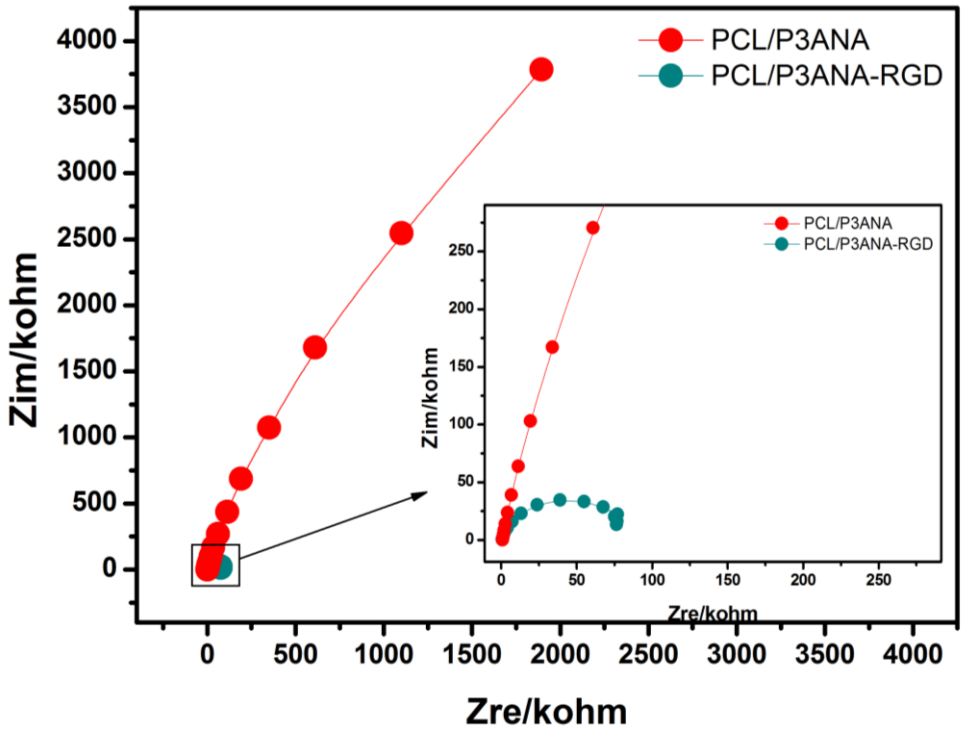

Figure 3.31 : Nyquist plots of PCL/P3ANA and PCL/P3ANA-RGD nanofibers.

Table 3.7 : Fitting values for the equivalent circuit elements by the simulation of the impedance spectra of BMP-2/PCL/P3ANA and PCL/P3ANA-RGD nanofibers.

	Rs(Ω)	C_{dl} (μF)	R_{ct}(1) (kΩ)	Rct(2) (kΩ)	C (μF)	Q(CPE) (10^{-6})(Ω^{-1})	Rp(kΩ)	W(10-5) ($Ssec^5/cm^2$)	n	Chi-squared error (10^{-4})
PCL/P3ANA R(CR)(QR)W	840.2	9.36	12.00	-	-	2.58	13.37	26.61	0.9	8.99
BMP2/PCL/P3ANA R(CR)(CR)(QR)W	517.5	1.30	20.79	7.67	40.58	4.54	22.0	21.42	0.7	4.40
PCL/P3ANA-RGD R(CR)(CR)(QR)W	683.1	2.15	61.30	11.14	109.5	7.68	28.34	121.00	0.8	1.35

3.5 Cell culture studies on BMP-2/PCL/P3ANA and RGD/PCL/P3ANA nanofibers

3.5.1 Cytotoxicity of nanofibers

The cytotoxicity of PCL, PCL/P3ANA and BMP-2 or RGD peptide immobilized nanofibers were determined by *in vitro* toxicology using the MTT assay after culturing Saos-2 cells on nanofibers for 1 day (Figure 3.32). MTT assay is based on the detection of the purple formazan crystals whose amount is proportional to the number of viable and adherent cells, since only metabolically active cells are able to produce dehydrogenase enzymes on their mitochondria and reduce the yellow tetrazolium salt to purple formazan crystals. The viability of Saos-2 cells cultured on nanofibers was compared with the viability of the cells seeded on cover glasses. The relative viability of Saos-2 cells was about 92 %, 91 %, 94 % and 93% after incubation with PCL, PCL/P3ANA, BMP-2/PCL/P3ANA and PCL/P3ANA-RGD nanofiber mats, respectively. Cell viability is in correlation with cellular adhesion (Chua et al., 2005; Kar, Pandey, & Rana, 2014) and structure of the scaffold (Zonari et al., 2012). Nanofibers showed to be nontoxic and enable for cell attachment and growth (Tan, Dalilottojari, Pingguan-Murphy, Ahmad, & Akbar, 2014).

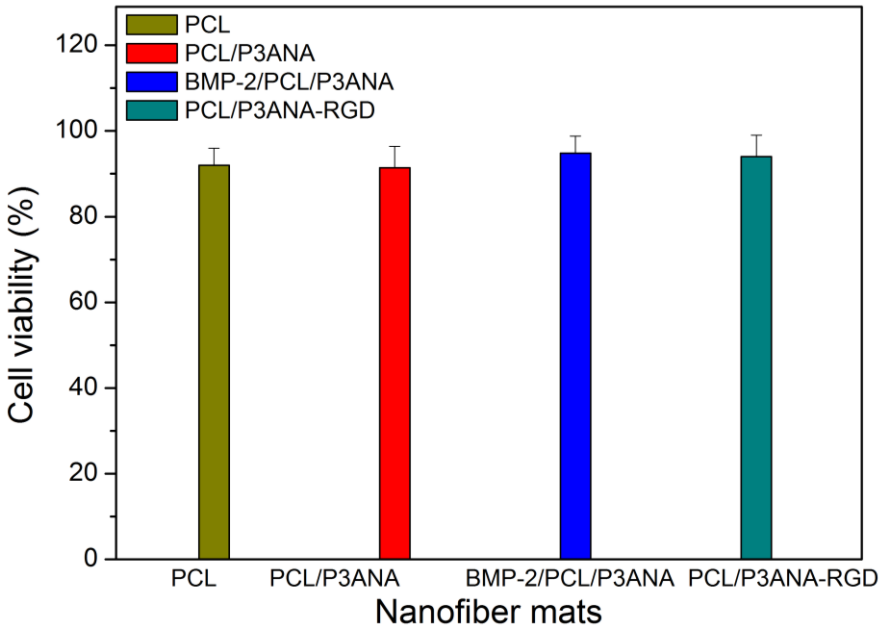

Figure 3.32 : Relative viability of Saos-2 cells cultured on PCL, PCL/P3ANA, BMP-2/PCL/P3ANA and PCL/P3ANA-RGD nanofibers for 1 day.

3.5.2 Cell proliferation

Resazurin test was used to measure the proliferation of cells cultured on PCL, PCL/P3ANA, BMP-2/PCL/P3ANA and PCL/P3ANA-RGD nanofibers. Quantitative evaluation of cells was performed every two days, until the 9th day of culture (Figure 3.33). Resazurin is a non-toxic dye which allows continuous measurement of cell populations by indicating whether cells are able to metabolize resazurin to resorufin. The metabolic rate is directly proportional to the number of viable cells (Zhang et al., 2009). The number of cells cultured on nanofibers was compared to cells on cover glasses. All nanofiber mats were able to sustain cell adhesion and proliferation. An increase in resazurin reduction from day 1 to day 9 was observed, which indicates an increase in cell number. Higher cell proliferation was observed on nanofibers compared to cover glass surface. This can be attributed to the porous structure of the nanofibers (Patrício, Domingos, Gloria, & Bártolo, 2013) since it is known that smooth surfaces reduce cell attachment and proliferation (Tryoen-Tóth et al., 2002). At day one, even though cell proliferation onto nanofibers was higher compared to coverglass, there was no significant difference between PCL, PCL/P3ANA and BMP-2/PCL/P3ANA nanofibers. This result was in correlation with MTT data which obtained after 1 day and related with adhesion of cell onto nanofibers. The cell proliferation was the highest for the RGD peptide immobilized nanofibers. From 3

day, the addition of P3ANA to the nanofiber structure enhanced cell adhesion and proliferation compared to PCL nanofibers, an effect that can possibly be ascribed to the hydrophilic nature of P3ANA. From day 3 to 9, the highest proliferation was observed when the cells were cultured on RGD biofunctionalized nanofibers. BMP-2 immobilization also significantly favored cell proliferation compared to PCL and PCL/P3ANA nanofibers. PCL/P3ANA-RGD and BMP-2/PCL/P3ANA nanofibers significantly favoured the attachment and proliferation of Saos-2 cells compared to coverglass and nanofibers of PCL and PCL/P3ANA.

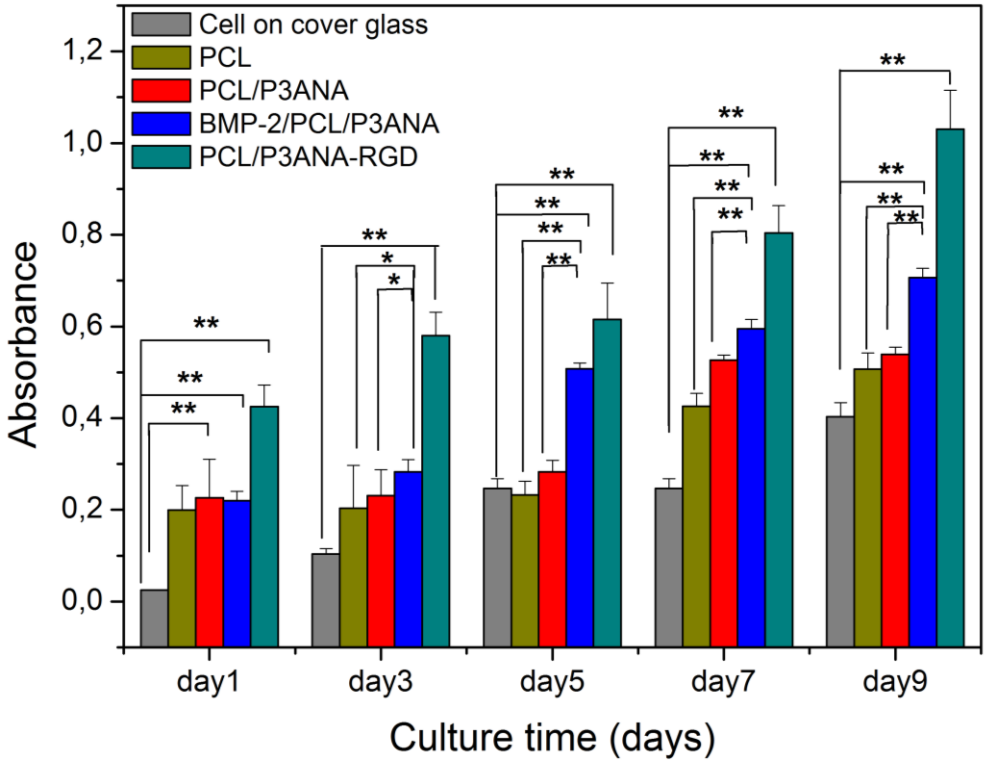

Figure 3.33 : Cell proliferation on nanofibers according to the resazurin assay. The asterisks indicate significant differences (*p<0.05 and ** p<0.01).

These results for the difference in proliferation behavior of cells were also evidenced with SEM images of cell distribution in nanofiber scaffolds after 9 days culture (Figure 3.34). Beside the quantification of the number of cells, cellular behavior is also an important parameter to determine the potential usage of materials for tissue engineering scaffolds. SEM images of nanofibers showed that cells adhered on the surfaces of the PCL, PCL/P3ANA, BMP-2/PCL/P3ANA and PCL/P3ANA-RGD nanofibers which indicate that nanofiber scaffolds possessed biocompatibility for cell attachment (Haider et al., 2014). The cells attached on PCL, PCL/P3ANA and BMP-

2/PCL/P3ANA nanofibers were elongated and oriented along the fiber. The cells cultured on PCL/P3ANA-RGD nanofibers were proliferated by spreading on the nanofiber mat and covered the scaffold (Serafim, Mallet, Pascaretti-Grizon, Stancu, & Chappard, 2014). In correlation with resazurin test, the number of cells on the PCL/P3ANA-RGD nanofibers was highest compared to PCL and PCL/P3ANA nanofibers suggesting that RGD was effective to enhance the cell attachment and the interaction between cells and nanofibers.

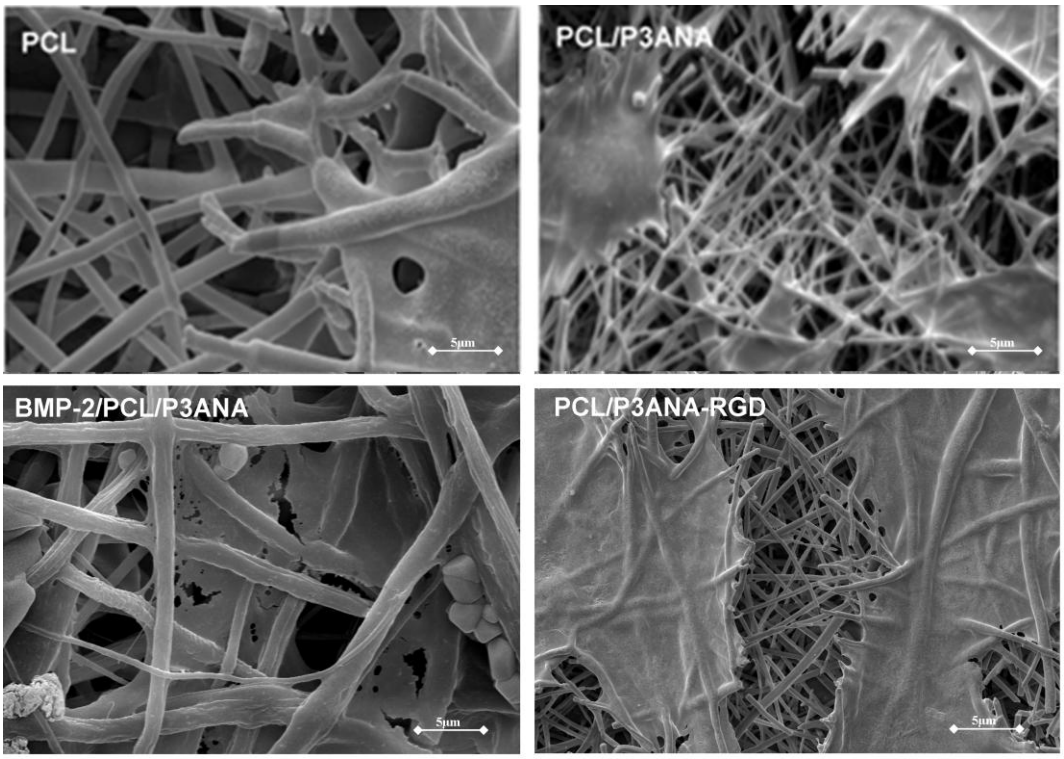

Figure 3.34 : SEM images of Saos-2 cells cultured on glass coverslips PCL, PCL/P3ANA, BMP-2/PCL/P3ANA and PCL/P3ANA-RGD nanofibers.

3.5.3 Immunofluorescence staining

Cell morphology and adhesion behavior on the nanofibers was investigated by fluorescent staining (Figure 3.35). Saos-2 cells adhered and spread on both cover glasses and nanofibers. The phalloidin stained actin in cells on PCL and PCL/P3ANA nanofibers is oriented in a direction parallel to the main cellular axis while cells seeded on coverslip exhibit a shorter morphology and random organization (Y. J. Park et al., 2006). Cell morphology on the PCL and PCL/P3ANA nanofibers is similar to each other. Cells exhibit elongated and spindle-like morphology which is characteristic for Saos-2 cell line (Tuzlakoglu et al., 2005).

However, the adhesion and spreading of the cells on cover glass was limited compared to cells on nanofibers. It can be observed that PCL, PCL/P3ANA, BMP-2/PCL/P3ANA and PCL/P3ANA-RGD nanofibers supported cell attachement and cell growth (Cho et al., 2014). Saos-2 cells on PCL or PCL/P3ANA nanofibers were polygonal in shape while cells on BMP-2 functionalized nanofibers exhibited osteocyte-like morphology (Prideaux et al., 2014). Cell morphology on the PCL/P3ANA-RGD nanofibers was similar to those on PCL and PCL/P3ANA nanofibers. BMP-2/PCL/P3ANA nanofibers induced adherent-cell type actin stress fibers (Y. J. Park et al., 2006) while PCL or PCL/P3ANA nanofibers did not induce actin extensions. These results indicate that all the nanofibers enhance cell attachment and proliferation and the PCL/P3ANA nanofibers functionalized with BMP-2 are biologically active by promoting actin-stress-fiber formation in the cells. The adhesion and spreading of the cells on nanofibers was favored compared to cells on cover glass which was in correlation with resazurin test and SEM images.

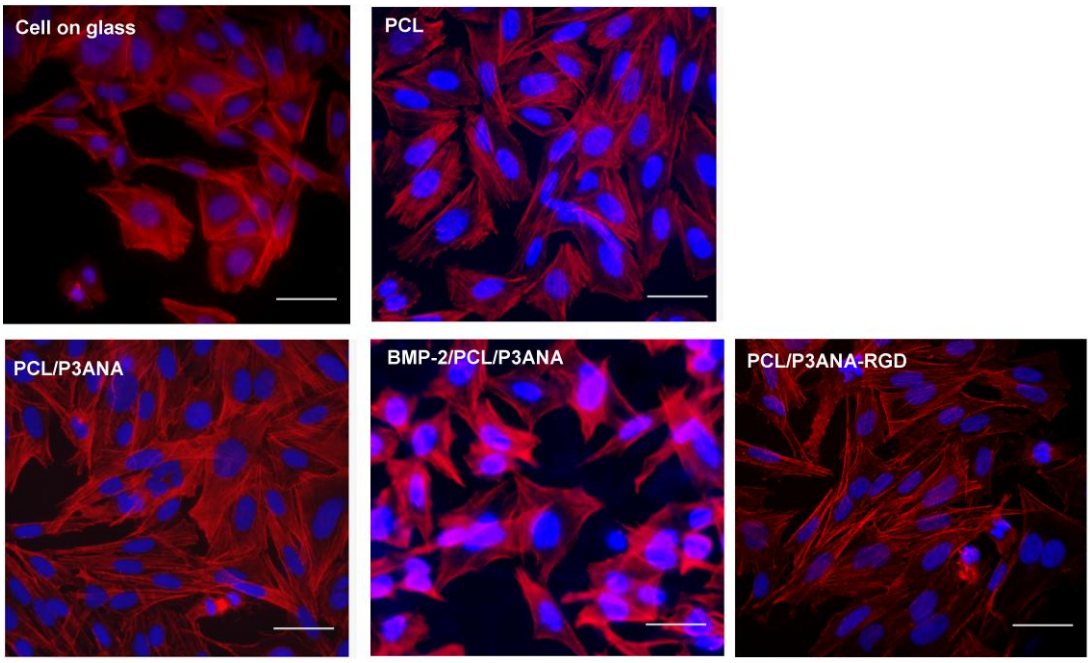

Figure 3.35 : Morphology of Saos-2 cells cultured on glass coverslips, PCL, PCL/P3ANA, BMP-2/PCL/P3ANA and PCL/P3ANA-RGD. Fluorescence images of staining for F-actin (red) and nuclei (blue) in cells (scale bar= 50 µm).

3.5.4 Alkaline phosphatase activity

ALP is an enzyme which plays an important role in bone matrix mineralization process and therefore a good marker of osteogenic phenotype (Liu, Sanghvi, Burnell,

& Howard, 1987). ALP activity of Saos-2 cells cultured for 14 days on cover glass, PCL, PCL/P3ANA, BMP-2/PCL/P3ANA and PCL/P3ANA-RGD nanofibers is represented in Figure 3.36. The ALP activity of cells on nanofibers was higher than that of those on cover glass. RGD immobilization increased the ALP activity of the cells which is in correlation with reported data in the literature (Beuvelot et al., 2009; Sofia et al., 2001; X. Wang et al., 2014). Cells on BMP-2 immobilized nanofibers exhibited the highest ALP activity. ALP activity is closely associated with sites of active bone formation (Vaziri, Vahabi, Torshabi, & Hematzadeh, 2012) and Saos-2 cells can differentiate into osteocyte-like cells under mineralizing conditions. The presence of BMP-2 on nanofibers induced the transition of cells to osteocyte-like cells (Prideaux et al., 2014). Saos-2 cells exhibit several osteoblastic features and synthesize ALP and mineral deposits and bone-related molecules (Beuvelot et al., 2009). ALP is an an early bone marker and enzyme which has essential role for bone matrix mineralization process and ossification (F. Yang et al., 2005).

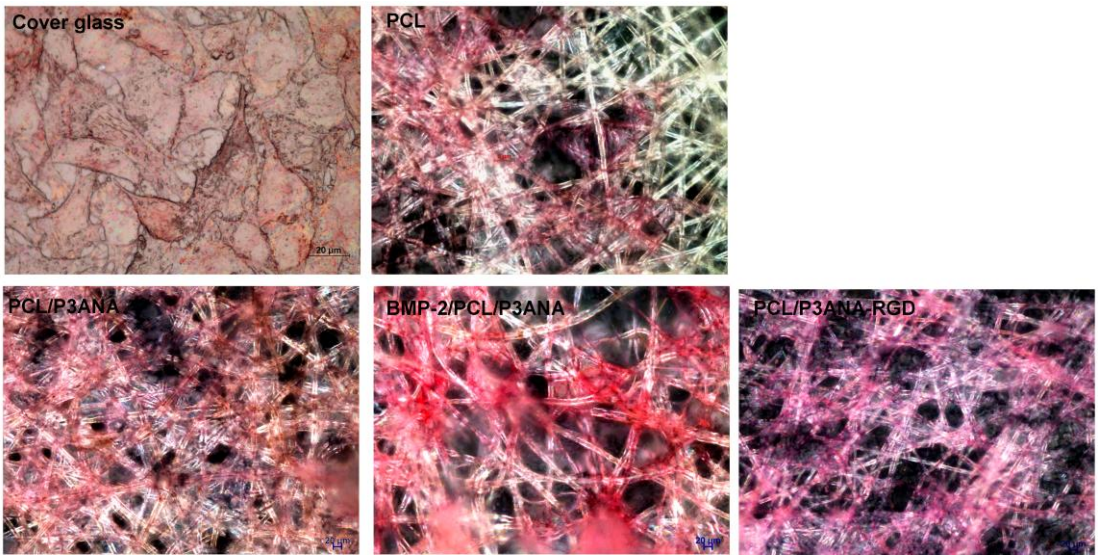

Figure 3.36 : ALP activity of cells on glass coverslips, PCL, PCL/P3ANA, BMP-2/PCL/P3ANA and PCL/P3ANA-RGD.

3.5.5 Mineralization Assay

Saos-2 cells were stained with Alizarin red S, which forms complexes with calcium, to monitor the presence of calcium deposits on day 14 (Figure 3.37). Calcium deposits, which are important indications of the middle stage of osteogenesis were detected by staining on day 14. Calcium deposits were observed as red/orange nodules in the areas of cell growth (Figure 3.37) (Hwang et al., 2008). The images

obtained after Alizarin red S staining correlates with the literature (Hwang et al., 2008; B. S. Kim et al., 2015). Compared to cover glass, the amount of calcium deposits are higher when cells cultured on PCL/P3ANA, BMP-2/PCL/P3ANA and PCL/P3ANA-RGD nanofibers. BMP-2 immobilized nanofibers displayed the highest amount of calcium deposits among all nanofibers and cover glass, which indicates a higher degree of osteogenesis (C.-H. Chang et al., 2015). The amount of calcium deposits on the cells cultured on the PCL/P3ANA-RGD nanofibers were higher compared to PCL and PCL/P3ANA nanofibers, which indicates a higher osteogenic activity (C.-H. Chang et al., 2015). After 14 days, both ALP activity and Ca deposition were increased on the BMP-2 and RGD immobilized nanofibers which is supported by the previous studies (Evangelista et al., 2007; Shin et al., 2005). When the ALP activity and Ca deposition results evaluated, the general trend found in these assays correlated well with that of the proliferation results obtained from Rezasurin assay and SEM. RGD peptide immobilized materials supports not only the adhesion and proliferation but also the cellular functions (Lee et al., 2007). The enhanced osteogenic activity of the cells on RGD peptide immobilized nanofibers can be related with favored cell attachement and its correlation with long-term cellular function (Shin et al., 2005).

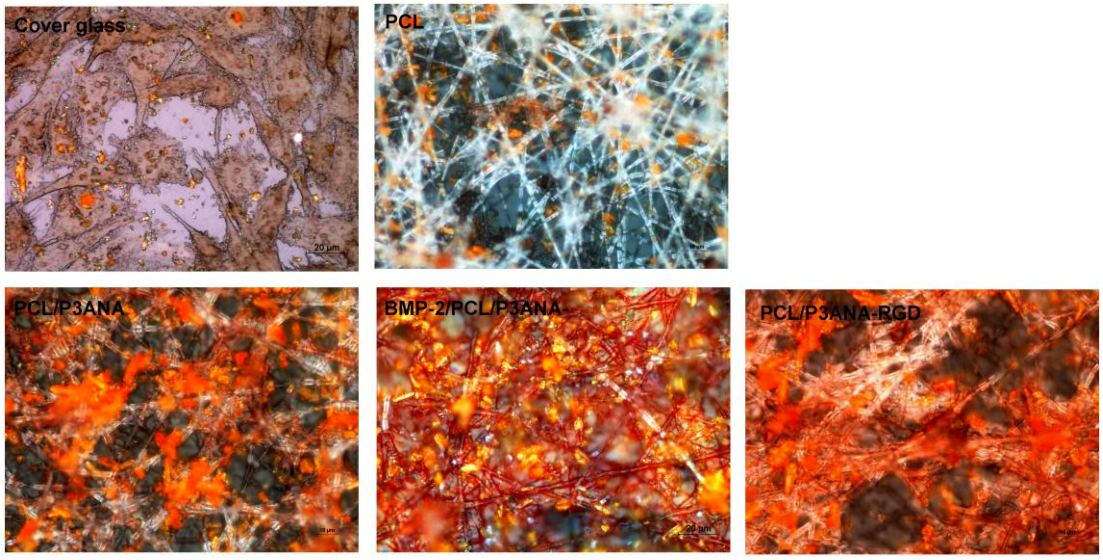

Figure 3.37 : Alizarin red S staining of Saos-2 cells on glass coverslips, PCL, PCL/P3ANA, BMP-2/PCL/P3ANA and PCL/P3ANA-RGD.

3.6 Electrical stimulation of BMSCs on PCL/P3ANA nanofibers

Stem cells have the capacity to develop and differentiate into their fate in vitro in the presence of a chemical or physical stimulation. Different types of cells have different differentiation lineages, which involve specific pathways. Electrical stimulations have positive effect on bone regeneration, therefore bone marrow mesenchymal stem cells (BMSCs) which can differentiate into osteogenic lineage were used to study the effect of electrical field on to the differentiation of the cells into bone feature.
There must be suitable support which can provide an electrical field to the cells. The PCL/P3ANA nanofibers were used in electrical stimulation of BMSCs since P3ANA as a conductive polymer delivers electrical signal directly to the cells cultured on the nanofiber. BMSCs were cultured on the conductive PCL/P3ANA nanofibers and stimulated electrically. The effect of electrical stimulation on to the viability and proliferation of cells as well as the the osteogenic activity was determined.

3.6.1 Cell viability after electrical stimulation

The cell viability was assessed by in vitro toxicology using the MTT assay after culturing BMSCs onto the PCL/P3ANA nanofibers for 2 days and applying electrical stimulation on the third day. The cells cultured onto the PCL/P3ANA nanofibers without electrical stimulation were used as control. Figure 3.38 represents the cell viability according to applied AC voltage and frequency. The viability of cells was the highest when frequency of 1 kHz was applied. At 1 kHz frequency, the cell viability was 78 % and 88% for the cells stimulated with 200 mV/mm and 400 mV/mm AC voltage. At 0.5 kHz frequency, the cell viability was decreased (71 % for 200 mV/mm and 78% for 400 mV/mm) compared to viability at 1 kHz. At frequency of 0.5 kHz and 1 kHz, the highest viability was observed when cells stimulated with 400 mV/mm. When 800 mV/mm AC voltage at any frequency was applied, cell viability was below 50%. The frequencies of 5 kHz and 10 kHz caused a dramatic decrease in cell viability; more than half of the cells were dead after applying high frequencies. The cell death at higher voltage and frequencies can be related with the rupture of the cell membrane and thus with the disruption of normal functions of the cells (Min et al., 2014). In order to avouid the cell stress and compromising the viability of the cells, it was decided to continue the cell culture

experiments with frequency values of 0.5 kHz and 1 kHz which exhibited good cell attachment.

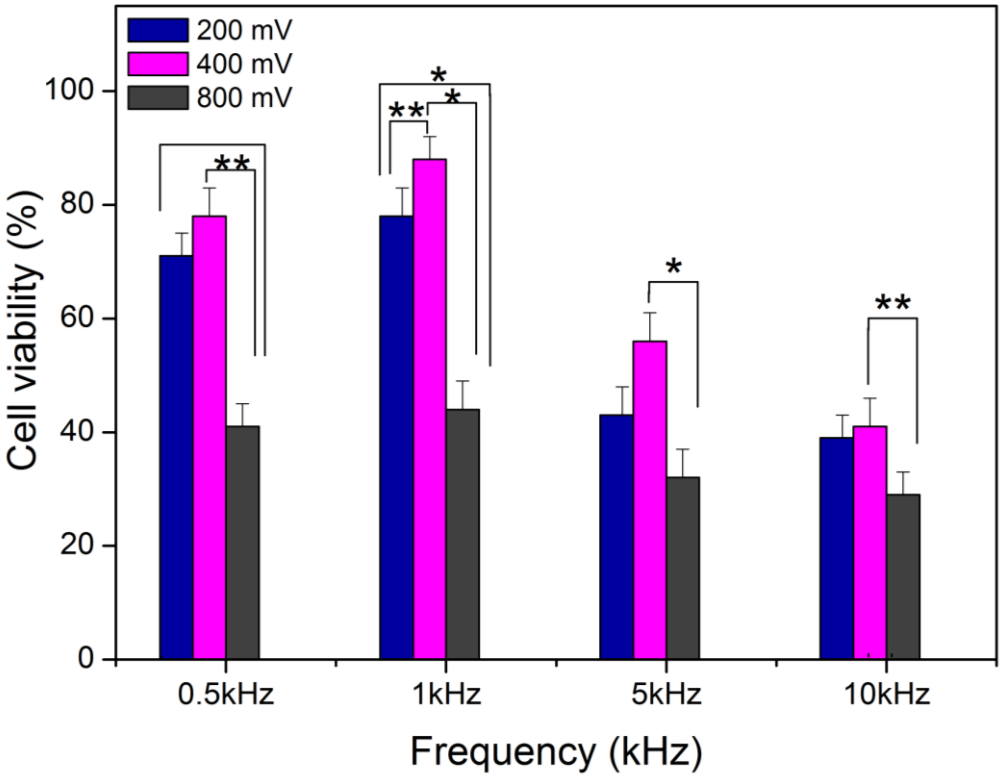

Figure 3.38 : Relative viability of BMSCs cultured on PCL/P3ANA nanofibers with electrical stimulation at different frequency (0.5 kHz, 1 kHz, 5 kHz and 10 kHz) and AC voltages (200 mV, 400 mV and 800 mV).

3.6.2 The effect of electrical stimulation on cell proliferation

Resazurin test was used to measure the proliferation of cells after stimulated with 0.5 kHz (Figure 3.39) and 1 kHz (Figure 3.40) frequency at increasing AC voltage (200 mV/mm, 400 mV/mm and 800 mV/mm). For both 0.5 kHz and 1 kHz frequency, an increase in resazurin reduction, thus in cell number from day 1 to day 9 was observed when cells stimulated either with 200 mV/mm and 400 mV/mm. In correlation with MTT data, 800 mV AC voltage inhibited the cell attachment and proliferation. The high voltage was found to be detrimental to BMSCs and to have an adverse effect on the cell proliferaiton. Higher voltages or frequencies affect the adhesion and proliferation of cells by disturbing cell membrane (Markx, 2008; Sebastian, Buckle, & Markx, 2007). 1 kHz frequency enhanced the cell proliferation more than 0.5 kHz. From day 1, the highest cell proliferation was observed when the cells stimulated

with 400 mV AC voltage at 1 kHz frequency. It can be related with induction of voltage-gated calcium ion channel on the cell membrane (Brighton et al., 1985). Because 400 mV exceeds the the transmembrane potential (100 mV) threshold and results transduction of cellular signals through Ca-ion channel which alters the Ca ion concentration in the cells (Lorich et al., 1998).

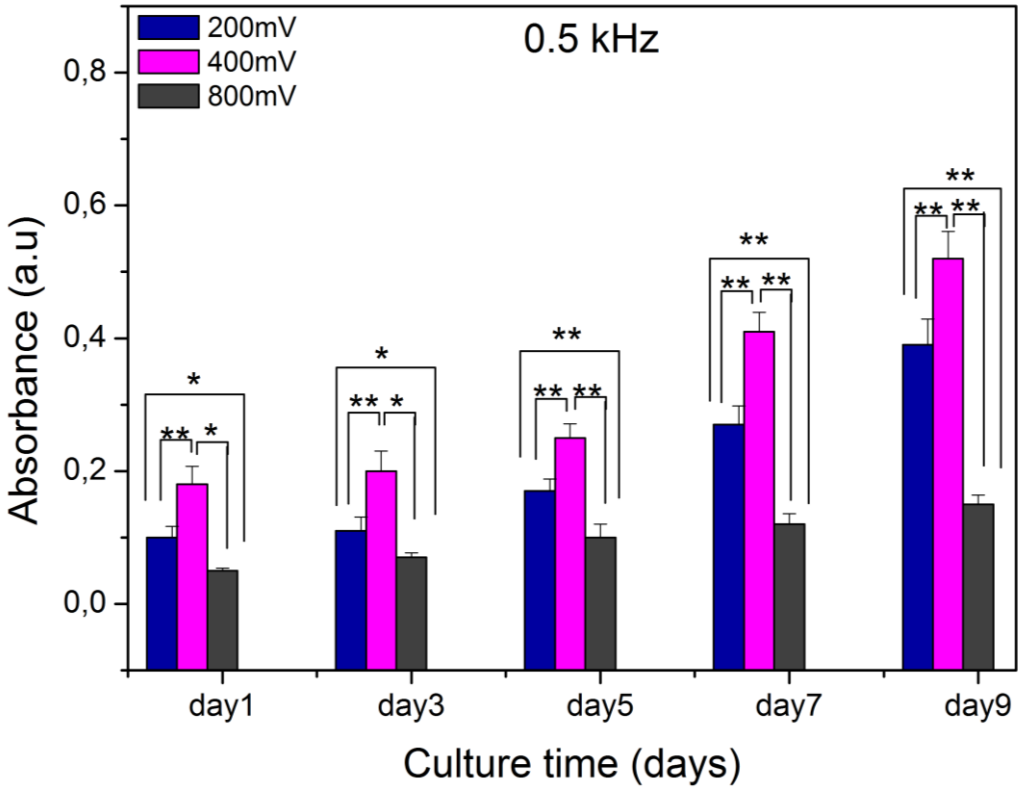

Figure 3.39 : Cell proliferation on PCL/P3ANA nanofibers depending on applied voltage at 0.5 kHz. The asterisks indicate significant differences (*p<0.05 and ** p<0.01).

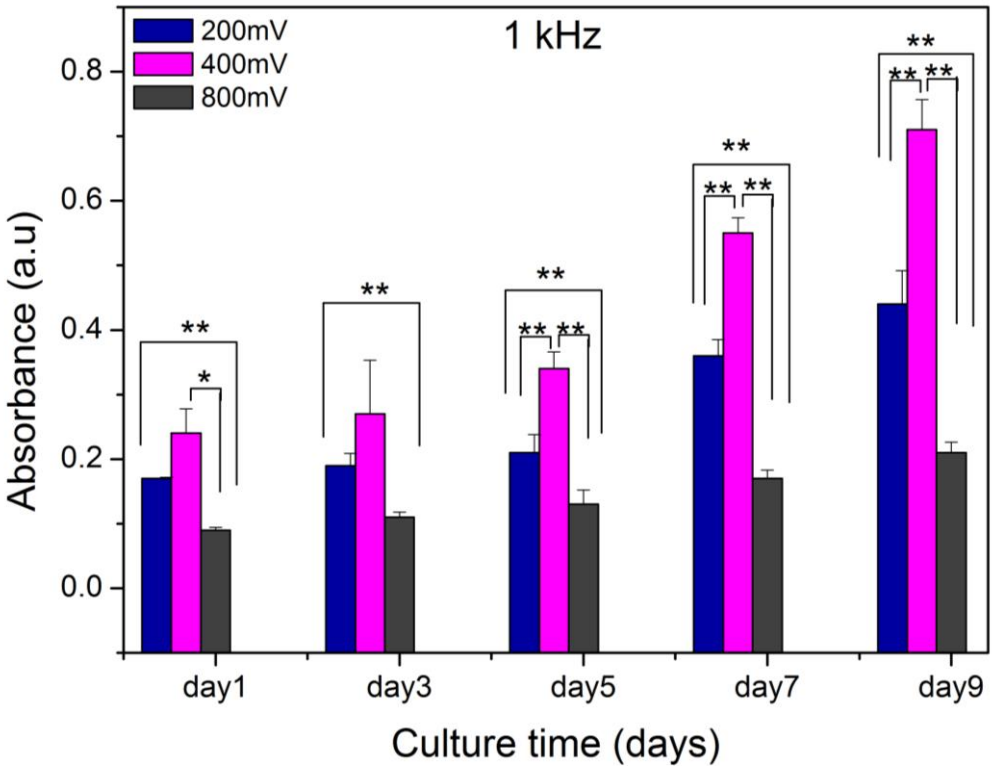

Figure 3.40 : Cell proliferation on PCL/P3ANA nanofibers depending on applied voltage at 1 kHz. The asterisks indicate significant differences (*p<0.05 and ** p<0.01).

3.6.3 The effect of electrical stimulation on the morphology of BMSCs

The distribution and spreading of the BMSCs which were stimulated with 0.5 kHz (Figure 3.41) and 1 kHz (Figure 3.42) frequency at increasing AC voltage (200 mV, 400 mV and 800 mV) after 9 days culture were monitored with SEM. These SEM images for the difference in proliferation behavior of the cells were in correlation with resazurin reduction obtained at 9^{th} day of culture. SEM images of BMSCs showed that cells adhered on the surfaces of the nanofibers after stimulated at 0.5 kHz and 1 kHz with the voltages of 200 mV/mm and 400 mV/mm which indicated that electrical stimulation favored cell attachment and proliferation (Haider et al., 2014). The morphology of the cells is an important indicator to understand the material is whether suitable as tissue engineering scaffold or not. Also, morphology of cells can help us to understand the impact of the electrical stimulation on the cells. The cells cultured on the PCL/P3ANA nanofibers under electrical stimulation, proliferated by spreading on the nanofiber mats and covered the scaffold (Serafim et al., 2014). In correlation with the resazurin test, the number of cells after stimulated at 1 kHz frequency was higher compared to ones at 0.5 kHz. The cells stimulated

with 800 mV/mm at both frequency (0.5 kHz and 1 kHz) did not spread on the nanofiber mat, which can be related with low viability under these conditions. SEM images indicated that P3ANA in the nanofiber structure was capable of delivering electrical signal to the cells and the 400 mV/mm at 1 kHz frequency was the most effective electrical stimulation condition in enhancing attachment and proliferation of the BMSCs.

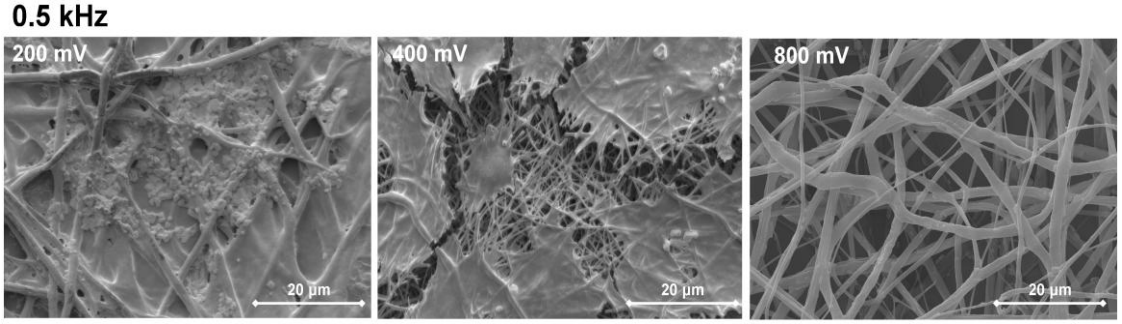

Figure 3.41 : SEM images of BMSCs on PCL/P3ANA nanofibers depending on applied voltage at 0.5 kHz.

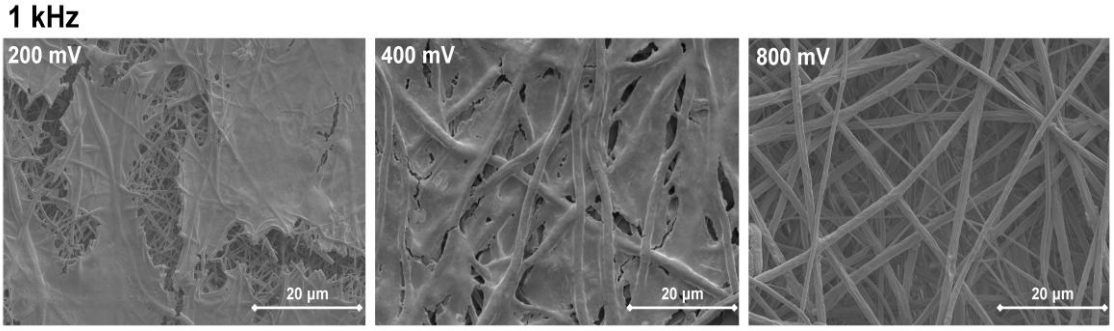

Figure 3.42 : SEM images of BMSCs on PCL/P3ANA nanofibers depending on applied voltage at 1 kHz.

The cell morphology of BMSCs cultured on the PCL/P3ANA nanofibers under electrical stimulation was characterized by fluorescence staining at 14 th day of culture. The phalloidin stained actin in the cells while DAPI was used for nuclei staining. As observed with SEM, the fluorescence images also showed that the cells stimulated at frequency of 0.5 kHz (Figure 3.43) exhibited limited spreading compared to the cells cultured under the frequency of 1 kHz (Figure 3.44). The BMSCs stimulated under 800 mV/mm voltage at the frequency of 0.5 kHz or 1 kHz exhibited rounded morphology. The cell density at this voltage (800 mV/mm) was lower compared to other voltages (200 mV/mm and 400 mV/mm) which was in

correlation with resazurin test and SEM images. Fluorescence images of BMSCs after stimulation with 800 mV/mm voltage supported the decreased viability at this applied voltage. 800 mV/mm voltage showed an adverse effecte on the stable cell attachment and cell coverage (Cho et al., 2014). The morphology of the BMSCs stimulated with 200 mV/mm and 400 mV/mm voltages showed notable difference. The cells under these conditions were widely spreaded and distributed randomly throughout the nanofibers (Madhurakkat Perikamana et al., 2015). Under these conditions (voltages of 200 mV/mm, 400 mV/mm and frequencies of 0.5 kHz and 1 kHz), BMSCs showed osteocyte-like morphology (Prideaux et al., 2014) and the applied voltages and frequencies favored adherent-cell type actin extensions (Y. J. Park et al., 2006). In parallel to the results of resazurin and SEM, it was found that 400 mV/mm at 1 kHz promoted more actin-fiber formation compared to 200 mV/mm voltage. Fluorescence staining images indicated that 200 mV/mm, 400 mV/mm at 0.5 kHz and 1 kHz enhaced the cell attachment, proliferation and osteogenic activity.

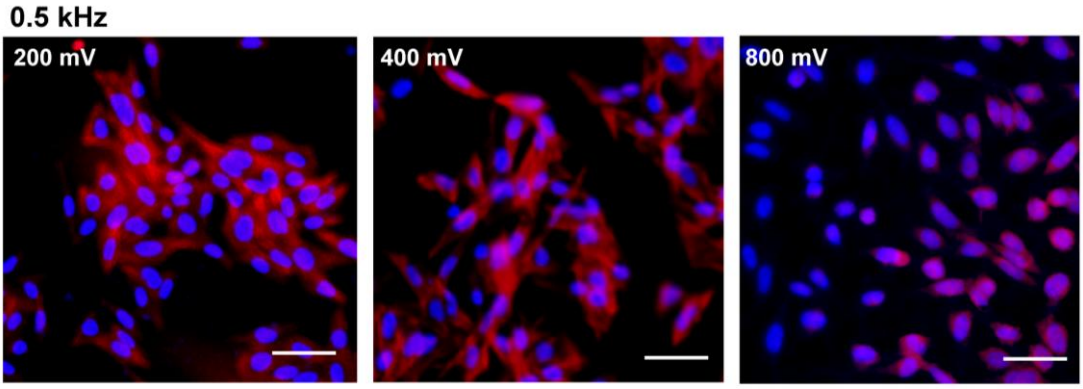

Figure 3.43 : Morphology of BMSCs on PCL/P3ANA nanofibers depending on applied voltage at 0.5 kHz. Fluorescence images of staining for F-actin (red) and nuclei (blue) in cells (scale bar= 50 μm).

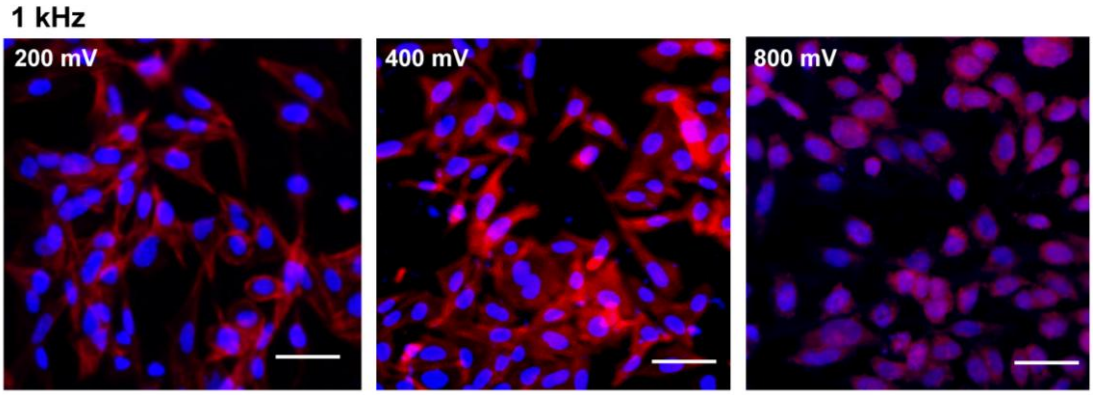

Figure 3.44 : Morphology of BMSCs on PCL/P3ANA nanofibers depending on applied voltage at 1 kHz. Fluorescence images of staining for F-actin (red) and nuclei (blue) in cells cultured for 3 days (scale bar = 50 μm).

3.6.4 The effect of electrical stimulation on alkaline phosphatase activity

The effect of electical stimulation on the osteogenic differentiation and activity of BMSCs was investigated by staining for ALP and Ca deposits by Alizarin red S. The BMSCs cultured on the nanofibers under AC voltage (200 mV, 400 mV and 800 mV) at 0.5 kHz (Figure 3.45) and 1 kHz (Figure 3.46) frequency was stained for ALP at 14 day of culture. ALP activity of the cells stimulated at 1 kHz frequency was higher when the cells stimulated at 0.5 kHz. At both frequency, the cells stimulated with voltage of 800 mV exhibited almost no ALP activity which can be related with low viability at this conditions. When 200 mV voltage applied to the BMSCs, the cells showed modarate ALP activity. The electrical stimulus of 400 mV voltage at 1 kHz frequency provided a microenvironment that promotes the highest ALP activity. The increased ALP activity can be related with gap junctions which plays essential role in differentiated bone tissue by enabling propagation of ions, nutrients and metabolites between adjoining cells (Stains & Civitelli, 2005).

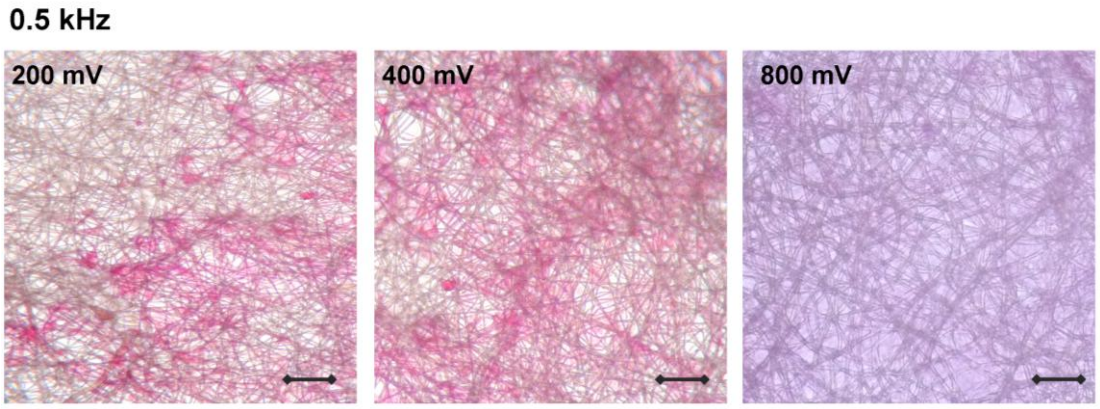

Figure 3.45 : ALP activity of BMSCs on PCL/P3ANA nanofibers depending on applied voltage at 0.5 kHz (scale bar= 100 μm).

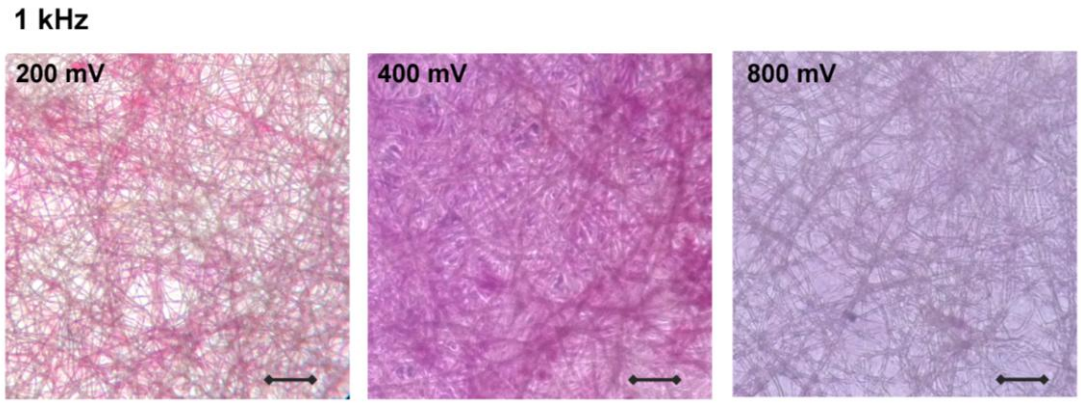

Figure 3.46 : ALP activity of BMSCs on PCL/P3ANA nanofibers depending on applied voltage at 1 kHz (scale bar= 100 μm).

3.6.5 The effect of electrical stimulation on mineralization assay

Calcium deposits, which are important indications of the middle stage of osteogenesis were detected by staining with Alizarin red S on day 14, in order to investigate the effect of electical stimulation on the BMSCs. Ca deposition involves many reactions, such as excreted extracellular proteins binding with calcium phosphate (Aubin, 1998; Boskey & Posner, 1984; Herbertson & Aubin, 1995). The hydroxylapatite is calcium phosphate salt with the formula of $(Ca,X)_{10}(PO_4)_6$, where X are cations (magnesium, sodium, strontium ions) that can replace calcium ions (LeGeros, 2002). This mineral is one of the main components of the bone and the accumulation of Ca is called mineralization (Lorich et al., 1998) which is an essential process for bone tissue to gain mechanical properties (Anderson, 1989). The calcium mineral deposits cover the nanofiber mats where the differentiated cells attach. The

BMSCs cultured on the PCL/P3ANA nanofibers under AC voltage (200 mV, 400 mV and 800 mV) at 0.5 kHz (Figure 3.47) and 1 kHz (Figure 3.48) frequency. After Alizarin red s staining, calcium deposits were observed as red/orange nodules in the areas of cell growth. In correlation with ALP activity, the cells stimulated at 1 kHz frequency showed higher osteogenic activity revealed by higher Ca deposits. The amount of Ca deposits was the highest after applying 400 mV at 1 kHz. At higher voltage (800 mV), the osteogenic activity of the cells were low.

Both ALP activity and Ca depositon data exhibited similar trend to the proliferation results. Electrical stimulation of 400 mV at 1 kHz favored the bone matrix mineralization process and ossification (F. Yang et al., 2005). The electrical stimulation data suggested that P3ANA in the nanofiber structure was capable of delivering, interacting and mediating the electrical signaling process within the seeded BMSCs (Yow et al., 2011).

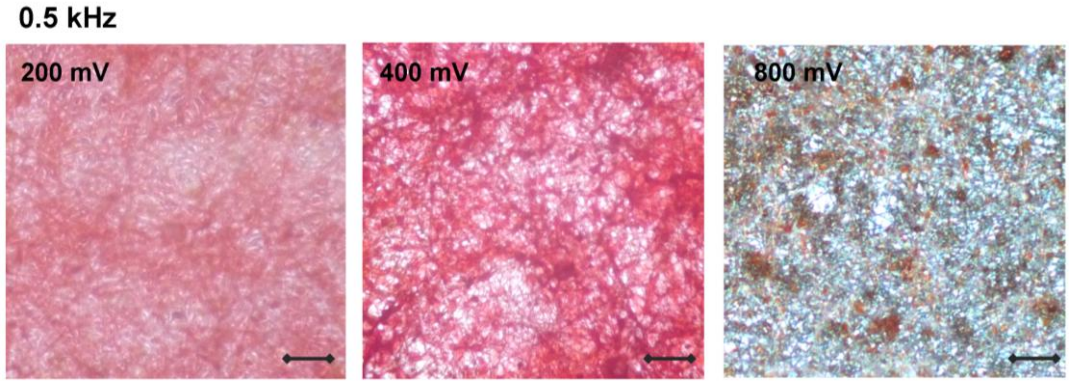

Figure 3.47 : Ca deposits of BMSCs on PCL/P3ANA nanofibers depending on applied voltage at 0.5 kHz (scale bar= 100 μm).

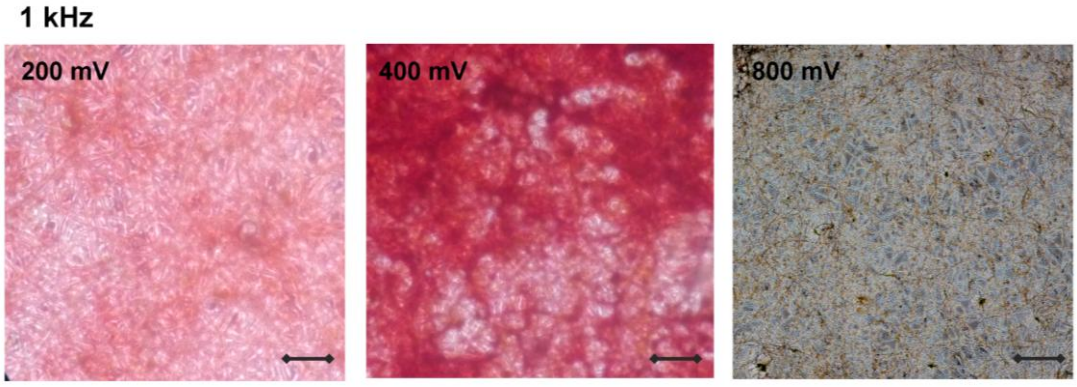

Figure 3.48 : Ca deposits of BMSCs on PCL/P3ANA nanofibers depending on applied voltage at 1 kHz (scale bar= 100 μm).

The mechanisms of how cells respond to electrical stimulation are very complex and remain largely unknown. However, there are some possible mechanisms for enhanced osteogenic activity under electrical stimulation. The cell membrane can sense the changes in the environment such as electrical signals. Several membrane proteins sense and use external electrical stimuli to regulate cellular functions since the electrical stimuli affect the movement of the charges within these proteins (Bezanilla, 2008). These membrane proteins have negatively charged chemical groups such as carboxylates or phosphates which caused a negative cell membrane. There is a transmembrane potential membrane in the order of 100 mV across the cell membrane due to the uneven distribution of ions. The potential difference between the inside and outside of the cell membrane starts the signal transduction processes. Electrical stimulation can cause a potential difference on cell mebrane by changing the ion concentration across the membrane and can trigger signaling pathways such as Calcium/calmodulin (Aaron et al., 2004). This pathway can induce the level of transforming factor-beta (TGF-β) which involves bone formation. The enhanced osteogenic activity and mineralization under electrical stimulus can stem from the induction of voltage-gated calcium ion channel on the surface of the cells (Brighton et al., 1985; Min et al., 2014) Because this ion channel can detect the changes in the membrane potential of the cell and cause an alteration of the cellular calcium ion concentration which can in turn induce multiple physiological pathways. Mild electrical stimulation can enhance the proliferation, cell growth and osteogenic activity of the cells (Min et al., 2014). Electrical stimulation favors differentiation of osteoblastic feature and enhances osteogenic activity by increasing gene expression of TGF-β, ALP and BMPs.

4. CONCLUSIONS

Tissue engineering (TE) is an important filed, which implies the use of organ-specific cells for seeding a scaffold that serves as a three-dimensional template for tissue regeneration. The cells seeded onto scaffolds, proliferate, migrate and differentiate into the specific tissue while secreting the extracellular matrix components required creating the tissue. The scaffold having an ideal surface chemistry and microstructure serves as a mimic for the ECM and plays a critic role in tissue regeneration by providing temporary support for the cells. Therefore, fabrication of a scaffold, which can provide necessary support and bioactive signals for cells, is important. In this study, bioactive and electroactive electrospun nanofibers fabricated in order to use as a scaffold in bone tissue engineering. Electrospun poly(ε-caprolactone)/poly(m-anthranilic acid) (PCL/P3ANA) nanofibers were fabricated by addition of increasing amounts of P3ANA to the PCL solutions. The higher amount of P3ANA resulted in higher (-COOH) group density on the nanofibers. The diameter of nanofibers was slighly decreased with the increasing P3ANA content in the nanofiber structure. The surface roughness and BET surface area were increased with the decrease in fiber diameter. The large surface area and roughness of the nanofibers provided more available sites for biofunctionalization of the nanofibers and enhanced the interaction between cells and the nanofibers. The increase in P3ANA amount in the nanofiber structure were resulted an increase in Young's modulus, toughness and the ultimate strenght of the nanofibers. The decrease in fiber diameter resulted increase of BET surface area, in addition it caused higher modulus and strength. The mechanical properties of PCL/P3ANA nanofibers changed due to P3ANA amount which changed the structural properties of the nanofibers. The increase of P3ANA amount in the PCL/P3ANA nanofibers resulted lower charge transfer resistance values which indicates higher conductivity. Since, PCL/P3ANA nanofibers were aimed to use as electroactive and bioactive tissue engineering scaffolds, the nanofiber mat containing the highest amount of P3ANA

with highest surface area, best mechanical and electrochamical properties was chosen for biofunctionalization and cell studies.

Biofunctionalization of the PCL/P3ANA nanofibers was achieved with covalent immobilization of proteins onto the nanofibers by using EDC/NHS activation process. The covalent immobilization has been widely applied to several kinds of substrates in varying concentrations of EDC and NHS The success of covalent immobilization is mainly affected by the concentraions of EDC, EDC. Therefore, it was aimed to investigate the optimum EDC/NHS concentration for surface activation of PCL/P3ANA nanofibers. Equal amounts of EDC/NHS (EDC/NHS=5/5 mM and EDC/NHS=50/50 mM), excess amount of EDC over NHS (EDC/NHS=5/0.5 mM) and excess amount of NHS over EDC (EDC/NHS=0.5/5mM) were used for the activation of carboxyl groups of PCL/P3ANA nanofibers. These concentrations were selected since very large concentrations of EDC or NHS result the formation of the byproducts at the surface which can prevent the formation of -COOsuc surface and affect the success of the surface activation. In the case of EDC and NHS concentrations are very low, and then the surface activation reaction remains incomplete. After surface activation of the PCL/P3ANA nanofibers, albumin as a model protein was covalently immobilized onto the nanofibers. AFM images showed that surface roughness of the nanofibers was increased after albumin immobilization. The amount of bound albumin was changed depending on the activation of the carboxyl groups of P3ANA. Elemental analyses and EDX-mapping of nitrogen atoms showed that the distribution of the albumin on the surface of nanofibers is affected by the distribution of activated -COOH groups of P3ANA. Electrochemical Impedance Spectroscopy (EIS) analysis showed that the nanofibers become resistive due to albumin immobilization and the higher charge transfer resistance was observed for the nanofibers activated with 50/50 mM of EDC/NHS. It was found that 50/50 mM of EDC/NHS was the most effective concentration for the activation of PCL/P3ANA nanofibers.

After determination of the suitable nanofiber mat and the optimum concentrations of EDC/NHS for covalent immobilization, PCL/P3ANA nanofibers were biofunctionalized with BMP-2 and RGD peptide for *in vitro* cells studies. FTIR-ATR and EIS data confirmed the successful immobilization of BMP-2 and RGD peptide onto the nanofibers. The double layer capacitance and charge transfer values were

increased after protein immobilization on the surface of nanofibers. The amounts of covalently immobilized BMP-2 and RGD peptide were determined by BCA protein assay and with elemental analyzes of N atoms by EDX. Contact angle measurements showed the changes of the surface properties from hydrophobic to hydrophilic after protein immobilization. Hydrophilicity of a surface is an important factor to enhance the interaction between cells and nanofibers by creating a favorable interface between them. The effects of BMP-2 and RGD functionalization of nanofibers on the attachment, proliferation and osteogenic activity of Saos-2 cells were investigated. Nanofibers showed to be nontoxic and enable for cell attachment and growth. The cell proliferation was the highest for the RGD peptide immobilized nanofibers. Cell viability is in correlation with cellular adhesion and structure of the scaffold. All nanofiber mats were able to sustain cell adhesion and proliferation according to resazurin assay. An increase in resazurin reduction from day 1 to day 9 was observed, which indicates an increase in cell number. Higher cell proliferation was observed on nanofibers compared to cover glass surface. This can be attributed to the porous structure of the nanofibers. These results for the difference in proliferation behavior of cells were also evidenced with SEM images. The cells attached on PCL, PCL/P3ANA, BMP-2/PCL/P3ANA and PCL/P3ANA-RGD nanofibers were were proliferated by spreading on the nanofiber mats and covered the scaffold. In correlation with resazurin test, the number of cells on the PCL/P3ANA-RGD nanofibers was highest compared to other nanofibers. Cell morphology and adhesion behavior on the nanofibers was also investigated by fluorescent staining. Cell morphology was polygonal in shape on the PCL, PCL/P3ANA and PCL/P3ANA-RGD nanofibers is similar to each other. Cells exhibit elongated and spindle-like morphology which is characteristic for Saos-2 cell line. The cells on BMP-2 functionalized nanofibers exhibited osteocyte-like morphology. BMP-2/PCL/P3ANA nanofibers induced adherent-cell type actin stress fibers while PCL or PCL/P3ANA nanofibers did not induce actin extensions. ALP activity and calcium deposition of Saos-2 cells cultured for 14 days on cover glass, PCL, PCL/P3ANA, BMP-2/PCL/P3ANA and PCL/P3ANA-RGD nanofibers were investigated. ALP is an enzyme which plays an important role in bone matrix mineralization process and therefore a good marker of osteogenic phenotype. ALP activity is closely associated with sites of active bone formation. Saos-2 cells exhibit several osteoblastic features and synthesize ALP and mineral deposits and bone-related molecules. The cells on

BMP-2 immobilized nanofibers exhibited the highest ALP activity and the highest amount of calcium deposits among all nanofibers and cover glass, which indicates a higher degree of osteogenesis. When the ALP activity and Ca deposition results evaluated, the general trend found in these assays correlated well with that of the proliferation results obtained from Rezasurin assay and SEM.

The effects of electrical stimulation on the differentiation of cells into bone feature and the ability of PCL/P3ANA nanofibers to deliver the electrical signals to the cell were investigated. For electrical stimulation studies BMSCs were used since they can differentiate into osteogenic lineage under the applied electrical field. Eletrical stimulation was applied to the cells with the electric field (voltage difference per unit distance) of 200 mV/mm, 400 mV/mm and 800 mV/mm at frequency of 0.5 kHz, 1 kHz, 5 kHz and 10 kHz. The viability of cells was the highest when frequency of 1 kHz was applied. At frequency of 0.5 kHz and 1 kHz, the highest viability was observed when cells stimulated with 400 mV/mm. When 800 mV/mm AC voltage at any frequency was applied, cell viability was below 50%. The higher frequencies (5 kHz and 10 kHz) caused a dramatic decrease in cell viability. The proliferation of BMSCS was evaluated and from day 1 to day 9, proliferation was observed when cells stimulated either with 200 mV/mm and 400 mV/mm. 800 mV AC voltage inhibited the cell attachment and proliferation. The morphology of the cells under electrical stimulation was observed with SEM and fluorescence staining. The cells cultured on the PCL/P3ANA nanofibers under electrical stimulation, proliferated by spreading on the nanofiber mats. The cells stimulated with 800 mV/mm at did not spread on the nanofiber mat and showed rounded morphology, which can be related with low viability under these conditions. The cell death at higher voltage and frequencies can be related with the rupture of the cell membrane. At 200 mV/mm and 400 mV/mm voltages BMSCs showed osteocyte-like morphology with adherent-cell type actin extensions. Osteogenic differentiation of BMSCs were investigated by staining for ALP activity and Ca deposits. ALP activity and Ca depositon data exhibited similar trend to the proliferation results. The cells stimulated with voltage of 800 mV exhibited almost no ALP activity or mineralization. The BMSCs showed modarate osteogenic activity at 200 mV voltage. The highest mineralization and ALP activity was observed when BMSCs stimulated with 400 mV at 1 kHz which can be related with induction of voltage-gated calcium ion channel on the cell membrane by exceeding the transmembrane potential threshold. The electrical stimulation data also

suggested that P3ANA in the nanofiber structure was capable of delivering, interacting and mediating the electrical signaling process within the seeded BMSCs.

REFERENCES

Aaron, R. K., Boyan, B. D., Ciombor, D. M., Schwartz, Z., & Simon, B. J. (2004). Stimulation of growth factor synthesis by electric and electromagnetic fields. *Clinical orthopaedics and related research, 419*, 30-37.

Adey, W. R. (1993). Biological effects of electromagnetic fields. *Journal of cellular biochemistry, 51*(4), 410-416.

Agarwal, S., Wendorff, J. H., & Greiner, A. (2008). Use of electrospinning technique for biomedical applications. *Polymer, 49*(26), 5603-5621.

Ahsan, T., Doyle, A., & Nerem, R. (2009). Stem cell research. *Principles of Regenerative Medicine*, 28-47.

Anderson, H. (1989). Mechanism of mineral formation in bone. *Laboratory investigation; a journal of technical methods and pathology, 60*(3), 320-330.

Annabi, N., Fathi, A., Mithieux, S. M., Weiss, A. S., & Dehghani, F. (2011). Fabrication of porous PCL/elastin composite scaffolds for tissue engineering applications. *The Journal of Supercritical Fluids, 59*, 157-167.

Aubin, J. E. (1998). Advances in the osteoblast lineage. *Biochemistry and Cell Biology, 76*(6), 899-910.

Bae, S. E., Choi, J., Joung, Y. K., Park, K., & Han, D. K. (2012). Controlled release of bone morphogenetic protein (BMP)-2 from nanocomplex incorporated on hydroxyapatite-formed titanium surface. *Journal of controlled release, 160*(3), 676-684.

Balacheva, A., Iliev, I., Detcheva, R., Dzimbova, T., Pajpanova, T., & Golovinsky, E. (2012). In vitro assessment of the cytotoxic effects of novel RGD analogues. *BioDiscovery, 4*.

Bendrea, A.-D., Cianga, L., & Cianga, I. (2011). Review paper: progress in the field of conducting polymers for tissue engineering applications. *Journal of biomaterials applications, 26*(1), 3-84.

Benyoucef, A., Huerta, F., Vázquez, J., & Morallon, E. (2005). Synthesis and in situ FTIRS characterization of conducting polymers obtained from aminobenzoic acid isomers at platinum electrodes. *European Polymer Journal, 41*(4), 843-852.

Beuvelot, J., Portet, D., Lecollinet, G., Moreau, M. F., Basle, M. F., Chappard, D., & Libouban, H. (2009). In vitro kinetic study of growth and mineralization of osteoblast-like cells (Saos-2) on titanium surface coated with a RGD functionalized bisphosphonate. *Journal of Biomedical Materials Research Part B: Applied Biomaterials, 90*(2), 873-881.

Bezanilla, F. (2008). How membrane proteins sense voltage. *Nature reviews Molecular cell biology, 9*(4), 323-332.

Bianco, P., & Robey, P. G. (2001). Stem cells in tissue engineering. *Nature, 414*(6859), 118-121.

Bidez, P. R., Li, S., MacDiarmid, A. G., Venancio, E. C., Wei, Y., & Lelkes, P. I. (2006). Polyaniline, an electroactive polymer, supports adhesion and proliferation of cardiac myoblasts. *Journal of Biomaterials Science, Polymer Edition, 17*(1-2), 199-212.

Birner, S., Uhl, C., Bayer, M., & Vogl, P. (2008). *Theoretical model for the detection of charged proteins with a silicon-on-insulator sensor.* Paper presented at the Journal of Physics: Conference Series.

Blau, H. M., Brazelton, T., & Weimann, J. (2001). The evolving concept of a stem cell: entity or function? *Cell, 105*(7), 829-841.

Borra, R. C., Lotufo, M. A., Gagioti, S. M., Barros Fde, M., & Andrade, P. M. (2009). A simple method to measure cell viability in proliferation and cytotoxicity assays. *Braz Oral Res, 23*(3), 255-262.

Boskey, A., & Posner, A. (1984). Bone structure, composition, and mineralization. *The Orthopedic clinics of North America, 15*(4), 597-612.

Bouhekka, A., & Bürgi, T. (2012). In situ ATR-IR spectroscopy study of adsorbed protein: Visible light denaturation of bovine serum albumin on TiO2. *Applied Surface Science, 261*, 369-374. doi: http://dx.doi.org/10.1016/j.apsusc.2012.08.017

Brighton, C. T., Hozack, W. J., Brager, M. D., Windsor, R. E., Pollack, S. R., Vreslovic, E. J., & Kotwick, J. E. (1985). Fracture healing in the rabbit fibula when subjected to various capacitively coupled electrical fields. *Journal of orthopaedic research, 3*(3), 331-340.

Campos, A. d., & Franchetti, S. M. M. (2005). Biotreatment effects in films and blends of PVC/PCL previously treated with heat. *Brazilian Archives of Biology and Technology, 48*, 235-243.

Casper, C. L., Yang, W., Farach-Carson, M. C., & Rabolt, J. F. (2007). Coating Electrospun Collagen and Gelatin Fibers with Perlecan Domain I for Increased Growth Factor Binding. *Biomacromolecules, 8*(4), 1116-1123. doi: 10.1021/bm061003s

Chang, B.-Y., & Park, S.-M. (2010). Electrochemical impedance spectroscopy. *Annual Review of Analytical Chemistry, 3*, 207-229.

Chang, C.-H., Yeh, S.-Y., Lee, B.-H., Chen, C.-J., Su, C.-T., Lin, Y.-T., . . . Chen, H.-Y. (2015). Osteogenic Surface Modification Based on Functionalized Poly-P-Xylylene Coating. *PLoS One, 10*(9), e0137017.

Chen, G., Ushida, T., & Tateishi, T. (2000). Hybrid biomaterials for tissue engineering: A preparative method for PLA or PLGA–collagen hybrid sponges. *Advanced Materials, 12*(6), 455-457.

Cheung, H.-Y., Lau, K.-T., Lu, T.-P., & Hui, D. (2007). A critical review on polymer-based bio-engineered materials for scaffold development. *Composites Part B: Engineering, 38*(3), 291-300.

Cho, H.-j., Madhurakkat Perikamana, S. K., Lee, J.-h., Lee, J., Lee, K.-M., Shin, C. S., & Shin, H. (2014). Effective Immobilization of BMP-2 Mediated by Polydopamine Coating on Biodegradable Nanofibers for Enhanced in Vivo Bone Formation. *ACS Applied Materials & Interfaces, 6*(14), 11225-11235. doi: 10.1021/am501391z

Chua, K.-N., Lim, W.-S., Zhang, P., Lu, H., Wen, J., Ramakrishna, S., . . . Mao, H.-Q. (2005). Stable immobilization of rat hepatocyte spheroids on galactosylated nanofiber scaffold. *Biomaterials, 26*(15), 2537-2547.

Cosnier, S., Dawod, M., Gorgy, K., & Da Silva, S. (2003). Synthesis and electrochemical characterization of a new electropolymerizable hydrophilic viologen designed for enzyme wiring. *Microchimica Acta, 143*(2-3), 139-145.

Dagli, U., Guler, Z., & Sarac, A. S. (2015). Covalent Immobilization of Tyrosinase on Electrospun Polyacrylonitrile/Polyurethane/Poly (m-anthranilic acid) Nanofibers: An Electrochemical Impedance Study. *Polymer-Plastics Technology and Engineering, 54*(14), 1494-1504.

Dai, J., Baker, G. L., & Bruening, M. L. (2006). Use of porous membranes modified with polyelectrolyte multilayers as substrates for protein arrays with low nonspecific adsorption. *Analytical Chemistry, 78*(1), 135-140.

Dash, M. P., Tripathy, M., Sasmal, A., Mohanty, G. C., & Nayak, P. L. (2010). Poly(anthranilic acid)/multi-walled carbon nanotube composites: spectral, morphological, and electrical properties. *Journal of Materials Science, 45*(14), 3858-3865. doi: 10.1007/s10853-010-4441-4

De Crombrugghe, A., Yunus, S., & Bertrand, P. (2008). Grafting and characterization of protein on polyaniline surface for biosensor applications. *Surface and Interface Analysis, 40*(3-4), 404-407.

De Vrieze, S., Van Camp, T., Nelvig, A., Hagström, B., Westbroek, P., & De Clerck, K. (2009). The effect of temperature and humidity on electrospinning. *Journal of Materials Science, 44*(5), 1357-1362.

Degasne, I., Basle, M., Demais, V., Hure, G., Lesourd, M., Grolleau, B., . . . Chappard, D. (1999). Effects of roughness, fibronectin and vitronectin on attachment, spreading, and proliferation of human osteoblast-like cells (Saos-2) on titanium surfaces. *Calcif Tissue Int, 64*(6), 499-507.

Douarche, C., Cortès, R., De Villeneuve, C. H., Roser, S., & Braslau, A. (2008). DNA adsorption at functionalized Si/buffer interfaces studied by x-ray reflectivity. *The Journal of chemical physics, 128*(22), 225108.

Ducker, R. E., Montague, M. T., & Leggett, G. J. (2008). A comparative investigation of methods for protein immobilization on self-assembled monolayers using glutaraldehyde, carbodiimide, and anhydride reagents. *Biointerphases, 3*(3), 59-65. doi: 10.1116/1.2976451

Ehrbar, M., Lütolf, M. P., Rizzi, S. C., Hubbell, J. A., & Weber, F. E. (2008). Artificial extracellular matrices for bone tissue engineering. *Bone, 42*, S72.

Elzubair, A., Elias, C. N., Suarez, J. C. M., Lopes, H. P., & Vieira, M. V. B. (2006). The physical characterization of a thermoplastic polymer for endodontic obturation. *Journal of dentistry, 34*(10), 784-789.

Engler, A. J., Sen, S., Sweeney, H. L., & Discher, D. E. (2006). Matrix elasticity directs stem cell lineage specification. *Cell, 126*(4), 677-689.

Evangelista, M. B., Hsiong, S. X., Fernandes, R., Sampaio, P., Kong, H.-J., Barrias, C. C., . . . Granja, P. L. (2007). Upregulation of bone cell differentiation through immobilization within a synthetic extracellular matrix. *Biomaterials, 28*(25), 3644-3655.

Feng, X., Chen, N., Zhou, J., Li, Y., Huang, Z., Zhang, L., . . . Yan, X. (2015). Facile synthesis of shape-controlled graphene–polyaniline composites for high performance supercapacitor electrode materials. *New Journal of Chemistry, 39*(3), 2261-2268.

Ficen, S. Z., Guler, Z., Mitina, N., Finiuk, N., Stoika, R., Zaichenko, A., & Ceylan, S. E. (2013). Biophysical study of novel oligoelectrolyte-based nonviral gene delivery systems for mammalian cells. *J Gene Med, 15*(5), 193-204. doi: 10.1002/jgm.2710

Flemming, R., Murphy, C., Abrams, G., Goodman, S., & Nealey, P. (1999). Effects of synthetic micro-and nano-structured surfaces on cell behavior. *Biomaterials, 20*(6), 573-588.

Foulds, I., & Barker, A. (1983). Human skin battery potentials and their possible role in wound healing. *British Journal of Dermatology, 109*(5), 515-522.

Fromigue, O., Marie, P., & Lomri, A. (1998). Bone morphogenetic protein-2 and transforming growth factor-b2 interact to modulate human bone marrow stromal cell proliferation and differentiation. *Journal of cellular biochemistry, 68*(4), 411-426.

Gigante, A., Manzotti, S., Bevilacqua, C., Orciani, M., Di Primio, R., & Mattioli-Belmonte, M. (2008). Adult mesenchymal stem cells for bone and cartilage engineering: effect of scaffold materials. *European journal of histochemistry: EJH, 52*(3), 169.

Gilde, F., Maniti, O. l., Guillot, R., Mano, J. F., Logeart-Avramoglou, D., Sailhan, F. d. r., & Picart, C. (2012). Secondary structure of rhBMP-2 in a protective biopolymeric carrier material. *Biomacromolecules, 13*(11), 3620-3626.

Giray, D., Balkan, T., Dietzel, B., & Sezai Sarac, A. (2013). Electrochemical impedance study on nanofibers of poly(m-anthranilic acid)/polyacrylonitrile blends. *European Polymer Journal, 49*(9), 2645-2653. doi: http://dx.doi.org/10.1016/j.eurpolymj.2013.06.012

Golshaei, R., Guler, Z., & Sarac, S. A. (2016). (Au/PANA/PVAc) nanofibers as a novel composite matrix for albumin and streptavidin immobilization. *Mater Sci Eng C Mater Biol Appl, 60*, 260-275. doi: 10.1016/j.msec.2015.11.046

Gomez, L. A., Alekseev, A. E., Aleksandrova, L. A., Brady, P. A., & Terzic, A. (1997). Use of the MTT assay in adult ventricular cardiomyocytes to assess viability: effects of adenosine and potassium on cellular survival. *Journal of molecular and cellular cardiology, 29*(4), 1255-1266.

Grdadolnik, J., & Maréchal, Y. (2001). Bovine serum albumin observed by infrared spectrometry. I. Methodology, structural investigation, and water uptake. *Biopolymers, 62*(1), 40-53. doi: 10.1002/1097-0282(2001)62:1<40::AID-BIP60>3.0.CO;2-C

Gu, H., Su, X. d., & Loh, K. P. (2005). Electrochemical impedance sensing of DNA hybridization on conducting polymer film-modified diamond. *The Journal of Physical Chemistry B, 109*(28), 13611-13618.

Guler, Z., Erkoc, P., & Sarac, A. S. (2015). Electrochemical impedance spectroscopic study of single-stranded DNA-immobilized electroactive polypyrrole-coated electrospun poly(ε-caprolactone) nanofibers. *Materials Express, 5*(4), 269-279. doi: 10.1166/mex.2015.1249

Guler, Z., & Sarac, A. S. (2016). Electrochemical impedance and spectroscopy study of the EDC/NHS activation of the carboxyl groups on poly(ε-caprolactone)/poly(m-anthranilic acid) nanofibers. *Express Polymer Letters, 10*(2), 96-110. doi: 10.3144/expresspolymlett.2016.11

Haider, A., Gupta, K. C., & Kang, I.-K. (2014). Morphological effects of HA on the cell compatibility of electrospun HA/PLGA composite nanofiber scaffolds. *BioMed research international, 2014*.

Han, D., Song, J., Ding, X., Xu, X., & Niu, L. (2007). Fabrication and characterization of self-doped poly (aniline-co-anthranilic acid) nanorods in bundles. *Materials Chemistry and Physics, 105*(2), 380-384.

Haynesworth, S., Goshima, J., Goldberg, V., & Caplan, A. (1992). Characterization of cells with osteogenic potential from human marrow. *Bone, 13*(1), 81-88.

Heliotis, M., Ripamonti, U., Ferretti, C., Kerawala, C., Mantalaris, A., & Tsiridis, E. (2009). The basic science of bone induction. *British Journal of Oral and Maxillofacial Surgery, 47*(7), 511-514.

Herbertson, A., & Aubin, J. E. (1995). Dexamethasone alters the subpopulation make-up of rat bone marrow stromal cell cultures. *Journal of Bone and Mineral Research, 10*(2), 285-294.

Ho, M.-H., Wang, D.-M., Hsieh, H.-J., Liu, H.-C., Hsien, T.-Y., Lai, J.-Y., & Hou, L.-T. (2005). Preparation and characterization of RGD-immobilized chitosan scaffolds. *Biomaterials, 26*(16), 3197-3206.

Hronik-Tupaj, M., Rice, W. L., Cronin-Golomb, M., Kaplan, D. L., & Georgakoudi, I. (2011). Osteoblastic differentiation and stress response of human mesenchymal stem cells exposed to alternating current electric fields. *Biomedical engineering online, 10*(1), 9.

Hwang, N. S., Varghese, S., Lee, H. J., Zhang, Z., Ye, Z., Bae, J., . . . Elisseeff, J. (2008). In vivo commitment and functional tissue regeneration using human embryonic stem cell-derived mesenchymal cells. *Proceedings of the National Academy of Sciences, 105*(52), 20641-20646.

Hwang, N. S., Varghese, S., Zhang, Z., & Elisseeff, J. (2006). Chondrogenic differentiation of human embryonic stem cell-derived cells in arginine-glycine-aspartate-modified hydrogels. *Tissue engineering, 12*(9), 2695-2706.

Jakub, #352, irc, Hobzov, R., #225, Kostina, N., . . . lek. (2012). Morphological characterization of nanofibers: methods and application in practice. *J. Nanomaterials, 2012*, 121-121. doi: 10.1155/2012/327369

Jalili, R., Hosseini, S. A., & Morshed, M. (2005). The effects of operating parameters on the morphology of electrospun polyacrilonitrile nanofibres. *Iranian Polymer Journal, 14*(12), 1074.

Jang, J.-H., Castano, O., & Kim, H.-W. (2009). Electrospun materials as potential platforms for bone tissue engineering. *Advanced drug delivery reviews, 61*(12), 1065-1083.

Kar, K. K., Pandey, J. K., & Rana, S. K. (2014). *Handbook of Polymer Nanocomposites. Processing, Performance and Application: Volume B: Carbon Nanotube Based Polymer Composites*: Springer.

Karande, T., & Agrawal, C. (2008). *Function and Requirement of Synthetic Scaffolds in Tissue Engineering*: Boca Raton, FL: CRC Press.

Kartsogiannis, V., & Ng, K. W. (2004). Cell lines and primary cell cultures in the study of bone cell biology. *Molecular and cellular endocrinology, 228*(1), 79-102.

Kempen, D. H., Creemers, L. B., Alblas, J., Lu, L., Verbout, A. J., Yaszemski, M. J., & Dhert, W. J. (2010). Growth factor interactions in bone regeneration. *Tissue Engineering Part B: Reviews, 16*(6), 551-566.

Khalil, A., Shaaban, A., Azab, M., Mahmoud, A., & Metwally, A. (2013). Synthesis, characterization and morphology of polyanthranilic acid micro-and nanostructures. *Journal of Polymer Research, 20*(6), 1-10.

Khandanlou, R., Ahmad, M. B., Shameli, K., Saki, E., & Kalantari, K. (2014). Studies on Properties of Rice Straw/Polymer Nanocomposites Based on Polycaprolactone and Fe3O4 Nanoparticles and Evaluation of Antibacterial Activity. *International journal of molecular sciences, 15*(10), 18466-18483.

Kilpadi, K. L., Sawyer, A. A., Prince, C. W., Chang, P. L., & Bellis, S. L. (2004). Primary human marrow stromal cells and Saos-2 osteosarcoma cells use different mechanisms to adhere to hydroxylapatite. *Journal of Biomedical Materials Research Part A, 68*(2), 273-285.

Kim, B. S., Park, K. E., Kim, M. H., You, H. K., Lee, J., & Park, W. H. (2015). Effect of nanofiber content on bone regeneration of silk fibroin/poly (ε-caprolactone) nano/microfibrous composite scaffolds. *International journal of nanomedicine, 10*, 485.

Kim, T. G., & Park, T. G. (2006). Biomimicking extracellular matrix: cell adhesive RGD peptide modified electrospun poly (D, L-lactic-co-glycolic acid) nanofiber mesh. *Tissue engineering, 12*(2), 221-233.

Kityakarn, S., Pooarporn, Y., Songsiriritthigul, P., Worayingyong, A., Robl, S., Braun, A. M., & Wörner, M. (2012). (Photo) Electrochemical characterization of nanoporous TiO 2 and Ce-doped TiO 2 sol–gel film electrodes. *Electrochimica Acta, 83*, 113-124.

Laurencin, C. T., & Nair, L. S. (2008). *Nanotechnology and tissue engineering: the scaffold*: CRC Press.

Lee, M. H., Adams, C. S., Boettiger, D., DeGrado, W. F., Shapiro, I. M., Composto, R. J., & Ducheyne, P. (2007). Adhesion of MC3T3-E1 cells to RGD peptides of different flanking residues: Detachment strength and correlation with long-term cellular function. *Journal of Biomedical Materials Research Part A, 81*(1), 150-160.

LeGeros, R. Z. (2002). Properties of osteoconductive biomaterials: calcium phosphates. *Clinical orthopaedics and related research, 395*, 81-98.

Li, L., Zhou, G., Wang, Y., Yang, G., Ding, S., & Zhou, S. (2015). Controlled dual delivery of BMP-2 and dexamethasone by nanoparticle-embedded electrospun nanofibers for the efficient repair of critical-sized rat calvarial defect. *Biomaterials, 37*, 218-229.

Li, M., Guo, Y., Wei, Y., MacDiarmid, A. G., & Lelkes, P. I. (2006). Electrospinning polyaniline-contained gelatin nanofibers for tissue engineering applications. *Biomaterials, 27*(13), 2705-2715.

Li, M., Mondrinos, M. J., Gandhi, M. R., Ko, F. K., Weiss, A. S., & Lelkes, P. I. (2005). Electrospun protein fibers as matrices for tissue engineering. *Biomaterials, 26*(30), 5999-6008.

Li, W. J., Laurencin, C. T., Caterson, E. J., Tuan, R. S., & Ko, F. K. (2002). Electrospun nanofibrous structure: a novel scaffold for tissue engineering. *Journal of biomedical materials research, 60*(4), 613-621.

Liang, D., Hsiao, B. S., & Chu, B. (2007). Functional electrospun nanofibrous scaffolds for biomedical applications. *Advanced drug delivery reviews, 59*(14), 1392-1412.

Lim, J.-S., Kook, M.-S., Jung, S., Park, H.-J., Ohk, S.-H., & Oh, H.-K. (2014). Plasma treated high-density polyethylene (HDPE) medpor implant immobilized with rhBMP-2 for improving the bone regeneration. *Journal of Nanomaterials, 2014*, 5.

Lim, J. Y., Shaughnessy, M. C., Zhou, Z., Noh, H., Vogler, E. A., & Donahue, H. J. (2008). Surface energy effects on osteoblast spatial growth and mineralization. *Biomaterials, 29*(12), 1776-1784.

Liu, C., Sanghvi, R., Burnell, J., & Howard, G. (1987). Simultaneous demonstration of bone alkaline and acid phosphatase activities in plastic-embedded sections and differential inhibition of the activities. *Histochemistry, 86*(6), 559-565.

Lo, K. W.-H., Ulery, B. D., Ashe, K. M., & Laurencin, C. T. (2012). Studies of bone morphogenetic protein-based surgical repair. *Advanced drug delivery reviews, 64*(12), 1277-1291.

Lorich, D. G., Brighton, C. T., Gupta, R., Corsetti, J. R., Levine, S. E., Gelb, I. D., . . . Pollack, S. R. (1998). Biochemical pathway mediating the response of bone cells to capacitive coupling. *Clinical orthopaedics and related research, 350*, 246-256.

Lu, X., Dou, H., Yuan, C., Yang, S., Hao, L., Zhang, F., . . . Zhang, X. (2012). Polypyrrole/carbon nanotube nanocomposite enhanced the electrochemical capacitance of flexible graphene film for supercapacitors. *Journal of Power Sources, 197*, 319-324.

Lu, X., Zhang, W., Wang, C., Wen, T.-C., & Wei, Y. (2011). One-dimensional conducting polymer nanocomposites: synthesis, properties and applications. *Progress in Polymer Science, 36*(5), 671-712.

Ma, B., Xie, J., Jiang, J., Shuler, F. D., & Bartlett, D. E. (2013). Rational design of nanofiber scaffolds for orthopedic tissue repair and regeneration. *Nanomedicine (Lond), 8*(9), 1459-1481. doi: 10.2217/nnm.13.132

Madhurakkat Perikamana, S. K., Lee, J., Ahmad, T., Jeong, Y., Kim, D.-G., Kim, K., & Shin, H. (2015). Effects of immobilized BMP-2 and nanofiber morphology on in vitro osteogenic differentiation of hMSCs and in vivo collagen assembly of regenerated bone. *ACS Applied Materials & Interfaces, 7*(16), 8798-8808.

Manjubala, I., Ponomarev, I., Wilke, I., & Jandt, K. D. (2008). Growth of osteoblast-like cells on biomimetic apatite-coated chitosan scaffolds. *Journal of Biomedical Materials Research Part B: Applied Biomaterials, 84*(1), 7-16.

Markx, G. H. (2008). The use of electric fields in tissue engineering: A review. *Organogenesis, 4*(1), 11-17.

Markx, G. H., & Davey, C. L. (1999). The dielectric properties of biological cells at radiofrequencies: applications in biotechnology. *Enzyme and Microbial Technology, 25*(3), 161-171.

Martina, M., & Hutmacher, D. W. (2007). Biodegradable polymers applied in tissue engineering research: a review. *Polymer International, 56*(2), 145-157.

Marx, S., Jose, M. V., Andersen, J. D., & Russell, A. J. (2011). Electrospun gold nanofiber electrodes for biosensors. *Biosensors and Bioelectronics, 26*(6), 2981-2986.

Matsumoto, H., & Tanioka, A. (2011). Functionality in Electrospun Nanofibrous Membranes Based on Fiber's Size, Surface Area, and Molecular Orientation. *Membranes (Basel), 1*(3), 249-264. doi: 10.3390/membranes1030249

Mattioli-Belmonte, M., Giavaresi, G., Biagini, G., Virgili, L., Giacomini, M., Fini, M., . . . Giardino, R. (2003). Tailoring biomaterial compatibility: in vivo tissue response versus in vitro cell behavior. *The International journal of artificial organs, 26*(12), 1077-1085.

Mayr-Wohlfart, U., Fiedler, J., Günther, K. P., Puhl, W., & Kessler, S. (2001). Proliferation and differentiation rates of a human osteoblast-like cell line (SaOS-2) in contact with different bone substitute materials. *Journal of biomedical materials research, 57*(1), 132-139.

McCaig, C. D., Rajnicek, A. M., Song, B., & Zhao, M. (2005). Controlling cell behavior electrically: current views and future potential. *Physiological reviews, 85*(3), 943-978.

Mehedintu, M., & Berg, H. (1997). Proliferation response of yeast Saccharomyces cerevisiae on electromagnetic field parameters. *Bioelectrochemistry and bioenergetics, 43*(1), 67-70.

Meng, S., Rouabhia, M., & Zhang, Z. (2011). *Electrical stimulation in tissue regeneration*: INTECH Open Access Publisher.

Meng, S., Zhang, Z., & Rouabhia, M. (2011). Accelerated osteoblast mineralization on a conductive substrate by multiple electrical stimulation. *Journal of bone and mineral metabolism, 29*(5), 535-544.

Mezey, É., Chandross, K. J., Harta, G., Maki, R. A., & McKercher, S. R. (2000). Turning blood into brain: cells bearing neuronal antigens generated in vivo from bone marrow. *Science, 290*(5497), 1779-1782.

Min, Y., Liu, Y., Poojari, Y., Wu, J.-C., Hildreth III, B. E., Rosol, T. J., & Epstein, A. J. (2014). Self-doped polyaniline-based interdigitated electrodes for electrical stimulation of osteoblast cell lines. *Synthetic Metals, 198*, 308-313.

Mohamad, N. R., Marzuki, N. H. C., Buang, N. A., Huyop, F., & Wahab, R. A. (2015). An overview of technologies for immobilization of enzymes and surface analysis techniques for immobilized enzymes. *Biotechnology & Biotechnological Equipment, 29*(2), 205-220. doi: 10.1080/13102818.2015.1008192

Murphy, C. M., Haugh, M. G., & O'Brien, F. J. (2010). The effect of mean pore size on cell attachment, proliferation and migration in collagen-glycosaminoglycan scaffolds for bone tissue engineering. *Biomaterials, 31*(3), 461-466. doi: 10.1016/j.biomaterials.2009.09.063

Müller, W. E., Wang, X., Diehl-Seifert, B., Kropf, K., Schloßmacher, U., Lieberwirth, I., . . . Schröder, H. C. (2011). Inorganic polymeric phosphate/polyphosphate as an inducer of alkaline phosphatase and a modulator of intracellular Ca 2+ level in osteoblasts (SaOS-2 cells) in vitro. *Acta biomaterialia, 7*(6), 2661-2671.

Nakanishi, K., Sakiyama, T., Kumada, Y., Imamura, K., & Imanaka, H. (2008). Recent advances in controlled immobilization of proteins onto the surface of the solid substrate and its possible application to proteomics. *Current Proteomics, 5*(3), 161-175.

Nisbet, D., Forsythe, J. S., Shen, W., Finkelstein, D., & Horne, M. K. (2008). Review paper: a review of the cellular response on electrospun nanofibers for tissue engineering. *Journal of biomaterials applications*.

Orr, A. W., Helmke, B. P., Blackman, B. R., & Schwartz, M. A. (2006). Mechanisms of mechanotransduction. *Developmental cell, 10*(1), 11-20.

Otto, T. N., Habicht, W., Dinjus, E., & Zimmerman, M. (2012). Catalyst characterization with FESEM/EDX by the example of silver-catalyzed epoxidation of 1, 3-butadiene. *Scanning Electron Microscopy*, 367.

Ozkan, M., Pisanic, T., Scheel, J., Barlow, C., Esener, S., & Bhatia, S. (2003). Electro-optical platform for the manipulation of live cells. *Langmuir, 19*(5), 1532-1538.

Paletta, J. R. J., Bockelmann, S., Walz, A., Theisen, C., Wendorff, J. H., Greiner, A., . . . Schofer, M. D. (2010). RGD-functionalisation of PLLA nanofibers by surface coupling using plasma treatment: influence on stem cell differentiation. *Journal of Materials Science: Materials in Medicine, 21*(4), 1363-1369.

Panić, V., Dekanski, A., Mišković-Stanković, V., & Nikolić, B. (2009). The study of capacitance change during electrolyte penetration through carbon-supported hydrous ruthenium oxide prepared by the sol-gel procedure. *Chemical and Biochemical Engineering Quarterly, 23*(1), 23-30.

Park, J.-Y., & Park, S.-M. (2009). DNA hybridization sensors based on electrochemical impedance spectroscopy as a detection tool. *Sensors, 9*(12), 9513-9532.

Park, Y. J., Kim, K. H., Lee, J. Y., Ku, Y., Lee, S. J., Min, B. M., & Chung, C. P. (2006). Immobilization of bone morphogenetic protein-2 on a nanofibrous chitosan membrane for enhanced guided bone regeneration. *Biotechnology and applied biochemistry, 43*(1), 17-24.

Patra, S., & Munichandraiah, N. (2005). Insoluble poly(anthranilic acid) confined in Nafion membrane by chemical and electrochemical polymerization of anthranilic acid. *Synthetic Metals, 150*(3), 285-290. doi: http://dx.doi.org/10.1016/j.synthmet.2005.03.001

Patrício, T., Domingos, M., Gloria, A., & Bártolo, P. (2013). Characterisation of PCL and PCL/PLA scaffolds for tissue engineering. *Procedia CIRP, 5*, 110-114.

Pauliukaite, R., Ghica, M. E., Fatibello-Filho, O., & Brett, C. M. (2010). Electrochemical impedance studies of chitosan-modified electrodes for application in electrochemical sensors and biosensors. *Electrochimica Acta, 55*(21), 6239-6247.

Phipps, M. C., Clem, W. C., Catledge, S. A., Xu, Y., Hennessy, K. M., Thomas, V., . . . Bellis, S. L. (2011). Mesenchymal stem cell responses to bone-mimetic electrospun matrices composed of polycaprolactone, collagen I and nanoparticulate hydroxyapatite. *PLoS One, 6*(2), e16813. doi: 10.1371/journal.pone.0016813

Pittenger, M. F., Mackay, A. M., Beck, S. C., Jaiswal, R. K., Douglas, R., Mosca, J. D., . . . Marshak, D. R. (1999). Multilineage potential of adult human mesenchymal stem cells. *Science, 284*(5411), 143-147.

Polat, E., Güler, Z., Balkan, T., & Sarac, A. S. (2016). Covalent streptavidin immobilization on electrospun poly(m-anthranilic acid)/polycaprolactone nanofibers and cytocompatibility. *Journal of Bioactive and Compatible Polymers: Biomedical Applications*. doi: 10.1177/0883911515621572

Prideaux, M., Wijenayaka, A. R., Kumarasinghe, D. D., Ormsby, R. T., Evdokiou, A., Findlay, D. M., & Atkins, G. J. (2014). SaOS2 Osteosarcoma cells as an in vitro model for studying the transition of human osteoblasts to osteocytes. *Calcif Tissue Int, 95*(2), 183-193. doi: 10.1007/s00223-014-9879-y.

Qin, Y. (2010). *Micromanufacturing engineering and technology*: William Andrew.
Rabiller-Baudry, M., & Gouttefangeas, F. Coupling of SEM-EDX and FTIR-ATR to (quantitatively) investigate organic fouling on porous organic composite membranes.

Radecka, M., Wierzbicka, M., & Rekas, M. (2004). Photoelectrochemical cell studied by impedance spectroscopy. *Physica B: Condensed Matter, 351*(1), 121-128.

Randles, J. E. B. (1947). Kinetics of rapid electrode reactions. *Discussions of the faraday society, 1*, 11-19.

Ravichandran, R., Sundarrajan, S., Venugopal, J. R., Mukherjee, S., & Ramakrishna, S. (2010). Applications of conducting polymers and their issues in biomedical engineering. *Journal of the Royal Society Interface, 7*(Suppl 5), S559-S579.

Rezwan, K., Chen, Q., Blaker, J., & Boccaccini, A. R. (2006). Biodegradable and bioactive porous polymer/inorganic composite scaffolds for bone tissue engineering. *Biomaterials, 27*(18), 3413-3431.

Rodríguez-Sevilla, E., Ramírez-Silva, M.-T., Romero-Romo, M., Ibarra-Escutia, P., & Palomar-Pardavé, M. (2014). Electrochemical quantification of the antioxidant capacity of medicinal plants using biosensors. *Sensors, 14*(8), 14423-14439.

Sachlos, E., & Czernuszka, J. (2003). Making tissue engineering scaffolds work. Review: the application of solid freeform fabrication technology to the production of tissue engineering scaffolds. *Eur Cell Mater, 5*(29), 39-40.

Safaeijavan, R., Soleimani, M., Divsalar, A., Eidi, A., & Ardeshirylajimi, A. (2013). Biological behavior study of gelatin coated PCL nanofiberous electrospun scaffolds using fibroblasts. *Journal of Paramedical Sciences, 5*(1).

Salgado, A. J., Coutinho, O. P., & Reis, R. L. (2004). Bone tissue engineering: state of the art and future trends. *Macromolecular bioscience, 4*(8), 743-765.

Sam, S., Touahir, L., Salvador Andresa, J., Allongue, P., Chazalviel, J. N., Gouget-Laemmel, A. C., . . . Djebbar, S. (2010). Semiquantitative Study of the EDC/NHS Activation of Acid Terminal Groups at Modified Porous Silicon Surfaces. *Langmuir, 26*(2), 809-814. doi: 10.1021/la902220a

Sargeant, T. D., Rao, M. S., Koh, C.-Y., & Stupp, S. I. (2008). Covalent functionalization of NiTi surfaces with bioactive peptide amphiphile nanofibers. *Biomaterials, 29*(8), 1085-1098. doi: http://dx.doi.org/10.1016/j.biomaterials.2007.11.002

Scheufler, C., Sebald, W., & Hülsmeyer, M. (1999). Crystal structure of human bone morphogenetic protein-2 at 2.7 Å resolution. *Journal of molecular biology, 287*(1), 103-115.

Schmidt, C. E., Shastri, V. R., Vacanti, J. P., & Langer, R. (1997). Stimulation of neurite outgrowth using an electrically conducting polymer. *Proceedings of the National Academy of Sciences, 94*(17), 8948-8953.

Sebastian, A., Buckle, A. M., & Markx, G. H. (2007). Tissue engineering with electric fields: Immobilization of mammalian cells in multilayer aggregates using dielectrophoresis. *Biotechnology and bioengineering, 98*(3), 694-700.

Serafim, A., Mallet, R., Pascaretti-Grizon, F., Stancu, I.-C., & Chappard, D. (2014). Osteoblast-like cell behavior on porous scaffolds based on poly (styrene) fibers. *BioMed research international, 2014*.

Sharma, B., & Elisseeff, J. H. (2004). Engineering structurally organized cartilage and bone tissues. *Annals of biomedical engineering, 32*(1), 148-159.

Shin, H., Temenoff, J. S., Bowden, G. C., Zygourakis, K., Farach-Carson, M. C., Yaszemski, M. J., & Mikos, A. G. (2005). Osteogenic differentiation of rat bone marrow stromal cells cultured on Arg–Gly–Asp modified hydrogels without dexamethasone and β-glycerol phosphate. *Biomaterials, 26*(17), 3645-3654.

Shukla, S. K., Quraishi, M., & Prakash, R. (2008). A self-doped conducting polymer "polyanthranilic acid": an efficient corrosion inhibitor for mild steel in acidic solution. *Corrosion Science, 50*(10), 2867-2872.

Siggelkow, H., Schenck, M., Rohde, M., Viereck, V., Tauber, S., Atkinson, M. J., & Hüfner, M. (2002). Prolonged culture of HOS 58 human osteosarcoma cells with 1, 25-(OH) 2-D3, TGF-beta, and dexamethasone reveals physiological regulation of alkaline phosphatase, dissociated osteocalcin gene expression, and protein synthesis and lack of mineralization. *Journal of cellular biochemistry, 85*(2), 279-294.

Sill, T. J., & von Recum, H. A. (2008). Electrospinning: applications in drug delivery and tissue engineering. *Biomaterials, 29*(13), 1989-2006.

Smith, S. D., McLeod, B. R., Liboff, A. R., & Cooksey, K. (1987). Calcium cyclotron resonance and diatom mobility. *Bioelectromagnetics, 8*(3), 215-227.

Sofia, S., McCarthy, M. B., Gronowicz, G., & Kaplan, D. L. (2001). Functionalized silk-based biomaterials for bone formation. *Journal of biomedical materials research, 54*(1), 139-148.

Sophia, I. A., Gopu, G., & Vedhi, C. (2012). Synthesis and Characterization of Poly Anthranilic Acid Metal Nanocomposites. *Open Journal of Synthesis Theory and Applications, Vol.01No.01*, 8. doi: 10.4236/ojsta.2012.11001

Spagnuolo, M., & Liu, L. (2012). Fabrication and degradation of electrospun scaffolds from l-tyrosine-based polyurethane blends for tissue engineering applications. *ISRN Nanotechnology, 2012*.

Stains, J. P., & Civitelli, R. (2005). Cell-to-cell interactions in bone. *Biochemical and biophysical research communications, 328*(3), 721-727.

Staros, J. V., Wright, R. W., & Swingle, D. M. (1986). Enhancement by N-hydroxysulfosuccinimide of water-soluble carbodiimide-mediated coupling reactions. *Analytical Biochemistry, 156*(1), 220-222. doi: http://dx.doi.org/10.1016/0003-2697(86)90176-4

Tan, A., Dalilottojari, A., Pingguan-Murphy, B., Ahmad, R., & Akbar, S. (2014). In vitro chondrocyte interactions with TiO 2 nanofibers grown on Ti–6Al–4V substrate by oxidation. *Ceramics International, 40*(6), 8301-8304.

Tribet, C., Porcar, I., Bonnefont, P., & Audebert, R. (1998). Association between hydrophobically modified polyanions and negatively charged bovine serum albumin. *The Journal of Physical Chemistry B, 102*(7), 1327-1333.

Tryoen-Tóth, P., Vautier, D., Haikel, Y., Voegel, J. C., Schaaf, P., Chluba, J., & Ogier, J. (2002). Viability, adhesion, and bone phenotype of osteoblast-like cells on polyelectrolyte multilayer films. *Journal of biomedical materials research, 60*(4), 657-667.

Tuzlakoglu, K., Bolgen, N., Salgado, A., Gomes, M. E., Piskin, E., & Reis, R. (2005). Nano-and micro-fiber combined scaffolds: a new architecture for bone tissue engineering. *Journal of Materials Science: Materials in Medicine, 16*(12), 1099-1104.

Vacareanu, L., Catargiu, A.-M., & Grigoras, M. (2012). An electrochemical study of two self-dopable water-soluble aniline derivatives: electrochemical deposition of copolymers. *Journal of analytical methods in chemistry, 2012*.

Vats, A., Tolley, N., Bishop, A., & Polak, J. (2005). Embryonic stem cells and tissue engineering: delivering stem cells to the clinic. *Journal of the Royal Society of Medicine, 98*(8), 346-350.

Vaziri, S., Vahabi, S., Torshabi, M., & Hematzadeh, S. (2012). In vitro assay for osteoinductive activity of different demineralized freeze-dried bone allograft. *Journal of periodontal & implant science, 42*(6), 224-230.

Voicu, R., Boukherroub, R., Bartzoka, V., Ward, T., Wojtyk, J. T. C., & Wayner, D. D. M. (2004). Formation, Characterization, and Chemistry of Undecanoic Acid-Terminated Silicon Surfaces: Patterning and Immobilization of DNA. *Langmuir, 20*(26), 11713-11720. doi: 10.1021/la047886v

Volpato, F. Z., Almodóvar, J., Erickson, K., Popat, K. C., Migliaresi, C., & Kipper, M. J. (2012). Preservation of FGF-2 bioactivity using heparin-based nanoparticles, and their delivery from electrospun chitosan fibers. *Acta biomaterialia, 8*(4), 1551-1559.

Wan, Y., Chang, P., Yang, Z., Xiong, G., Liu, P., & Luo, H. (2015). Constructing a novel three-dimensional scaffold with mesoporous TiO2 nanotubes for potential bone tissue engineering. *Journal of Materials Chemistry B, 3*(27), 5595-5602. doi: 10.1039/C5TB00609K

Wang, C., Dong, Y., Sengothi, K., Tan, K., & Kang, E. (1999). In-vivo tissue response to polyaniline. *Synthetic Metals, 102*(1), 1313-1314.

Wang, C., Yan, Q., Liu, H. B., Zhou, X. H., & Xiao, S. J. (2011). Different EDC/NHS activation mechanisms between PAA and PMAA brushes and the following amidation reactions. *Langmuir, 27*(19), 12058-12068. doi: 10.1021/la202267p

Wang, X., Tolba, E., Schröder, H. C., Neufurth, M., Feng, Q., Diehl-Seifert, B., & Müller, W. E. (2014). Effect of bioglass on growth and biomineralization of SaOS-2 cells in hydrogel after 3D cell bioprinting. *PLoS One, 9*(11), e112497.

Wang, Y., Wang, G., Chen, L., Li, H., Yin, T., Wang, B., . . . Yu, Q. (2009). Electrospun nanofiber meshes with tailored architectures and patterns as potential tissue-engineering scaffolds. *Biofabrication, 1*(1), 015001.

Wang, Z.-G., Wang, Y., Xu, H., Li, G., & Xu, Z.-K. (2009). Carbon nanotube-filled nanofibrous membranes electrospun from poly (acrylonitrile-co-acrylic acid) for glucose biosensor. *The Journal of Physical Chemistry C, 113*(7), 2955-2960.

Wannatong, L., Sirivat, A., & Supaphol, P. (2004). Effects of solvents on electrospun polymeric fibers: preliminary study on polystyrene. *Polymer International, 53*(11), 1851-1859.

Warren, L., Walker, J., Anderson, D., Rhodes, C., & Buckley, L. (1989). A study of conducting polymer morphology the effect of dopant anions upon order. *Journal of the Electrochemical Society, 136*(8), 2286-2295.

Wei, Y., Lelkes, P. I., MacDiarmid, A. G., Guterman, E., Cheng, S., Palouian, K., & Bidez, P. (2004). Electroactive polymers and nanostructured materials for neural tissue engineering. *Contemporary topics in advanced polymer science and technology. Peking University Press, Beijing, China*, 430-436.

Wise, D. L., Wnek, G. E., Trantolo, D. J., Cooper, T. M., & Gresser, J. D. (1998). *Photonic Polymer Systems: Fundamentals: Methods, and Applications*: CRC Press.

Wisse, E., Spiering, A., Dankers, P. Y., Mezari, B., Magusin, P. C., & Meijer, E. (2011). Multicomponent supramolecular thermoplastic elastomer with peptide-modified nanofibers. *Journal of Polymer Science Part A: Polymer Chemistry, 49*(8), 1764-1771.

Wissink, M. J. B., Beernink, R., Pieper, J. S., Poot, A. A., Engbers, G. H. M., Beugeling, T., . . . Feijen, J. (2001). Immobilization of heparin to EDC/NHS-crosslinked collagen. Characterization and in vitro evaluation. *Biomaterials, 22*(2), 151-163. doi: http://dx.doi.org/10.1016/S0142-9612(00)00164-2

Woo, K. M., Chen, V. J., & Ma, P. X. (2003). Nano-fibrous scaffolding architecture selectively enhances protein adsorption contributing to cell attachment. *Journal of Biomedical Materials Research Part A, 67*(2), 531-537.

Woodruff, M. A., & Hutmacher, D. W. (2010). The return of a forgotten polymer—polycaprolactone in the 21st century. *Progress in Polymer Science, 35*(10), 1217-1256.

Yamazaki, M. (2007). *The chemical modification of chitosan films for improved hemostatic and bioadhesive properties*: ProQuest.

Yang, F., Williams, C. G., Wang, D.-a., Lee, H., Manson, P. N., & Elisseeff, J. (2005). The effect of incorporating RGD adhesive peptide in polyethylene glycol diacrylate hydrogel on osteogenesis of bone marrow stromal cells. *Biomaterials, 26*(30), 5991-5998.

Yang, Z., Wang, J., Luo, R., Maitz, M. F., Jing, F., Sun, H., & Huang, N. (2010). The covalent immobilization of heparin to pulsed-plasma polymeric allylamine films on 316L stainless steel and the resulting effects on hemocompatibility. *Biomaterials, 31*(8), 2072-2083. doi: http://dx.doi.org/10.1016/j.biomaterials.2009.11.091.

Yow, S.-Z., Lim, T. H., Yim, E. K., Lim, C. T., & Leong, K. W. (2011). A 3D electroactive polypyrrole-collagen fibrous scaffold for tissue engineering. *Polymers, 3*(1), 527-544.

Yu, D.-G., Williams, G. R., Gao, L.-D., Bligh, S. A., Yang, J.-H., & Wang, X. (2012). Coaxial electrospinning with sodium dodecylbenzene sulfonate solution for high quality polyacrylonitrile nanofibers. *Colloids and Surfaces A: Physicochemical and Engineering Aspects, 396*, 161-168.

Zainudin, N., Hairul, A. R. M., Yusoff, M. M., Tan, L. L., & Chong, K. F. (2014). Impedimetric graphene-based biosensor for the detection of Escherichia coli DNA. *Analytical Methods, 6*(19), 7935-7941.

Zander, N. E., Orlicki, J. A., Rawlett, A. M., & Beebe, T. P. (2012). Quantification of Protein Incorporated into Electrospun Polycaprolactone Tissue Engineering Scaffolds. *ACS Applied Materials & Interfaces, 4*(4), 2074-2081. doi: 10.1021/am300045y

Zehani, N., Dzyadevych, S. V., Kherrat, R., & Jaffrezic-Renault, N. J. (2014). Sensitive impedimetric biosensor for direct detection of diazinon based on lipases. *Frontiers in chemistry, 2*.

Zhang, X., Reagan, M. R., & Kaplan, D. L. (2009). Electrospun silk biomaterial scaffolds for regenerative medicine. *Advanced drug delivery reviews, 61*(12), 988-1006.

Zheng, W., Zhang, W., & Jiang, X. (2010). Biomimetic collagen nanofibrous materials for bone tissue engineering. *Advanced Engineering Materials, 12*(9), B451-B466.

Zhuang, H., Wang, W., Seldes, R. M., Tahernia, A. D., Fan, H., & Brighton, C. T. (1997). Electrical stimulation induces the level of TGF-β1 mRNA in osteoblastic cells by a mechanism involving calcium/calmodulin pathway. *Biochemical and biophysical research communications, 237*(2), 225-229.

Zipse, D. W. (1993). Health effects of extremely low-frequency (50 and 60 Hz) electric and magnetic fields. *Industry Applications, IEEE Transactions on, 29*(2), 447-458.

Zonari, A., Novikoff, S., Electo, N. R., Breyner, N. M., Gomes, D. A., Martins, A., . . . Goes, A. M. (2012). Endothelial differentiation of human stem cells seeded onto electrospun polyhydroxybutyrate/polyhydroxybutyrate-co-hydroxyvalerate fiber mesh. *PLoS One, 7*(4), e35422.

CURRICULUM VITAE

Name Surname: Zeliha GÜLER

Place and Date of Birth: 25.01.1986 Kırcaali

E-Mail: zelihaglr@gmail.com

EDUCATION:

B.Sc.: Istanbul University, Faculty of Science, Department of Biology, Istanbul TURKEY

M.Sc.: Istanbul University, Institute of Science and Engineering, Department of Biology, Istanbul TURKEY

Thesis: *"Cell Transfection and Cytotoxicity Studies of Newly Synthesized DNA Nanocarriers for Gene Delivery"*

PROFESSIONAL EXPERIENCE AND REWARDS:

- TUBITAK (Scientific and Technological Research Council of Turkey) Fellowship-2211C
- ERASMUS Scholarship, "Nova" University of Lisbon, Faculty of Science and Technology, Physics Department, Tissue Engineering Group, Lisbon-Portugal
- TUBITAK (Scientific and Technological Research Council of Turkey) Projects:
    - Researcher, Project No. 213M469, ITU (2014-2016)
    - Researcher, Project No. 1120200, ITU- SENTROMER DNA TECHNOLOGIES (2014-2016)
    - Researcher, Project No. 111T051, ITU-CZECH REPUBLIC (2012-2014)
- Researcher at TUBITAK on project SBAG-UKRAYNA-3 (109S258) (2010-2012)
- Young Researcher Award-2.place from the IEEE International Scientific Committee of E-HEALTH AND BIOENGINEERING

PUBLICATIONS, PRESENTATIONS AND PATENTS ON THE THESIS:

- **Guler Z.,** and Sarac A. S., 2016: Electrochemical impedance and spectroscopy study of the edc/nhs activation of the carboxyl groups on poly (ε-caprolactone)/poly (m-anthranilic acid) nanofibers, *eXPRESS Polymer Letters*, 10(2), 96-110.

- **Guler, Z.,** Silva J.C. Silva, Sarac, A.S, Enhanced Osteogenesis on Biofunctionalized Poly(m-anthranilic acid) Nanofibers (accepted 2016).

- **Guler, Z.,** Silva J.C. Silva, Sarac, A.S, RGD functionalized poly(ε-caprolactone)/poly(m-anthranilic acid) electrospun nanofibers as high performing scaffolds for bone tissue engineering (submitted).

- Polat E., **Guler Z.**, Balkan T., and Sarac A. S., 2015: Covalent Streptavidin Immobilization on Electrospun Poly(m-anthranilic acid) / Polycaprolactone Nanofibers and Cytocompatibility, *Journal of Bioactive and Biocompatible Polymers*.

- Golshaei R., **Guler Z.**, Sarac A.S., 2016: (Au/PANA/PVAc) nanofibers as a novel composite matrix for Albumin and streptavidin immobilization, *Materials Science and Engineering: C-Materials for Biological Applications*, 60, 260-275.

- **Guler Z.**, Erkoc P., and Sarac A.S, 2015: Electrochemical impedance spectroscopic study of single-stranded DNA-immobilized electroactive polypyrrole-coated electrospun poly(ε-caprolactone) nanofibers, *Materials express*, 5, 269-279.

- Dagli U., **Guler Z.**, Sarac A.S., 2015: Covalent Immobilization of Tyrosinase on Electrospun Polyacrylonitrile/Polyurethane/Poly(m-anthranilic acid) Nanofibers: An Electrochemical Impedance Study, *Polymer-Plastics Technology and Engineering*, 54, 14, 1494-1504.

- **Guler Z.,** Sarac A.S., 2015: BMP-2 immoblized PCL/P3ANA nanofibers for bone tissue engineering, *The 5 th IEEE International Conference on E-Health and Bioengineering – EHB*.

- **Guler Z.**, Sarac A.S., 2014: Bioactivation of Poly(m-anthranilic acid)/Poly(caprolactone) Nanofibers by Covalent Protein: Immobilization and Electrochemical Impedance Spectroscopic Characterization, *The MacroJournals Conference Paris 2014: Proceedings*.

- Guler, Z., Sarac A.S.,Biyoaktif, İletken Nanofiber Mat, NATIONAL PATENT APPLICATION (2016).

OTHER PUBLICATIONS, PRESENTATIONS AND PATENTS:

- Balkan, T., **Guler, Z.,** Morozova, M., Dytrych, P., Solcova, O., Sarac, A. S. 2016: The effect of deposition on electrochemical impedance properties of TiO_2/FTO photoanodes, *Journal of Electroceramics*, 1-10.

- Golshaei R, **Guler Z.**, Ünsal C., Sarac A.S., 2015: In situ spectroscopic and Electrochemical Impedance Study of Gold/Poly (Anthranilic acid) Core/Shell Nanoparticles, *European Polymer Journal*, 66, 502-512.

- Golshaei R., **Guler Z.**, Sarac A.S., 2015 Electrochemical Studies of Streptavidin Immobilization onto The (Gold/Poly Anthranilic Acid/Poly Vinyl Acetate) Nanofibers, 5th International Istanbul Textile Congress 2015: Innovative Technologies "Inspire to Innovate" (2015).

- Solcova O., Balkan T., **Guler Z.**, Morozova M., Dytrych P., Sarac A.S., 2014: New Preparation Route Of TiO2 Nanofibers By Electrospınnıng: Spectroscopic And Thermal Characterizations, *Science of Advance Materials*, 6, 2618-2624**.**

- Ficen S.Z.*, **Guler Z.*,** Mitina N., Finyuk N., Stoika R., Zaichenko A., Ceylan S.E., 2013: Biophysical Study of Novel Oligoelectrolyte Based Non-viral Gene Delivery Systems to Mammalian Cells, *Journal of Gene Medicine*,15 (5), 193-204 *Equal contribution-first author).

- Ficen S.Z, **Guler Z**, Mitina N., Zaichenko O., Filyak E., Ercelen S., 2011: Biophysical Study of Novel Oligoelectrolyte Vectors for Non-Viral Gene Delivery to Mammalian Cells. *Current Opinion in Biotechnology*, Volume 22, Supplement 1, S121.

- **Guler Z**., Erkoc P., Sarac A.S., 2013: Electrochemical Study of Polypyrrole Coated Electrospun Polycaprolactone Nanofibers and Their Potential Application in Biosensors, *Trends in Nanotechnology International Conference* (TNT2013).

- **Guler Z.**, Ficen S.Z, Mitina N., Zaichenko O., Ercelen S., 2012: Non-Viral Gene Delivery and Cytotoxicity Studies of Novel Oligoelectrolyte Based DNA Nanocarriers, *NanotechItaly2012 Promoting responsible innovation*, ISBN 978-886140-130-3, 369-370.

- **Guler Z.**, Balkan T., Demircioglu B., Sarac A.S., 2012: Synthesis and Characterization of PEDOT-PSS-TiO2 Films for Potential Use in Dye-Sensitized Solar Cell Applications, *NanotechItaly2012 Promoting responsible innovation*, ISBN 978-886140-130-3, 361-362.

- Birol S.Z, **Guler Z.**, Mitina N., Zaichenko A., Ercelen S., 2012: Investigation of interactions between newly synthesized block copolymer and DNA for non-viral gene delivery, *NanotechItaly2012 Promoting responsible innovation*, ISBN 978-886140-130-3, 351-352.

- Demircioglu B., Balkan T., **Guler Z.**, Sarac A.S., 2012: Preparation and Characterization of Polymer blends of PEDOT:PSS and PVAc, *NanotechItaly2012 Promoting responsible innovation*, ISBN 978-886140-130-3, 353-354.

- **Guler Z.**, Ficen S.Z, Skorokhoda T., Filyak Y., Ivanitska L., Mitina N., Stoika R., Zaichenko A., Ercelen S., 2011: Non-Viral Gene Delivery to HeLa cells Using Novel Oligoelectrolyte Vector, *International Conference Proceedings of PSRC,* ISBN 978-81-922428-3-5, 230-237.